UNIVERSITY OF AGDER

ENE 500 Master's Thesis

Measurements and analysis of spectral irradiance distributions in southern Norway

by

Helene Arnesen Hasla

Supervisor:
Anne Gerd Imenes and Margrethe Wold

This master's thesis is carried out as a part of the education at the University of Agder and is therefore approved as a part of this education. However, this does not imply that the University answers for the methods that are used or the conclusions that are drawn.

University of Agder, 2018

Faculty of Technology and Science

Department of Engineering

Abstract

The spectral response of the photovoltaic (PV) cell depends on which technology that is used and the outdoor performance of PV modules depends on solar irradiation, module temperature, and solar spectrum. Therefore, different locations should give different PV performance outcome. This thesis investigates local spectral irradiance measurements, which will be analysed to document irradiance conditions, and give an indication of which PV technology to prefer in Southern Norway.

A spectroradiometer is calibrated for use to measure the spectral irradiance at the University of Agder in Grimstad. From February to April in 2018, spectral irradiance data were collected. These data are used to analyse the spectral irradiance distribution during the months. Moreover, with the Simple Model for the Atmospheric Radiative Transfer of Sunshine version (SMARTS) and data from the nearby air station, different atmospheric parameters are analysed to test their influence on the spectra.

A literature review of the Average Photon Energy (APE) presented, and APE is used further to characterize the spectral irradiance. APE from this thesis work is from $1.95 - 2.1$ eV. The APE value is used to determine if the spectra are classified as blue rich or red rich. APE values from May and April are blue rich, while in February the majority of APE values are red rich.

In addition to analysing the atmospheric parameter with SMARTS, a model for a clear sky for each month is made. From the spectral irradiance measurements with a spectrometer, only the spectral irradiance from 300 to 900 nm influenced by noise. A model made in SMARTS gives the opportunity to get the complete spectrum.

Spectral response (SR) curves for a-Si, c-Si, CIGS, and CdTe PV modules is used to calculate their short circuit current density with both the measured data and the SMARTS models. The maximum power output is also calculated with the SMARTS models. The results show that CIGS gives best PV performance. However, the results for CIGS and c-Si is close and are both suitable PV technologies to use for the Southern Norway conditions.

Preface

This thesis is made as a completion of the master education in Renewable Energy. Yours truly has a bachelor degree in Renewable Energy from the Unversity of Agder and this thesis is the product of the master period, which is the last part of the Renewable Energy study at the University of Agder, Faculty of Technology and Science, Department of Engineering.

Several persons have contributed academically, practically and with support to this master thesis and I want to thank everybody who helped me during this process.

First of all, I want to thank Prof. Anne Gerd Imenes and Dr. Margrethe Wold, my supervisors, for dedicated and excellent guidance throughout this semester. Anne Gerd and Margrethe contributed with good advice and were always there to point me in the right direction.

I also want to thank Dr. Asadollah Bagheri for guidance to calibrate the spectrometer and Dr. Georgi Hristov Yordanov for solving the problem with the PC that controlled the measurements.

I want to thank Wenche Aas and Georg H. Hansen at NILU for their contribution concerning the data collected at Birkenes.

Finally, I would like to thank my boyfriend, family, and friends for being helpful and supportive during my time studying Renewable Energy at the University of Agder.

University of Agder, 11.05.2018

Helene Arnesen Hasla

Helene Arnesen Hasla

Individual Declaration

The individual student or group of students is responsible for the use of legal tools, guidelines for using these and rules on source usage. The statement will make the students aware of their responsibilities and the consequences of cheating. Missing statement does not release students from their responsibility.

1.	I hereby declare that my thesis is my own work and that I/We have not used any other sources or have received any other help than mentioned in the thesis.	☑
2.	I further declare that this thesis: - not been used for another exam at another department/university/university college in Norway or abroad; - does not refer to the work of others without it being stated; - does not refer to own previous work without it being stated; - have all the references given in the literature list; - is not a copy, duplicate or copy of another's work or manuscript.	☑
3.	I am aware that violation of the above is regarded as cheating and may result in cancellation of exams and exclusion from universities and colleges in Norway, see Universitets- og høgskoleloven §§4-7 og 4-8 og Forskrift om eksamen §§ 31.	☑
4.	I am aware that all submitted theses may be checked for plagiarism.	☑
5.	I am aware that the University of Agder will deal with all cases where there is suspicion of cheating according to the university's guidelines for dealing with cases of cheating.	☑
6.	I have incorporated the rules and guidelines in the use of sources and references on the library's web pages.	☑

Publishing Agreement

<table>
<tr><td colspan="2">Authorization for electronic publishing of
the thesis.

Author(s) have copyrights of the thesis.
This means, among other things, the exclusive right to make the work available to the general public (Åndsverkloven. §2).

All theses that fulfill the criteria will
be registered and published in Brage Aura and on UiA's web pages with author's approval.

Theses that are not public or are
confidential will not be published.</td></tr>
<tr><td>I hereby give the University of Agder a free right to
make the task available for electronic publishing:</td><td>Yes ☑</td></tr>
<tr><td>Is the thesis confidential?
(confidential agreement must be completed)</td><td>No ☑</td></tr>
<tr><td>- If yes:
Can the thesis be published when the confidentiality period is over?</td><td></td></tr>
<tr><td>Is the task except for public disclosure?
(contains confidential information. see Offl.
§13/Fvl. §13)</td><td>No ☑</td></tr>
</table>

Contents

List of Figures

List of Tables

Nomenclature

Constants

h	Plank constant	$6.63 \times 10^{-34}\, Js$
q	electronic charge	$1.60 \times 10^{-19}\, C$
v	velocity of light in vacum	$3.00 \cdot 10^{8}\, m/s$

Symbols

λ	wavelength	nm
λ_a	lower wavelength limit of an interval of the spectrum	nm
λ_b	upper wavelength limit of an interval of the spectrum	nm
λ_{eff}	effective wavelength	nm
$\mathbb{AM}$	air mass	
$\mathbb{GHI}$	global horizontal irradiance	$W/m^2/nm$
$\mathbb{GTI}$	global tilted irradiance	$W/m^2/nm$
$\Phi(\lambda)$	spectral photon flux density	$m^{-2}nm^{-1}s^{-1}$
AOD	aerosol optical depth at any wavelength	
AOD_{1020}	aerosol optical depth at 1020 nm	
AOD_{1640}	aerosol optical depth at 1640 nm	
AOD_{340}	aerosol optical depth at 340 nm	
AOD_{380}	aerosol optical depth at 380 nm	
AOD_{440}	aerosol optical depth at 440 nm	
AOD_{500}	aerosol optical depth at 500 nm	
AOD_{675}	aerosol optical depth at 675 nm	
AOD_{870}	aerosol optical depth at 870 nm	
APE	average photon energy	eV
Cd_2SnO_4	cadmium tin oxide	
Cds	cadmium sulfide	

CO_2	carbon dioxide	
CV	coefficient of variation	%
DIR	direct normal + circumsolar	$W/m^2/nm$
DNI	direct normal irradiance	W/m^2
$E(\lambda)$	spectral irradiance	$W/m^2/nm^2$
ETR	extraterrestrial spectrum	$W/m^2/nm$
FF	fill factor	
J_{SE}	short-circuit current density	$\mathrm{A/m^2}$
P_{mp}	maximum power output	$\mathrm{W/m^2}$
PW	precipitable water	cm
SnO_2	tin oxide	
SR	spectral response	A/W
T_{mod}	module temperature	K
UF	useful fraction	

Abbreviations

a -Si	amorphous silicon
$AERONET$	Aerosol Robotic Network
c -Si	crystalline silicon
$CdTe$	cadmium telluride
$CIGS$	copper indium gallium selenide
EQE	external quantum efficiency
IQE	internal quantum efficiency
PV	Photovoltaic(s)
QE	quantum efficiency
$SMARTS$	Simple Model for the Atmospheric Radiative Transfer of Sunshine version
STC	Standard Test Condition
TOC	transparent conductive oxide

1 Introduction

1.1 Background and motivation

Solar energy is one of the fastest growing renewable energy sources in the world, where the capacity is more than trebling over the past four years [1]. According to the International Energy Agency [2], solar PV will represent the largest annual capacity additions for renewable energy for the next five years, well above wind and hydro. This leads to a higher focus on producing more effective solar modules with the lowest cost. The effectiveness of the photovoltaic (PV) module is rated to standard test condition (STC) which is based on US conditions. Despite this, PV modules energy conversion mostly occurs at conditions differing from STC. [3] [4]

The spectral response of the PV cell depends on which technology that is used. The outdoor performance of PV modules depends on solar irradiation, module temperature, and solar spectrum. This dependence causes a difference between the actual solar spectrum under which the PV modules operates and the standard spectrum used for rating purposes from STC. The irradiance spectrum varies during the day, and the power output of the PV cells and modules will depend on the total in-plane irradiance and the instantaneous spectrum of the sunlight. This results in PV modules with a different spectral response having the same nominal power can have different instantaneous power output. This indicates that the different spectral irradiance has to be taken into account to achieve accurate predictions of the expected energy to be delivered over long periods—during which the incident spectrum may change significantly. The solar spectrum changes with geographical locations, which may lead to a difference in the energy output from PV installations. To know the effect of the spectral variations at any point would therefore be useful for the planners and investors of a PV system, to choose the PV modules best suited for a given location. In this thesis, local measurements will be presented and analyzed to give an indication of typical spectral irradiance conditions, and which PV technology to prefer, in Southern Norway.

To manage this, a unique index for the spectral irradiance distribution would be beneficial. In earlier studies average photon energy (APE) have already been investigated as a unique characteristic for the spectral irradiance distribution in several locations in the world with different climates. This parameter will also be used here, in order to compare with results from other graphical locations. [4] [5]

1.1.1 Problem

This thesis aims at presenting measurements and analysis of the spectral irradiance distributions in southern Norway. Solar irradiation data are collected, analysed and presented, both global irradiance and spectral irradiance distributions. The following steps will be introduced:

- Literature review of justification to use APE as a characterization of the spectral irradiance, the influence of atmospheric parameter on the spectrum, and the spectral effects on PV performance.
- Spectral irradiance measurements conducted in Grimstad by using a spectroradiometer.
- Calibration of the spectrometer, used for the measurements.

- Comparison of data from the Norwegian Insitute for Air Research (NILU) with spectral irradiance measurements data.
- A sensitivity analysis of different parameters affecting the solar spectral irradiance.
- Comparison of the measured spectral irradiance data with the model output produced from the modeling software SMARTS.
- The spectral response data from different PV technologies is analyzed with spectral irradiance measurements data.

1.1.2 Limitations

During the thesis, some problems occurred with the PC that controlled the measurements. The source of the problem was not discovered before late in April. This led to some lost data during the project.

Aerosol Optical Depth data from Birkenes is only available from late in April and May. The Cimel photometer had been sent to calibration in Spain during the winter, and there were also some technical problems after the photometer was back at Birkenes.

These limitations mean that the results presented are not representative for a full year. Ideally, measurements series should be conducted over several years (in meteorology, typically ten years is used for averaged data) in order to give a representative dataset taking into account year-to-year variations. However, as no such data material is currently available, this thesis is a start to try and identify typical conditions in Southern Norway and measurements should continue in the years ahead.

1.1.3 Thesis structure

The thesis is divided into eight sections. The following sections are:

Sections 1: The background, limitations, and problem are presented, and an overview of the methodology is defined.

Sections 2: The theoretical background to further reading of the thesis is presented.

Sections 3 A literature review of justification of the characterization parameter and earlier studies on the influence on the spectrum and PV performance.

Sections 4 The methodology and theory concerning the spectral irradiance measurements and modeling.

Sections 5 The collected data and results are presented and commented.

Sections 6 The results are discussed.

Sections 7 Recommendations for further work is presented.

Sections 8 The conclusion of the thesis is outlined.

2 Theoretical Background

This section explains how solar radiation reacts when entering the Earth's atmosphere. Characterizing methods of the spectral irradiance is also presented. In addition, utilization of the solar spectrum using PV, solar conversion efficiency, and the standard test conditions are explained.

2.1 Radiation through the atmosphere

The solar output originates from nuclear reactions within the Sun's hot core and is transmitted to the Sun's surface by radiation and convection. At Earth's average distance from the Sun, the radiation from the Sun per unit of time per unit of area on an ideal surface perpendicular to the Sun's rays is defined as $1,2608\ \text{kW/m}^2$. By the time the radiation reaches the Earth's surface, it has changed as a consequence of absorption and scattering in the Earth's atmosphere. In addition, the Suns radiation is affected by the altitude of the Sun, the distance from the Sun and day length. [6] [7]

The altitude of the Sun is the angle between its rays and a tangent to the Earth's surface at the observation point. The higher the Sun's altitude, the more concentrated is the radiation intensity per unit area at the Earth's surface and the shorter is the path length of the beam through the atmosphere. This decreases the atmospheric absorption. [6]

The distance from the Sun changes annually, producing seasonal variations in solar energy received by the Earth. This is caused by Earth's declination angle, which varies seasonally due to the tilt of the Earth on its axis of rotation and the rotation of the Earth around the Sun. The Earth is tilted by 23.45° and the declination angle varies plus or minus this amount. Also, the length of daylight affects the amount of radiation received; the longer the time the Sun shines, the greater is the quantity of radiation that a given portion of the Earth receives. [6] [8]

2.1.1 Air mass

The received solar spectrum depends on air mass, as the solar irradiance decreases when the air mass increase. The air mass is the path length as the light passes through the atmosphere and is calculated from the Sun's zenith angle, defined as the angle between the Sun and zenith, as shown in figure 2.1. The air mass measures the reduction in power of light as it transfers through the atmosphere and is absorbed by air and dust. The air mass number can be calculated by the equation:

$$AM = \frac{1}{\cos\theta} \tag{1}$$

where the θ is the Sun's zenith angle. [9]

When the air mass is one (AM1), the Sun is directly overhead. At an air mass of AM1.5, the angle between the Sun position and zenith angle is 48.2°. Outside the atmosphere, the air mass is defined as zero (AM0).

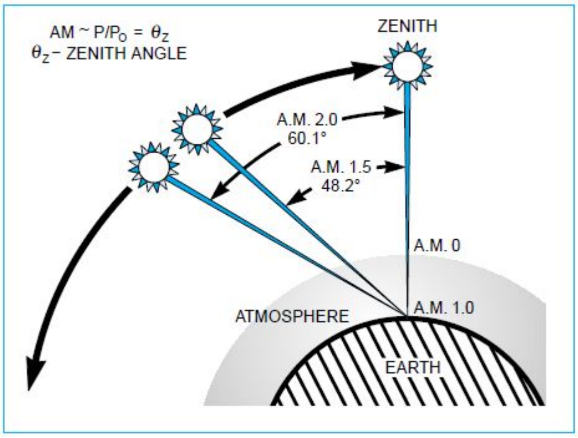

Figure 2.1: Air mass illustration [10]

2.1.2 Absorption in the atmosphere

When sunlight is passing through the Earth's atmosphere, it is reduced by about 30% by the time it reaches the Earth's surface. This reaction is a result of Rayleigh scattering by molecules in the atmosphere, scattering by aerosols and dust particles, absorption by atmospheric gases such as oxygen, ozone, water vapor (precipitable water) and carbon dioxide (CO2), and reflection of light. [7]

Absorption of sunlight below 300 nm is caused by ozone. Water vapor absorption, complemented by CO_2 absorption at longer wavelengths, produces the absorption bands around 1000 nm. Water vapor in the atmosphere is often measured in cm and then defined as precipitable water (PW). An illustration of this absorption is shown below in figure 2.2. [7]

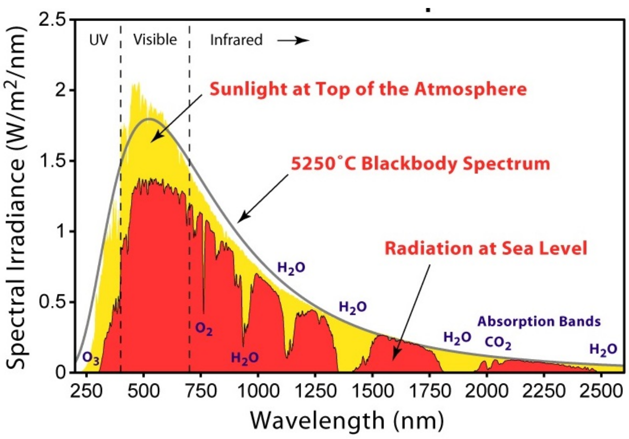

Figure 2.2: Absorption in the atmosohere and how it affects the spectrum [11]

To measure the amount of light that aerosols scatter and absorb in the atmosphere, aerosol optical depth (AOD) is used. If AOD is less than 0.05, it indicates that the sky is clear with relativity few aerosols and maximum visibility, while AOD around 1 indicates cloudy conditions. If AOD is above 2, it indicates very high concentrations of aerosols. [12]

When the sun's air mass is AM1, it has a diffuse component of about 10% when the sky is clear. When the AM increases or the sky is not clear, the diffuse component will increase. A significant cause of radiation reduction and scattering is clouds, where low altitude clouds (Cumulus or bulky) are effective in blocking sunlight. Nevertheless, of the direct radiation that is blocked by cumulus clouds, about half is recovered in the form of diffuse radiation. High altitude clouds (Cirrus or wispy) is not as effective in blocking sunlight, where about two-thirds of the direct beam radiation blocked are converted to diffuse radiation. On a cloudy day, most radiation that reaches the Earth's surface will be diffuse. The combination of direct and diffuse irradiation is defined as the global (G) irradiation. In figure 2.3, the AM 1.5 global spectrum is presented with it's diffuse and direct irradiation components, together with the extraterrestrial (AM0) spectrum. Global irradiance is the de [7]

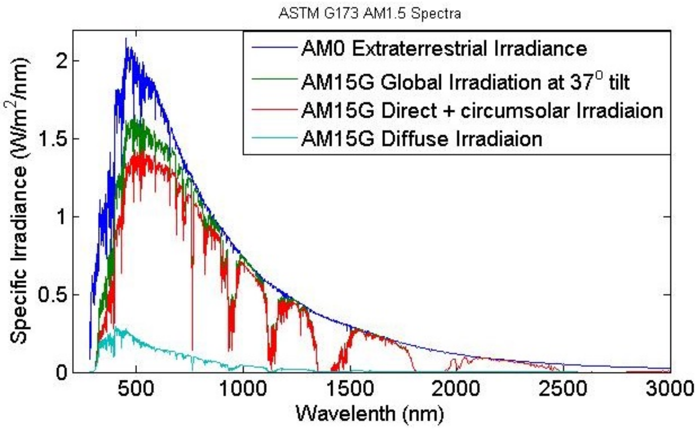

Figure 2.3: Global, direct and diffuse radiation for the AM1.5 spectrum together with the extraterrestrial (AM0) spectrum. [13].

2.2 Utilization of light with PV

A single PV cell is a semiconductor device that converts sunlight into direct current electricity. PV modules consist of many PV cells wired in series to produce higher voltage and in parallel to increase current. There are many types of PV modules, and the module structure is often different for different types of solar cells for various applications. The typical PV modules are crystalline silicon (c-Si), amorphous silicon (a-Si), cadmium telluride (CdTe), and copper indium gallium selenide solar cell (CiGS). [14]

The c-Si has the highest efficiency output, however, is also the most expensive type of silicon, because of the careful and slow manufacturing processes that are required. This is because of the ordered crystal structure, with each atom ideally lying in a pre-ordained position. [7] Figure 2.4 shows a schematic of a c-Si module. Encapsulating materials are used to resist heat, humidity, UV radiation and thermal cycling, electrically isolate components, and control, reduce, or eliminate moisture from entering. Ethaline vinyl acetate (EVA) is the most common most common material used for encapsulation. [15]

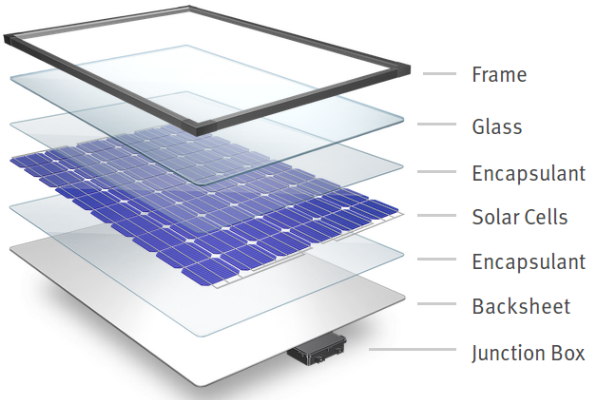

Figure 2.4: Schematic of a typical c-Si PV device. [15]

The a-Si was the first material thin film solar cells were based on. There is no long-range order in the structural arrangement of the atoms, results in areas within the material containing unsatisfied, or 'dangling' bonds in an a-Si solar cell. This gives rise to defects within the solar cell material that contributes to reduced efficiency. [7] Figure 2.5 illustrates a schematic a-Si module. The transparent conductive oxide (TCO) lets the sunlight enter and production of electrical current and voltage in the a-Si layer occurs. [16]

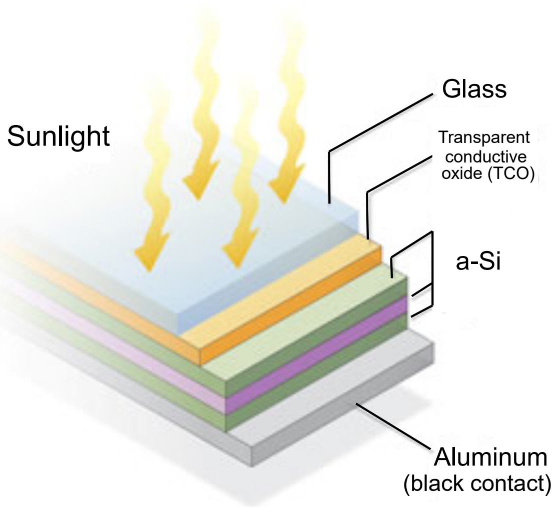

Figure 2.5: Schematic of a typical a-Si thin film PV device [16]

The CdTe PV solar cell is classified as a thin-film module. The CdTe thin film module represents the largest segment of commercial thin-film module production worldwide. The active layers in a CdTe thin-film module are just a few microns thick. Figure 2.6 shows an illustration of a typical CdTe thin-film PV device. TCO layers like SnO_2 or Cd_2SnO_4 are transparent to visible light and conductive to transport current efficiently. Intermediate layers like CdS help in both the electrical and growth properties between the TCO and CdTe. The CdTe film operates as the primary photoconversion layer and absorbs most visible light within the first micron of material. Together, the CdTe intermediate, and TCO layers from an electric field that converts light absorbed in the CdTe layer into current and voltage. On the back, metal is placed to form electrical contacts. All these layers are deposited on incoming glass and adapted into complete solar panels in just a few hours in the production. [17]

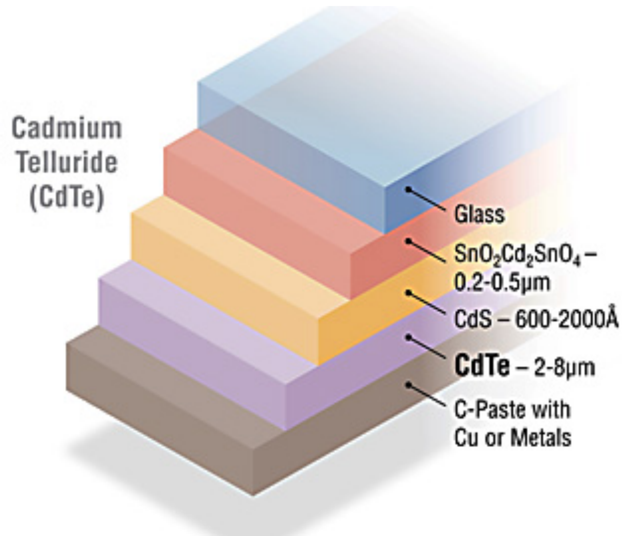

Figure 2.6: Illustration of a typical CdTe superstrate thin-film PV device. [17]

Another thin-film PV device is CIGS thin-film solar cell. This thin-film represents the highest-efficiency alternative for large-scale, commercial thin-film solar cells. In figure 2.7, an illustration of CIGS substrate thin-film PV device is presented. Here the layers are deposited on to glass, metal or polymer substrate. The top layer of the device, TOC, lets sunlight enter and production of electrical current and voltage in the lower layers occurs. [18]

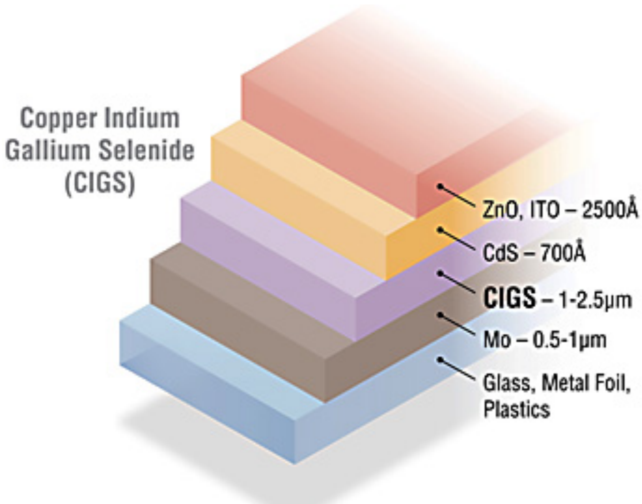

Figure 2.7: Illustration of a typical CIGS substrate thin-film photovoltaic device. [18]

2.2.1 Characterisics of the PV technologies

For PV technologies, quantum efficiency (QE) and spectral response (SR) are important device characterisics.

Quantum efficiency is defined as the number of electrons that move to the conduction band from the valence band per incident photon in the band-gap and collected by the solar cell. The band-gap is defined as the minimum amount of energy required for an electron to break free of its bound state. The conduction band contains unfilled energy levels, in which valence electrons can be excited and become conductive. The valence band contains filled energy levels with electrons that are bound to the nucleus of the atom and not conductive. [7] An illustration of the band-gap is shown in figure 2.8.

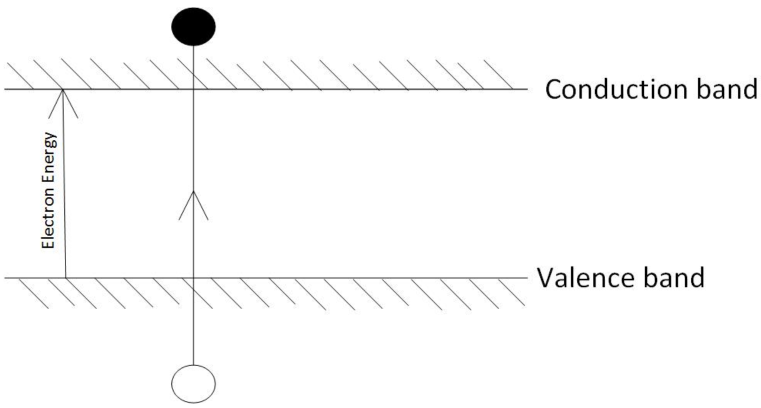

Figure 2.8: A illustration of band-gap

When the bandgap is in the range of $1.0-1.6$ eV, the maximum use can be made of incoming sunlight. This field limits the maximum achievable efficiency of solar cells to 44%. [7]

External quantum efficiency (EQE) is defined in equation 2, where EQE differs from the internal quantum efficiency (IQE) in that the latter excludes the fraction, R, of light reflected from the top surface of the solar cell. [7]

$$EQE = (1 - R) \times IQE \tag{2}$$

Spectral response (SR) is the ratio of the current generated by the solar cell and the source of power to the solar cell per wavelength. SR can be calculated as followed:

$$SR = \frac{q\lambda}{hc} EQE \tag{3}$$

where h is Planck's constant, c is the velocity of light in vacuum, λ is wavelength incident on the cell per unit time. [7]

The spectral response can be used to calculate the short-circuit current density (J_{SC}) of a PV device. [19] There are several ways to calculate the short-circuit current density. However, in this thesis, this equation is used:

$$J_{SE} = \int_{\lambda_a}^{\lambda_b} SR(\lambda) E(\lambda) d\lambda \tag{4}$$

Here, λ_a and λ_b are the lower and higher integration limits of the spectral irradiance, and $E(\lambda)$ is the spectral irradiance at wavelength λ. The unit of J_{SC} is A/m^2.

The maximum power P_{mp} is the product of fill factor FF, short-circuit current density J_{sc}, and open circuit voltage V_{oc} [20], as shown in this equation:

$$P_{mp} = FF \times J_{sc} \times V_{oc} \tag{5}$$

P_{mp} has the unit W/m^2. FF, J_{sc}, and V_{oc} for a single-junction solar cell can be found as a function of band-gap energy according to the Shockley-Queisser limit (solid lines) and experimental values for record-efficiency cells. [21] This is illustrated in figure 2.9. This gives the opportunity to find the ideal «record efficiency solar cell» parameters. All the parameters are for standard AM1.5 illumination at 1000 W/m^2.

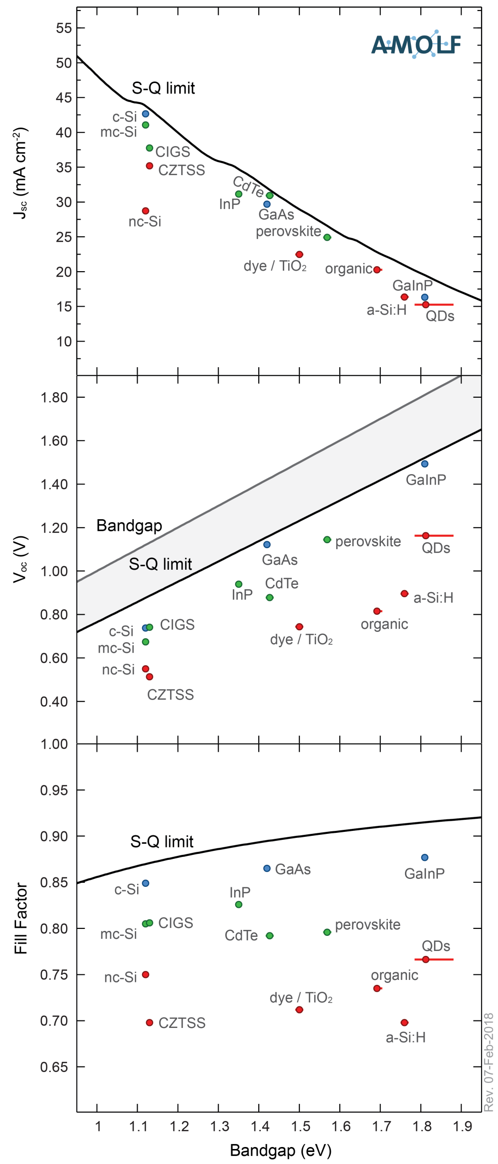

Figure 2.9: Single-junction solar cell parameters are shown as a function of band gap energy. [21]

2.3 Standard test conditions

To the compare the efficiency of PV modules, they are rated after Standard Test Conditions (STC). The performance of a PV module depends on temperature and irradiance. STC is defined when PV cell temperature is 25° C, the spectral distribution is AM 1.5 global, and standard intensity (E_{STC}) is set as a constant incoming in-plane solar irradiance of $1000\,\mathrm{W/m^2}$. [22]

The STC is based on the average atmospheric conditions for the 48 contiguous states of the United States of America (U.S.A.) over a period of one year, according to the following parameters:

- the 1976 U.S. Standard Atmosphere with temperature, pressure, aerosol density, air density, molecular species density specified in 33 layers.
- an absolute air mass of 1.5 (solar zenith angle 48.19° and tilted surface at 37°)
- Angstrom (unit length) turbidity at 500 nm of 0.084
- total column water vapor equivalent of 1.42 cm
- total column ozone equivalent of 0.34 cm
- surface spectral albedo (reflectivity) of light soil as documented in the Jet Propulsion Laboratory ASTER Spectral Reflectance Database. [22]

Figure 2.10 of the AM 1.5 standard spectrum with both extraterrestrial, terrestrial global 37° south facing tilt and direct(normal + circumsolar) spectrum. In this plot, the full spectrum is introduced over the wavelength range 0 to 4000 nm.

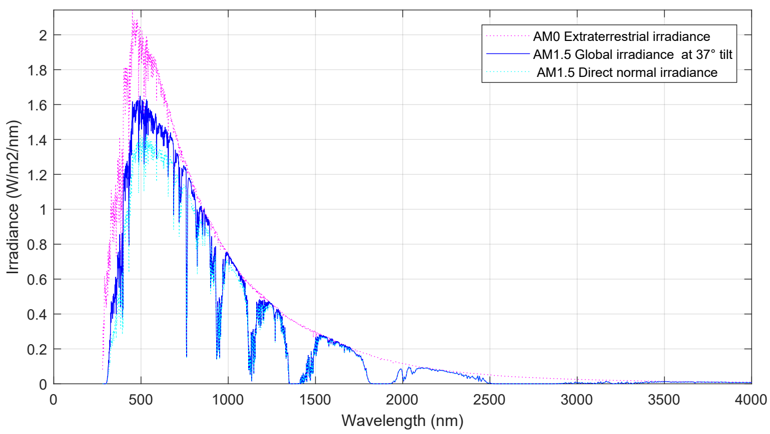

Figure 2.10: AM 1.5 standard spectrum

2.4 Spectral irradiance charactersation

To characterise the effect of the solar spectral variations, it is useful to define a parameter that can represent a spectral shift towards higher or lower energies. In this thesis, the average photon energy is used as the parameter. However, another parameter named useful fraction is mentioned in section 3, and is therefore briefly described as well.

2.4.1 Irradiance

Spectral irradiance is the photon flux multiplied by the energy of the photon per wavelength λ. It measures how much power is coming from all the photons received per second at the wavelength. This gives an impression of how much energy is being contributed at each wavelength. [23] Spectral irradiance is measured in $W \times m^{-3}$ and is defined as:

$$I_\lambda = \frac{\Phi \times E_\lambda}{\lambda} \tag{6}$$

where the Φ is the photon flux, E is the photon energy and λ is the wavelength.

The photon flux is defined as the number of photons (N) per unit time (t) and area (A) and can be described with this equation [24]:

$$\Phi = \frac{N}{t \times A} \tag{7}$$

2.4.2 Average photon energy

The average photon energy (APE) is one of the parameters that is used in literature to characterize spectral irradiation. The APE is an instantaneous value defined as ratio of total irradiance of the spectrum over photon flux density. The definition of APE, as proposed by Dirnberger et al. [3], is usually referred to as a finite integration interval, here expressed in the unit of joule (J):

$$APE = \frac{\displaystyle\int_{\lambda_a}^{\lambda_b} E(\lambda)\, d\lambda}{\displaystyle\int_{\lambda_a}^{\lambda_b} \Phi(\lambda)\, d\lambda} \tag{8}$$

APE is regularly expressed in electronvolt (eV) by converting J to eV with conversion factor.

The wavelength range used in the calculation of the APE influences its value. APE increases as more of the wavelength range is removed from the calculation.

The relationship between spectral irradiance and spectral photon flux density at wavelength λ is [9]:

$$\Phi(\lambda) = \frac{E(\lambda)}{hc/\lambda} \tag{9}$$

In addition to eq. 8, there is also an equivalent definition of APE suggested by Gueymard [25]

$$APE = \frac{hc}{\lambda_{eff}} \tag{10}$$

where λ_{eff} is the "effective wavelength", defined as

$$\lambda_{eff} = \frac{\displaystyle\int_{\lambda_a}^{\lambda_b} \lambda E(\lambda)\, d\lambda}{\displaystyle\int_{\lambda_a}^{\lambda_b} E(\lambda)\, d\lambda} \tag{11}$$

APE is dependent on atmospheric conditions and season. The spectral irradiance at short wavelengths decreases when there is a high absorption or scattering of short wavelength light. In these conditions, the incident spectrum is often referred to as a “red rich” because the average photon energy is moved towards the lower APE values, which corresponds to light at longer wavelengths. [5] [26]

When the long wavelength portion of the incoming light is attenuated, the opposite occurs, resulting in a “blue rich” spectrum and APE increases. Between the specific upper and lower wavelength limits, the APE of the standard AM 1.5 spectrum is often used as reference to determine if the spectral scattering is shifted in the direction toward blue or red wavelengths. [5] [26]

Overhead clouds and humid weather increase APE because the clouds absorb in the long wavelength part of the solar spectrum. Long wavelength region is attenuated, thereby making the spectrum more "blue rich" . [27]

2.4.3 Useful fraction

Another method to characterise the spectral irradiance is Useful fraction (UF). Unlike APE, UF is dependent on PV technology.

If the spectral irradiance encountered by a given PV device/cell is $G(\lambda)$ the total irradiance, G is defined as

$$G \equiv \int_0^{\infty} G(\lambda)\, d\lambda = \int_0^{\infty} E_\lambda \Phi(\lambda)\, d\lambda \tag{12}$$

UF is the ratio of the solar irradiance within the usable wavelength range of a PV device to the total solar irradiance and is defined as

$$UF \equiv \frac{1}{G} \int_0^{\lambda(E_g)} G(\lambda)\, d\lambda \tag{13}$$

where E_g is the band-gap of the solar device/cell which equates to a long wavelength cut-off of wavelength λ.

3 State of Art

This section presents a literature study for the thesis, which is divided into three subsections. The first subsection presents the justification to use APE as a characterization of the spectral irradiance is presented, first experimental investigation and then theoretical investigation.

The next subsection presents a review of the influence of spectral irradiance on the performance of different PV technologies. The final subsection, investigate the influence of the atmospheric parameters on the spectrum.

3.1 Investigations of APE

3.1.1 Experimental investigations of APE

Minemoto et al. (2009) [28] is the first to investigate if APE can be a unique characteristic of the solar spectrum. Their results are based on a statistical analysis conducted using spectral global tilted irradiation (GTI) data collected over three years on a surface equator-facing with a tilt angle of 15.3° in Kusatsu city, Japan. The results reproduced in figure 3.1, display the solar spectra with APE values from 1.86 to 2.04 eV. In the outcome of this analysis, the authors conclude that APE is a reasonable and useful index to describe the spectral irradiance distribution for evaluating the outdoor performance of PV modules. However, Minemoto et al. suggest that similar analysis has to be performed at different locations and climates to check the uniqueness universally.

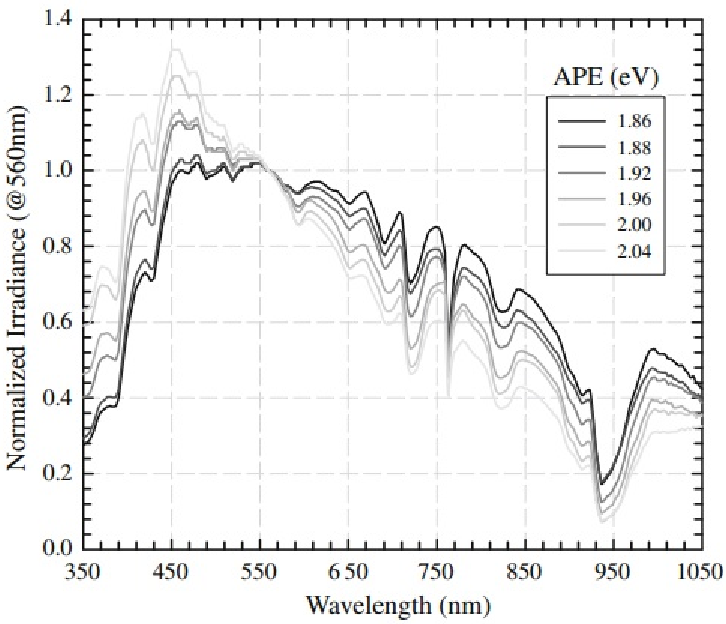

Figure 3.1: Results from Minemoto et al [28]. Solar spectra with APE values between 1.86-2.04 eV. The spectral irradiance is normalized with the irradiance at 560 nm for each spectrum.

Norton et al. (2015) [29] support the conclusion of Minemoto et al. that APE can identify a unique spectral irradiation distribution with low standard deviation. Their conclusion is based on the result of the analysis of two spectrally-resolved global horizontal irradiances (GHI) experimental datasets using different equipment at different locations and times of the year. The two locations have different climates and average atmospheric depths, where Ispra, Italy is classified as warm-temperate/fully humid/warm summer (Cfb), and Golden, Colorado, USA is classified as borderline between snow/fully humid/warm summer (Dfb) and arid/steppe/cold arid (BSk). The measurements were taken during two years, and the analysis followed the same methodology as Minemoto et al. Norton et al. also encourage the collection and analysis of data elsewhere in order to validate their conclusion.

Recently a study was carried out by Nofuentes et al.(2017) [5], using data from two Spanish locations, 333 km apart. This paper uses the same methodology as Minemoto et al. and Norton et al. The locations of the two spectroradiometers is in Jaén and Madrid, Spain. The spectroradiometers, which are the same brand and model, are used in each site with identical experimental protocols. The datasets are collected over two years with a tilted angle of 30°. Their results reproduced in fig 3.2a and 3.2b, show that the coefficient of variation, CV (ratio of the standard deviation to the mean), remains below 3.3 % over the 450–900 nm waveband, whereas values up to 5–11 % occur outside of it (which they mention can be explained by impacts of experimental uncertainty and the direct effect of aerosols and water vapor). By looking at these results, they conclude that APE cannot be a unique characteristic of the complete spectrum. However, they argue that APE may be considered approximately unique relative to the spectrum distribution under the climate of the two sites under scrutiny over the limited $450-900$ nm spectral range.

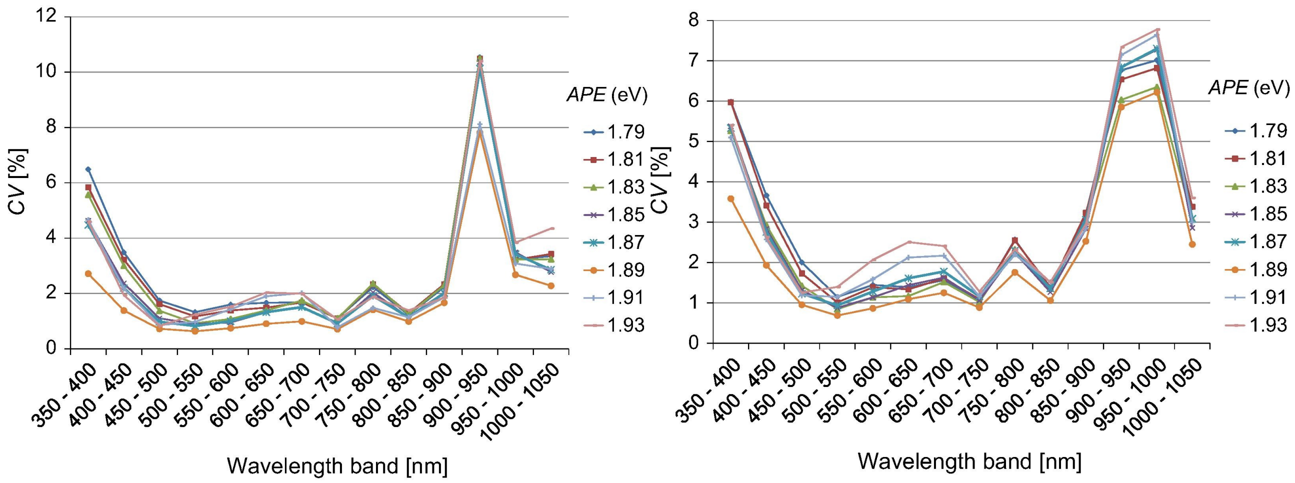

(a) (b)

Figure 3.2: Results from Nofuentes et al [5]. Coefficient of variation of every 50-nm band for spectral measurements grouped into 0.02-eV width APE intervals, over the range 1.79–1.93 eV (central values), for spectral data recorded in (a) Jaen and (b) Madrid.

In a study by Ishii et al. (2013) [4], which was carried out at four locations in Japan with different tilt angles, they estimated the net effect of the solar spectrum on the annual energy yield of c-Si and a-Si modules by two parameters, spectral factor (SP) and APE. In their results, the two parameters are quite consistent, where there is 1.2% difference between the estimations at most. They conclude that APE would be a useful index to quantify the effect of the solar spectrum on annual yield. Furthermore, they suggest that important work would be to confirm whether the approximate parameter can apply to different climate regions.

Louwen et al. (2016) [30] published results from Utrecht, The Netherlands, with solar spectral instruments installed on a 37° tilted surface facing due south. Here, they analyse the suitability of APE as an indicator of PV module performance as a function of spectral variation, by calculating the variation in measured spectra at a range of APE values. In addition they compare APE with other spectral indicators. In their results, APE is found as the best indicator of spectral variation on PV module performance, but no mention of its possible uniqueness. And like the other references, they recommend that this study is extended to other climatic zones to validate their conclusions.

Despite the positive result from Minemoto (2009) et al., Norton et al. (2015) and Nofuentes et al. (2017), the study by Dirnderger et al. (2015) [3] reject APE as a unique characteristic of the spectral distribution. Their conclusion is based on measurements taken over 3.5 years from Freiburg im Breisgau, Germany with instruments installed on a 35° tilted surface facing due south. In their conclusion, they establish that APE is not a good index to quantify the spectral impact on single-junction devices, and should rather be used for qualitative evaluations.

3.1.2 Theoretical investigation of APE uniqueness

A theoretical study of APE was conducted by Gueymard (2009), using the SMARTS spectral irradiance model (Gueymard, 2001) [25], to calculate the spectral mismatch correction factor on single- or multi-junction solar cells. In the study, the author evaluated the sensitivity of APE (Eq.10) and λ_{eff} (Eq.11) to three important variables that are known to affect the clear-sky direct spectrum most; air mass (AM), aerosol optical depth (AOD) and precipitable water (PW). AM and AOD influence λ_{eff} and APE so that the spectrum shifts toward longer wavelengths when they increase, while PW has a more limited but opposing effect. With two different set of conditions (AM1, AOD1, PW1) and (AM2, AOD2, PW2), Gueymard shows that the model could induce the same results in λ_{eff} and APE. He concludes that the APE is not a unique characteristic of the direct spectrum. Nevertheless, the study was looking at direct normal irradiance (DNI), which is known to be much more sensitive to AM, AOD, and PW than the global spectrum.

3.1.3 Summary of findings in the literature

To have a overview of the experimental investigations of APE, table 3.1 and 3.2 presented.

Table 3.1: Data from experimental investigations of APE

	Sapporo, Tosu, Gifu, Okinoerabu (Ishii)	**Jaén (Nofuentes)**	**Madrid (Nofuentes)**	**Kusatsu city (Minemoto)**
Country	Japan	Spain	Spain	Japan
Latitude (°)	43.1, 31.6, 35.4, 27.4	37.8	40.4	35.0
Longitude (°)	141.4, 130.5, 136.8, 128.6	-3.8	-3.7	136.0
Koeppen-Geiger climate classification	Dfa, Cfa, Cfa, Cfa	Csa	Csa	Cfa
Start wavelength (nm)	350	350	350	350
End wavelength (nm)	1700	1050	1050	1050
Start month	?-2008	01-2011	01-2011	01-2004
End month	?-2010	12-2013	12-2013	12-2006
Tilt angle	36°, 26°, 32°, 22°	30°	30°	15.3°
APE result	1.2-2.1 eV	1.79 - 1.93 eV	1.79 - 1.93 eV	1.86-2.04 eV

Table 3.2: Data from experimental investigations of APE

	Freiburg im Breisgau (Dirnderger)	**Utrecht (Louwen)**	**JRC (Norton)**	**NREL (Norton)**
Country	Germany	The Netherlands	Italy	USA
Latitude (°)	48.0	52.1	45.8	39.7
Longitude (°)	7.8	5.1	8.6	-105.2
Koeppen-Geiger climate classification	Cfb	Cfb	Cfb	Dfb-BSk
Start wavelength (nm)	350	350	400	400
End wavelength (nm)	1050	1050	1050	1050
Start month	01-06-2010	?-2015	02-2009	01-2012
End month	31-12-2013	?-2015	06-2010	04-2014
Tilt angle	30°	37°	Horizontal	Horizontal
APE result	1.84-1.91 eV	1.88+-0.012 eV	1.78 - 1.92 eV	1.78 - 1.94 eV

3.2 Spectral effects on PV performance

A study by Krawczynsk et al. (2011) [31] was carried out at Loughborough University, the UK, analysed of the variations of spectral irradiance and the effects on the accuracy of energy production and reference energy rating of PV modules. A meteorological station with facilities to measure PV module short-circuits currents and temperatures were designed and built. The station was equipped with three diode-array base grating spectroradiometers, three ventilated thermopile pyranometers, air humidity and temperature sensor and wind speed and wind direction sensor. Spectroradiometers and pyranometers were installed in a horizontal plane, 45° tilted plane and on a solar tracker. The measurements were taken over a 2-year period from 09-01-2009 to 31-12-2010. In their study, they concluded that the largest differences take place for low-level irradiance and most of the energy reaches the surface of the earth at the low air mass and light overcast conditions, with moderate spectral influences on total PV energy production. In addition, some of the seasonal variations of Pv module performance may have a partial explanation related to spectral variations of the sunlight and can be caused by reference sensor mismatch. The most accurate rating of the available energy for PV conversion can be given with the use of technology-specific current density. They suggest that utilization of spectroradiometers may have some advantages in a large-scale plant where different module technologies are used, as a way of irradiance data validation. Furthermore, they expect that for southern climates characterized by lower clouds cover, the influence of the spectral variations of the solar radiation may have a stronger effect on energy production.

Minemoto et al. (2007) [32] investigated the impact of spectral irradiance distribution and temperature on the outdoor performance of a-Si and mc-Si PV modules installed at Kusatsu city in Japan. Their results show that the output energy of a-Si modules mainly depends on spectrum distribution and is higher under blue-rich spectra. For the mc-Si module, the output energy is sensitive to module temperature but not to spectrum distribution. In addition, Minemoto et al. (2007) [33] also published an article of the investigation on the effects of spectral irradiance distributions on the outdoor performance of thin-film a-Si// c-Si stacked modules installed at Shiga-prefecture in Japan. The results revealed that more than 95% of annual total spectra were blue-rich compared to AM1.5 standard solar spectrum. The results also discovered that the outdoor performance of the modules had a higher spectral dependence than that of m-Si modules. The peak of the histogram of APE corresponded well to the peak of the outdoor performance. In their conclusion, they conclude that the actual spectral irradiance distribution is important in designing stacked PV modules.

Amillo et al. (2015) [34] investigated the magnitude of spectral influence on PV performance over Europe and Africa. They presented a method for calculating the effect of time-varying sunlight spectrum on the performance of PV modules by using spectrally-resolved irradiance data estimated from satellite data. The results compared spectral response data for c-Si, CdTe and single-junction a-Si modules with spectral satellite data to construct maps of the annual average spectral effect over Europe and Africa. The effect is small for all three module types in desert areas, while a positive effect of +2 to +4% is seen in most of Central and Northern Europe for CdTe and a-Si modules. The strongest effect is seen in tropical Africa, where CdTe modules may produce up to about 6% more energy due to spectral effects, while for a-Si modules, the effect may reach +10%. The study was only being performed for single-junction PV technologies and not multijunction PV technologies, as these have a more complicated behavior under varying spectra due to the varying spectral sensitivity of the different layers.

A study published in 2017 by Eke et al. [9] also discusses the influence of the spectrum on PV performance. The authors reviewed more than 200 studies, published in journals, conference proceedings, unpublished or only local data. For characterization of the spectra, they used APE and UF, which are represented in figure 3.3a. In their article, they conclude that the performance variation is strongly dependent on module type and that global solar radiation had a seasonal variation of 5%. This is illustrated in figure 3.3b. For clear sky days, spectrum has little influence for low bandgap material-based PV modules, where the efficiency varies only 4% or 5% between seasons for e.g., c-Si solar cells. However, for large bandgap materials, like an a-Si solar cell, this effect is severe, where the efficiency varies from −10% to +15% between seasons.

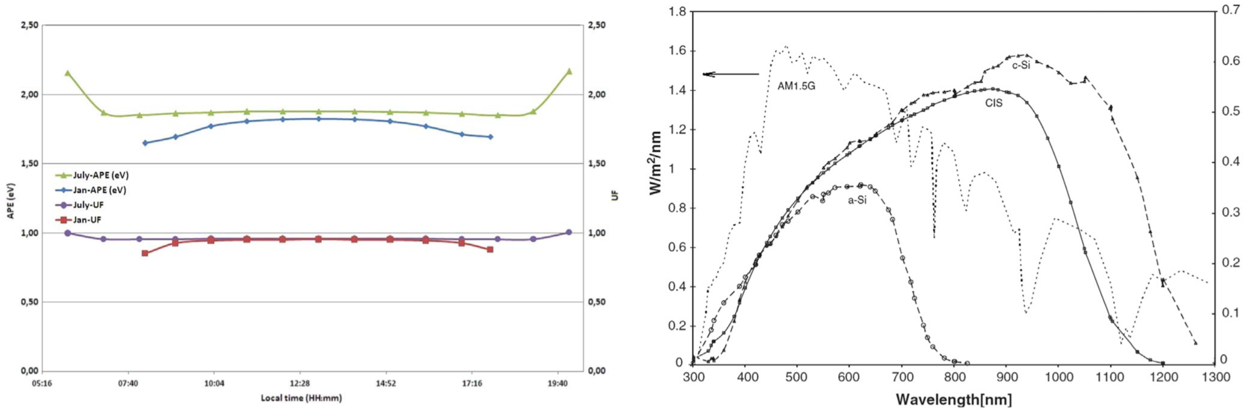

(a) **(b)**

Figure 3.3: Results from Eke et al. [9] Figure 3.3 (a) Calculated APE and UF values for clear sky days for a location of 37°N latitude . (b) Spectral responses of some module types and the AM1.5 G spectrum up to 1300 nm.

Dirnberger et al. [35] published in 2015 an article on the results from investigating the impact of varying spectral irradiance on the performance of different PV technologies. Spectral irradiance was measured and analysed from 01.06.2010 to 31.12.2013 in Freiburg im Breisgau, Germany. These measurements were used to quantify relative gains or losses quantified for five typical PV technologies with different band gaps and different spectral responses. The annual spectral impact was +3.4% for a-Si, +2.4% for CdTe, +1.4% for c-Si, +1.1% for high-efficiency c-Si and +0.6% for small-band-gap CIGS. Technologies with a large band gap presented spectral gains in summer and spectral losses in winter, and vice versa for small-band-gap technologies. The normalized spectral response data for single junction PV technologies shown in figure 3.4 is used further in this thesis.

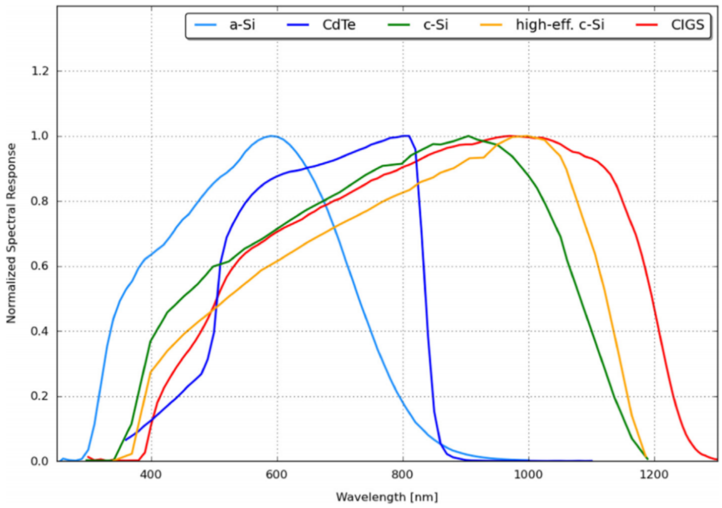

Figure 3.4: Data from Dirnberger et al. [35] The plot show typical, normalized spectral response data for single junction PV technologies.

3.3 Influence of atmospheric parameters on the spectrum

Nofuentes et al.(2017) [5] investigates the influence of the aerosol optical depth (AOD) and precipitable water (PW) on the spectrum. Results for the spectroradiometers, measurements of AOD, PW and other relevant atmospheric variables were obtained from the AERONET database. The reproduced figure 3.5a and 3.5b presents the seasonal variation of the daily mean and standard deviation of AOD500 (the aerosol optical depth at 500 nm in an atmospheric vertical column) and PW at Granada (the AERONET site of the University of Granada - 93 km to the south of Jean) and Madrid.

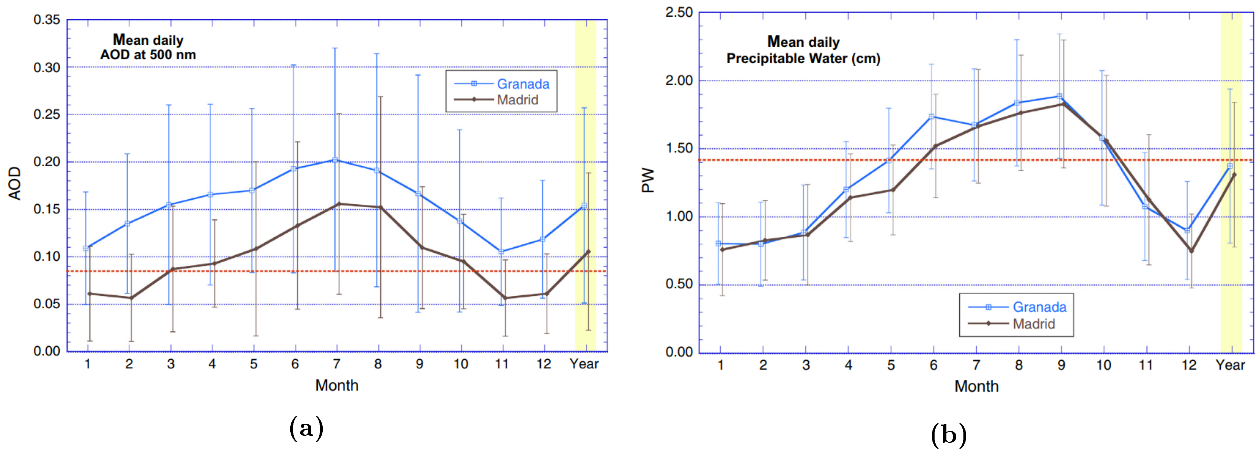

Figure 3.5: Results from Nofuentes et al [5]. (a) Daily mean and standard deviation of aerosol optical depth at 500 nm (AOD500). (B) Daily mean and standard deviation of precipitable water (PW). Results obtained from AERONET at Granada and Madrid on average for each month. The red horizontal dashed line indicates the value used to obtain the standard AM1.5G spectrum.

From figure 3.6a, the results of Nofuentes et al. [5] also show a SMARTS model was the intense water vapor absorption around 940 nm is the main source of concern for that band. Similarly, in figure 3.6b demonstrates that natural daily variations in AOD tend to affect the GTI spectrum mostly below 450 nm, and increase variability there.

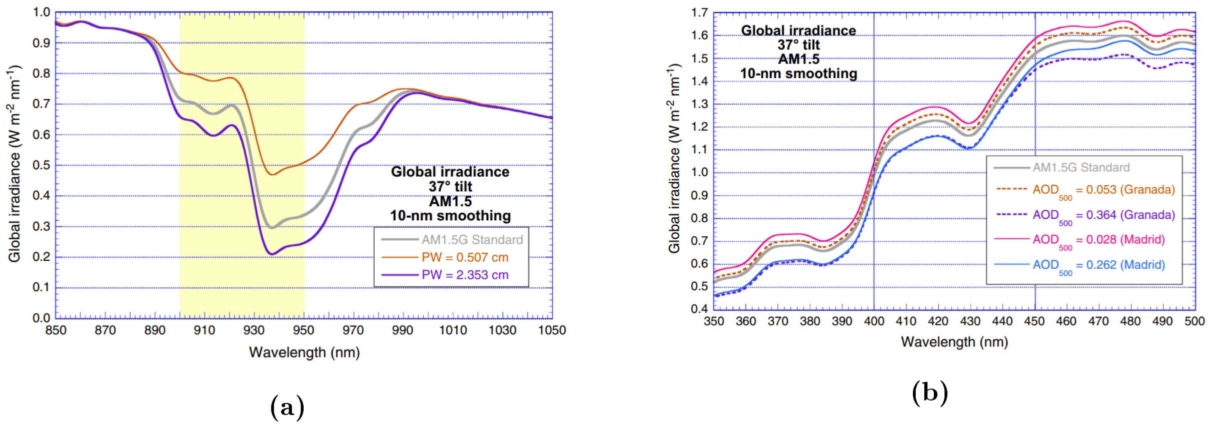

Figure 3.6: Results from Nofuentes et al [5]. Global tilted irradiance simulated with SMARTS for a 37° tilted surface facing the sun under standard conditions (a) under "near-extreme" PW conditions in and at Granada, (b) under "near-extreme" AOD conditions at Granada and Madrid.

This literature review demonstrates that APE cannot be considered as a unique characteristic of the complete spectrum, but APE may be considered approximately unique relative to the spectrum distribution under a limited range and will, therefore, be used further in this thesis from the wavelength range 300 - 900 nm.

The next section demonstrates that specific atmospheric parameters have the impact on the spectrum and this will be further analysed in this thesis. In addition, location and seasonal changes affect the PV performance, which will also be investigated for this location and season.

4 Methodology

This section addresses the methodology and theory concerning the spectral irradiance measurements and modeling.

The first subsection presents the spectrometer and its parameters and components, followed by a description of cosine corrector, fiber, and calibration procedure. Then the pyranometers, and locations and experimental set-up details are presented. Furthermore, data collection and filtrations and atmospheric data is presented. In the end, SMARTS modeling, PV details and Matlab is presented.

4.1 Spectrometer

Figure 4.1: HR2000+ spectrometer [36]

The High-Speed Miniature Fiber Optic Spectrometer HR2000+, produced by Ocean Optics, is used to measure solar spectra Figure 4.1). The HR2000+ is responsive from 200-1100 nm (UV-VIS-NIR), but the range and resolution depend on grating and entrance slit. [36] Figure 4.2 shows the spectrometer optical path and components. The spectrometers specifications are found in appendix A.

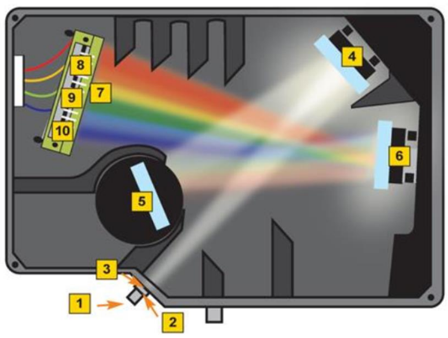

Figure 4.2: HR2000+ optical Components on the light path. 1. SMA connector , 2.Entrance slit, 3.Long pass absorbing filter, 4. Collimating mirror, 5. Grating, 6. Focusing mirror, 7. Detector collection lenses, 8. CCD detector, 9.Variable long pass filter, 10. UV windows (quartz). [36]

An available memory chip instructs the instrument on what and when and how to measure. Data programmed into a memory chip on HR2000+ includes wavelength calibration coefficients, linearity coefficients, and the serial number unique to each spectrometer. [36]

Free software from Ocean Optics will access the values on the memory chip. The HR2000+ can be controlled by OceanView software, which is a Java-based spectroscopy software platform that operates on Windows, Linux and Macintosh operating systems. The spectrometer is operating software reads merely values from the spectrometer. The HR2000+ Spectrometer connects to a PC via USB port. [36]

4.1.1 CCD detector

A CCD detector is a Charge Coupled Device detector and is a silicon-based multichannel array detector of UV, visible and near-infrared light. The CCD is divided up into a large number of small light-sensitive areas, also known as pixels. This can be used to build up an image of the scene of interest. When a photon of light falls within the area, it is defined by one of the pixels and converted into one or more electrons. The number of collected electrons is directly proportional to the intensity of the scene at each pixel. When the CCD is clocked out, the number of electrons in each pixel is measured, and the scene can be reconstructed. [37]

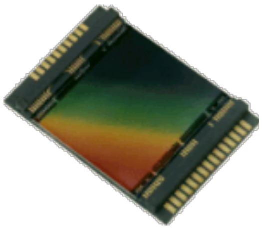

Figure 4.3: A typical CDD detector. [37]

4.1.2 Optical fiber cable and cosine corrector

An optical fiber cable is an assembly similar to an electrical cable. However, an optical fiber cable is used to carry light from one location to another or other. There exist different fibers, with different quality and functions. However, in this thesis work, a 25 meters patch cords fiber is used. [38] In Appendix A, the calibration certificate is presented.

A cosine corrector is an optical diffuser, which is connected to one fiber and a spectrometer to collect signal from a 180° point of view. A cosine corrector is specified for setups requiring the redistribution of incident light, like measuring spectral irradiance of a surface in air or other media. [39]

Figure 4.4: Cosine Corrector [39]

4.1.3 Noise

Noise during the measurements affect the measurement results. To prevent noise, different parameters are introduced under the calibration and data collection.

Noise equivalent irradiance (NEI) is defined as the standard deviation of the dark measurements times the instrument's response. NEI of a system is the level of flux density required to be equivalent to the noise present in the system. [40]

NEI depends on integration time, where NEI decreases with increasing integration time. To reduce the noise level of measurement, it is more efficient to increase the integration time as long as overexposure is avoided. As referred later in table 4.3, the integration time is set to 20 milliseconds under the data collection. However, under calibration of the spectrometer, the integration time needs to be set up to 2700 milliseconds. This is referred in table 4.1. [40] [41]

Further, by increasing the number of scans to average, the noise level is reduced proportionally to the square root of the number of repetitions. Scans to average are set to 100 scans under the data collection, while under the calibration of the spectrometer the scans to average are set to one. This is likewise presented in table 4.1 and 4.3. Furthermore, by cooling the detector, the NEI can be reduced. [40] [41]

Signal to noise ratio (SNR) is a measurement that compares the level of the desired signal to the level of background noise. [42]

A small number of Boxcar will increase the signal to noise ratio. Boxcar is a smoothing function and therefore it will also flatten the peaks in addition to increase the SNR. The Boxcar is set to zero under the data collection, while under the calibration, the Boxcar is set to 5.

4.1.4 Calibration of the spectrometer

Before the spectrometer can be used for spectral irradiance measurements, a calibration of the spectrometer needs to be done. This calibration is recommended to execute every 6 months to avoid noise in the spectral irradiance measurements collection.

The optic cable to the spectrometer is first connected to Deuterium-Halogen light sources for the UV-Vis-NI, the DH2000 Family, which is shown in figure 4.5. During treatment of the DH2000 Family, it is recommended to use safety glasses to avoid eye injury from the Deuterium-Halogen light. DH2000 Family specifications are found in appendix A.

Figure 4.5: DH2000 Family [43]

The deuterium lamp is turned on, and after 25 minutes the lamp is warmed up and ready to be used in the calibration. Using the software Ocean Optics, a new calibration can be created for "Absolute irradiance". The calibration details in the software are shown in table 4.1.

Table 4.1: Calibrations Details

	Deuterium Lamp	**Tungsten Halogen Lamp**
Warm Up Time	25 minutes	25 minutes
X-axis Ranges (Wavelength)	maximum 410 nm	minimum 350 nm
Intergration Time	2700 millsecond	2700 millsecond
Scans to Average	1	1
Boxcar Width (Smoothing function)	5	5
Fiber Diameter	3900 micron	3900 micron

With deuterium lamp, the wavelength range is set from 200 to 410 nm. When the calibration is finished with the deuterium lamp, the results can be controlled with a control file for the lamp that followed the instrument.

Next, the calibration can start with the tungsten halogen lamp. The halogen lamp also needs 25 minutes to warm up. Then the same procedure is followed, except now the wavelength range is set from 350 to 1100 nm. When the calibration is finished and controlled, the calibrations for the deuterium and halogen lamp are combined into one file to create a reference for the full wavelength range from 280 to 1100 nm. However, due to noise, in practice the useful wavelength range for the solar spectral irradiance measurements are from 300 to 900 nm.

4.2 Pyranometer

The pyranometer is an instrument that to measure the hemispherical solar radiation received by a plane surface, in W/m^2, from a 180° field of view. [44]

The pyranometer can be installed horizontally, tilted for a plane or array irradiance, positioned on a sun tracker with shadow-ring for diffuse measurements, or inverted for reflected radiation. In this thesis, the measurements from the pyranometer are used as control measurements with the measurements from the spectrometer and are installed in a 39° fixed tilted plane, just like the cosine corrector. [44]

Figure 4.6: Thermopile pyranometer [45]

The pyranometer has a thermopile detector, with strongly light-absorbing black paint that absorbs all wavelengths from the sun equally. A thermopile detector is a device that converts thermal energy into electrical energy. The detector creates a temperature difference between the body of the instrument and black surface of the sensors, which results in a small voltage that can be measured and translated into W/m^2. [44]

4.3 Location and experimental set-up

In this thesis, the measurements are taken at Grimstad in Southern Norway. The spectrometer is located at the University of Agder, at a rooftop dedicated for outdoor testing of PV modules. The location is shown on the map in figure 4.7 and experimental details are represented in table 4.2.

Figure 4.7: The location for this project is the University of Agder in Grimstad in Southern Norway, indicated by a red dot.

Table 4.2: Details of the experimental set-up.

Latitude	58.33°
Longitude	8.58°
Koeppen-Geiger climate classification	Cfb
Start wavelength	300 nm
End wavelength	900 nm
Start month	Feburary - 2018
End month	April - 2018
Tilt angle	39°

Figure 4.8a shows the view from the roof where the pyranometer and spectrometer optical sensor are set up. The sensors for recording irradiance and spectrum are shown in figure 4.8b, all wanted in place in the place of array of the PV modules at 39° tilt, facing directly south.

(a)

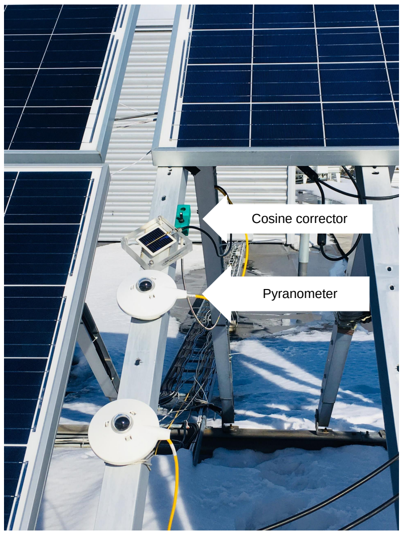

(b)

Figure 4.8: (a) View from the roof at UiA. (b) Spectrometer optical sensor with the pyronamteter and PV modules.

4.4 Data collection and filtration

When the spectrometer is calibrated, and the spectrometer cosine corrector is installed, the data collection is ready to start. The same software as for the calibration, Ocean Optics, used for the data collection. Now, the calibration file is used as the reference during the collection. The data collection details with the software are presented in table 4.3.

Table 4.3: Data collection details

Integration Time	20 millsecond
Scans to Average	100
Boxcar Width (Smooths)	0

At the beginning of the project work, the spectrometer was set up to take measurements automatically every 30 minutes. However, this was later changed to every 5 minutes to get more measurements during the day. After the data collection was complete, the dataset was filtrated, so only data between sunrise and sunset is included.

As mention in 1.1.2, only days with complete data are used in the results. The datasets are presented in table 4.4. Because the problem with the computer that the spectrometer was attached too, there is not data from the entire months, and there is also a variation on how many days with data set from each month. At the end of April and in May, the problem with the computer was solved. Nevertheless, to be able to filtrate latest the data in May, only data up to 19 May is included.

Table 4.4: Days with completed data set from each month.

Month	Days with completed measuments set	Total days	% of month
February	1 2 3 4 5 6 8 9 10 11 12	11 days	40%
March	8 9 10 11 12 14 15 16 17 18 20 22 23 27	14 days	45%
April	3 4 6 9 11 12 16 17 18 23 24 25 26 27 28 28 30	17 days	57%
May	2 3 4 5 6 7 8 9 10 11 12 13 14 15 16 17 18 19	18 days	60%

4.5 Atmospheric data

Data of atmospheric parameters close to the experimental set-up were in some cases difficult to achieve. Data on ozone and pressure from February to May for 2018 is not official before later this year. Therefore data from Oslo [46] form 2014 is used to as baseline in the sensitivity analyse. Moreover, data on PW was not found and therefore different PW values between minimum and maximum are used in the sensitivity analysis. Nevertheless, air mass for each day was found with the locations solar elevation. AOD data from April and May is measured at Norwegian Insitute for Air Research at Birkenes, which is the closest observertay of AOD to the experimental set-up. This is shown in figure 4.9. In the sensitivity analysis, AOD values between minimum and maximum is used.

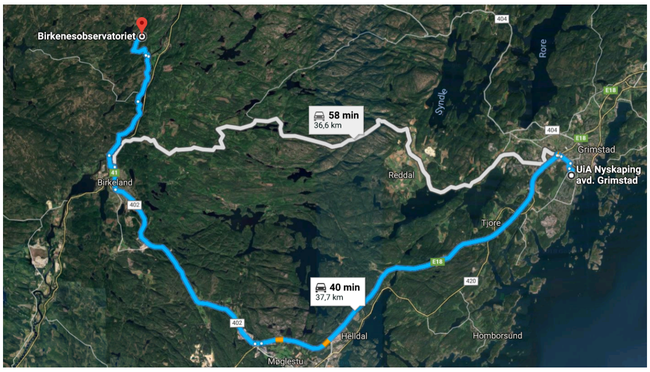

Figure 4.9: Distance between UiA and Birkenes observatory.

4.6 SMARTS

Simple Model for the Atmospheric Radiative Transfer of Sunshine version (SMARTS) is used to model spectral irradiance for calculating the spectral mismatch correction and is developed by Gueymard. The SMARTS model provides direct normal, global and diffuse horizontal and global tilted spectral irradiances for clear skies and 2002 wavelengths from 280 to 4000 nm. [47] SMARTS can be run through an Excel interface, and the model is configured through setup input cards, shown in figure 4.10.

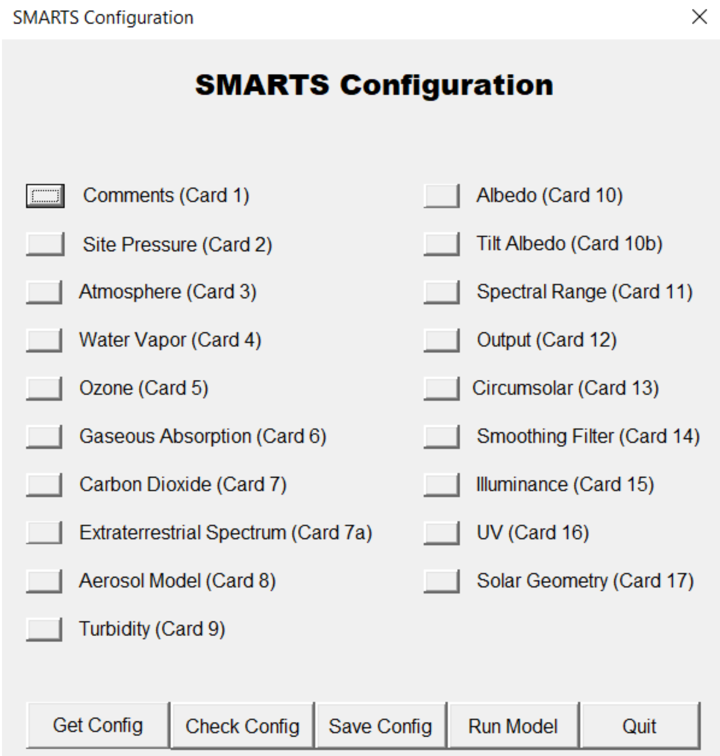

Figure 4.10: Simple Model of Atmospheric Radiative Transfer of Sunshine configuration.

In this thesis, SMARTS is used in a sensitivity analysis, where different atmospheric parameter is changed to see how the spectrum changes. Further, SMARTS is used to make a matching model for the full spectrum of one representative average spectrum for each month. The specification to SMARTS models for each month is presented in appendix B.

4.7 PV details

To find the short-circuit current density for PV technologies based on the average spectral irradiance for each month, equation 4 is used with the normalized SR values from Dirnberger et al. [35]. A plot of the normalized SR values from Dirnberger et al. is presented earlier in the section 3.2 in the literature review.

The normalized SR curves are multiplied with absolute SR values to find the absolute short-circuit current density. The absolute values are references from the PV Performance modeling collaborative and is shown in table 4.5. [48]

Table 4.5: Absolute SR vaules for the PV technologies.

PV technologies	Absolute SR
a-Si	0.35 A/W
CdTe	0.45 A/W
CIGS	0.65 A/W
c-Si	0.60 A/W

However, for the best performing PV technology, the power output should be compared. The maximum power P_{mp} is the product of fill factor FF, short-circuit current J_{sc}, and open circuit voltage V_{oc}. By assuming that all devices based on standard AM1.5 illumination at 1000 W/m^2, the ideal record efficiency solar cell parameters from figure 2.9 can find the P_{mp} with equation 5. The useful parameters from the figure are shown in table 4.6.

Table 4.6: Ideal «record efficiency solar cell» parameters for four PV technologies.

PV technologies	$\mathbf{V}_{oc}$	**FF**
a-Si	0.90 V	0.70
CdTe	0.89 V	0.79
CIGS	0.74 V	0.81
c-Si	0.74 V	0.85

4.8 Matlab

The spectrometer data are imported and analysed with the software package MATLAB R2017. Data for each day is used in large-scale calculations, which MATLAB executes efficiently.

The first MATLAB script (m-script) is designed to read every filtered dataset of irradiance for each day with a unit conversion from μW/cm^2/nm to W/m^2/nm, and then make an average spectrum which is saved as a text file and imported in the next m-script.

By using the data from the first m-script and atmospheric data, the next m-scripts is designed to produce following results for each month:

- Plot of mean spectral irradiance for each day in one month.
- An mean plot of spectral irradiance for each month.
- Irradiance (W/m^2) from the average plots, integrated into bands of 50 nm from 300 to 900 nm and together with its spectral irradiance fraction.
- Histogram of APE results (eV).
- Air Mass vs APE
- AOD vs APE
- Plot of spectral irradiance destribution for each day in one month around solar noon. (Solar noon is the definition when the Sun passes the location's meridian and reaches its highest position in the sky.)
- An average plot of spectral irradiance for each month at solar noon.
- Sensitivity analysis of Air Mass, AOD at 500 nm, Specific Precipitable Water, Ozone, and Pressure.
- Theoretical model vs experimental results for each month.

- The theoretical model from 0 to 3000 nm.
- The average irradiance from the pyranometer. The average is at the same period as the average of the measured spectrum, which is used to make the SMARTS spectrum.
- Short-circuit current density of PV technologies during the months.

The m-scrips for all calculations from Matlab is available in Appendix C.

5 Results

In this section, the results of this thesis are presented. The section is divided into four subsections; experimental results, sensitivity analysis, theoretical models of the experimental results, and PV results.

5.1 Experimental results

In this section, the spectral irradiance measurements for each month, both the average distribution for each day and an average of these days, is presented. In addition, the irradiance from the average spectral irradiance distribution within defined wavelength ranges is presented.

Furthermore, the APE results from measured days for each month is presented. This is illustrated in histograms and compared with air mass and AOD.

At the end of this section, the same procedure with results of the spectral irradiance measurements is investigated. Here, for solar noon conditions now only the results within two hours around solar noon are included.

5.1.1 Spectral irradiance measurements

Spectral irradiance measurements and irradiance results have been performed for February, March, April, and May in 2018.

Figure 5.1a shows the mean of the spectral irradiance measurements for each measured day in February, while figure 5.1b shows the average of these days. The shapes in figure 5.1a and 5.1b illustrate almost horizontal peaks with a small absorption trough around 600 nm. This is also the case with the highest spectral irradiance peak, also represented as "clear days," in figure 5.1a, which have a peak around 0.6 W/m^2/nm. The mean peak in 5.1b only has a peak around 0.3 W/m^2/nm.

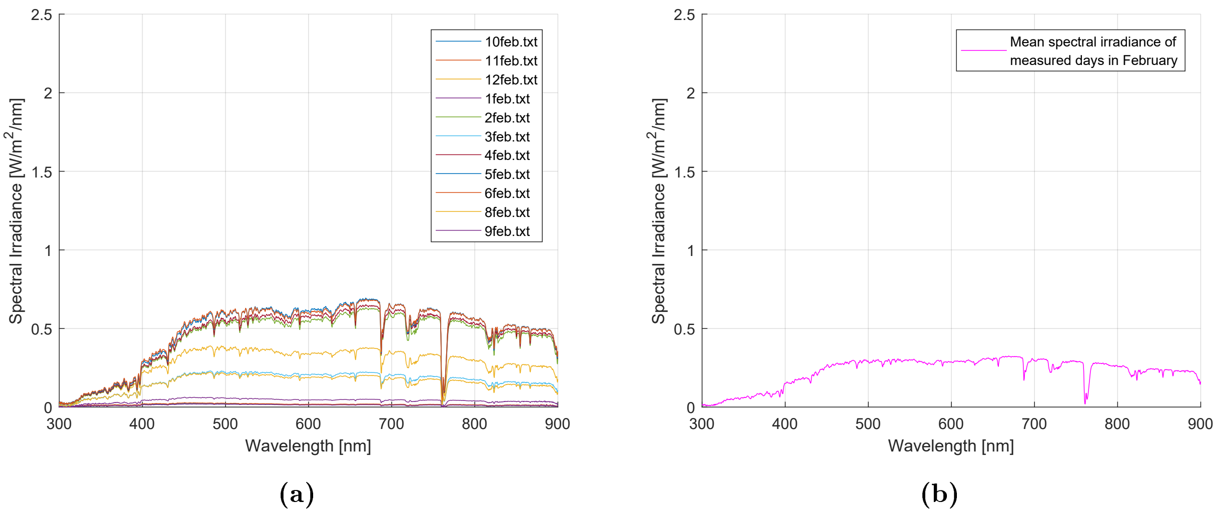

Figure 5.1: (a) Spectral irradiance measurements for each day with data in February. (b) Mean spectral irradiance for the measured days in February.

Table 5.1 shows the results of the irradiance from the mean spectrum in figure 5.1b integrated across spectral bands of 50 nm, from 300 nm to 900 nm. This demonstrates the distribution of the irradiance in the spectrum. In addition, the total irradiance from 300 nm to 900 nm is calculated, to determine the fraction of spectral irradiance within each 50 nm band. As demonstrated in table 5.1, the total irradiance between 300-900 nm is only 127 W/m^2 for the average spectrum in February.

Table 5.1: Mean irradiance from the integrated spectrum from measured days in February

Wavelength range $\Delta\lambda$ [nm]	Irradiance within $\Delta\lambda$ [W/m^2]	Spectral irradiance fraction [%]
300-350	1.56	1.26
350-400	3.80	2.98
400-450	8.90	7.0
450-500	13.07	10.26
500-550	13.55	10.64
550-600	13.41	10.52
600-650	13.53	10.62
650-700	14.10	11.04
700-750	12.95	10.16
750-800	11.39	8.94
800-850	10.77	8.46
850-900	10.37	8.14
300-900	**127.4**	**100**

Figure 5.2a shows the mean of the spectral irradiance measurements for each measured day in March, while figure 5.2b shows the average of these days.

Compared with the shape in figure 5.1a and 5.1b from the month before, the shapes are now in figure 5.2a and 5.2b more peaked and correspond better with the shape of an STC spectrum like figure 2.10. However, there is still a small absorption trough around 600 nm. This is most illustrated from the days with low spectral irradiance, but it also occurs on the day with the highest spectral irradiance in figure 5.2a, which has a peak value above 1 W/m^2/nm. The absorption trough is also illustrated in the monthly average spectral irradiance in figure 5.2b, where the peak is around 0.5 W/m^2/nm.

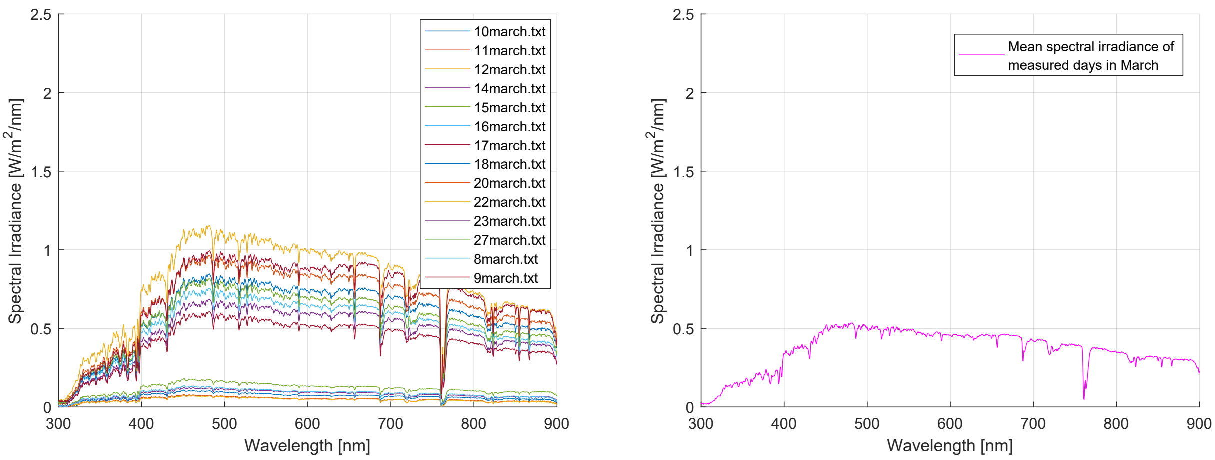

(a) (b)

Figure 5.2: (a) Spectral irradiance measurements for each day with data in March. (b) Mean spectral irradiance for the measured days in March

Table 5.2 shows the results of the irradiance from the mean spectrum irradiance in figure 5.2b integrated into bands of 50 nm, from 300 nm to 900 nm, to demonstrate the irradiance distribution. Moreover, the total irradiance from 300 nm to 900 nm is calculated, to determine the fraction of spectral irradiance within each 50 nm band. As demonstrated in table 5.2, the total irradiance between 300-900 nm has increased from the previous month to 219 W/m^2 for the average spectrum in March.

Table 5.2: Mean irradiance from the integrated spectrum from measured days in March.

Wavelength range Δλ [nm]	Irradiance within Δλ [W/m^2]	Spectral irradiance fraction [%]
300-350	4.40	2.01
350-400	9.76	4.46
400-450	19.68	8.99
450-500	25.59	11.69
500-550	24.52	11.20
550-600	23.54	10.75
600-650	22.43	10.24
650-700	21.90	10.0
700-750	19.67	8.98
750-800	16.87	7.70
800-850	15.80	7.21
850-900	14.83	6.77
300-900	**218.98**	**100**

Figure 5.3a shows the spectral irradiance measurements for each measured day in April, while figure 5.3b shows the average of these days.

In figure 5.3a and 5.3b, the trend from previous month is maintained. The absorption trough around 600 nm almost vanishes in the April results. The peak spectral irradiance in figure 5.3a is above 1 W/m^2/nm. In figure 5.3b, the average spectral irradiance has a peak value above 0.5 W/m^2/nm.

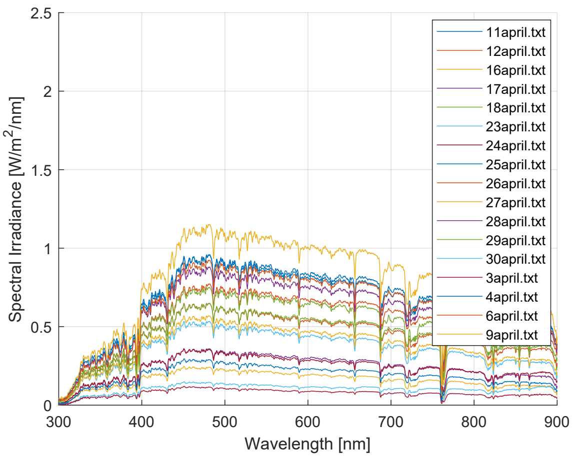

(a)

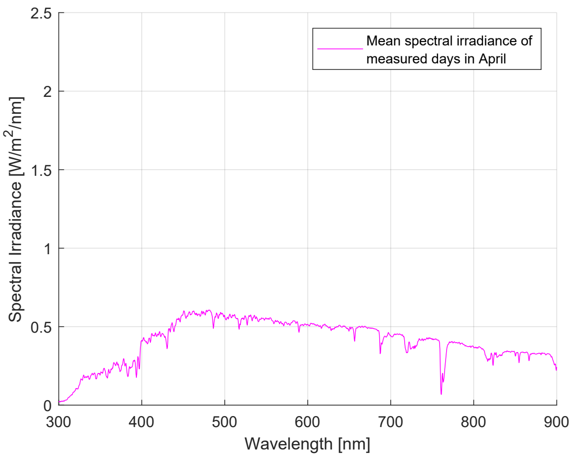

(b)

Figure 5.3: (a) Spectral irradiance measurements for each day with data in April. (b) Mean spectral irradiance for the measured days in April

Table 5.3 shows the results of the irradiance from the mean spectrum irradiance in figure 5.3b integrated into bands of 50 nm, from 300 nm to 900 nm. The total irradiance from 300 nm to 900 nm is calculated, to determine the fraction of spectral irradiance within each 50 nm band. As demonstrated in table 5.3, the total irradiance between 300-900 nm has increased from the previous month to 244 W/m^2 for the average spectrum in April.

Table 5.3: Mean irradiance from the integrated spectrum from measured days in April.

Wavelength range $\Delta\lambda$ [nm]	**Irradiance within $\Delta\lambda$ [W/m^2]**	**Spectral irradiance fraction [%]**
300-350	6.02	2.47
350-400	12.13	4.97
400-450	23.12	9.47
450-500	29.02	11.89
500-550	27.5	11.27
550-600	26.47	10.84
600-650	24.91	10.20
650-700	23.61	9.67
700-750	20.58	8.43
750-800	18.14	7.43
800-850	16.54	6.78
850-900	16.02	6.57
300-900	**244.06**	**100**

Figure 5.4a shows the mean of the spectral irradiance measurements for each measured day in May, while figure 5.4b shows the average of these days.

In figure 5.4a and 5.4b, the trend from previous two month is still maintained. In May, nearly all of the spectrum have similar spectral irradiance values, which is shown in figure 5.4a. In figure 5.4b, the monthly average spectral irradiance has a peak value around 0.75 W/m^2/nm.

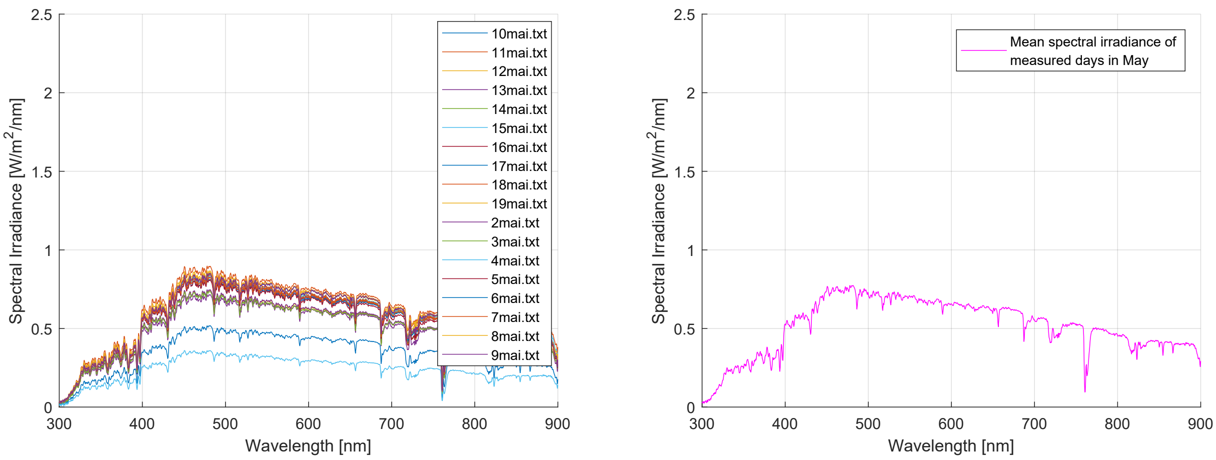

(a) **(b)**

Figure 5.4: (a) Spectral irradiance measurements for each day with data in May. (b) Mean spectral irradiance for the measured days in May.

Table 5.4 shows the results of the irradiance from the mean spectrum irradiance in figure 5.4b integrated into bands of 50 nm from 300 nm to 900 nm. The table shows that the spectrum in figure 5.4b is stronger peak than the spectrum in April. As demonstrated in table 5.4, the total irradiance between 300-900 nm has increased from the previous month to 309 W/m^2 for the average spectrum in May.

Table 5.4: Mean irradiance from the integrated spectrum from measured days in May

Wavelength range $\Delta\lambda$ [nm]	Irradiance within $\Delta\lambda$ [W/m^2]	Spectral irradiance fraction [%]
300-350	7.89	2.55
350-400	15.60	5.05
400-450	29.60	9.59
450-500	37.05	12.0
500-550	35.05	11.35
550-600	33.82	10.96
600-650	31.72	10.27
650-700	29.77	9.64
700-750	25.61	8.29
750-800	22.67	7.34
800-850	20.34	6.59
850-900	19.60	6.35
300-900	**308.72**	**100**

In table 5.5 an investigation on the mean spectral irradiance for each month has been done to decide if they can be classified as a red rich or blue rich spectrum. The irradiance between 450 to 500 nm and 600 to 650 nm is used to find the slope between the two wavelength ranges for each month. A spectrum that is more blue rich will have a negative slope and vice versa. For the table 5.5, the mean spectral irradiance from March, April, and May is a blue rich spectrum, while February is classified as red rich.

Table 5.5: Determine blue or red rich with slope from mean irradiance spctrum.

	February	**March**	**April**	**May**
450-500 nm	13.07	25.59	29.02	37.05
600-650 nm	13.53	22.43	24.91	31.72
slope	0.46	-3.16	-4.11	-5.33
red/blue rich	**red rich**	**blue rich**	**blue rich**	**blue rich**

5.1.2 APE

Figures 5.5-5.8 present histograms of APE values for each month. The APE results for March are higher than the APE results for February. Likewise for April and May, where April and May have higher APE values than March and February. Most of the APE values are between 1.95-2.01 eV in February, while in March most of the APE values are between 2.01-2.05 eV. All the measured days in April are between 2.03-2.07 eV, and in May all the APE results are between 2.05-2.07 eV.

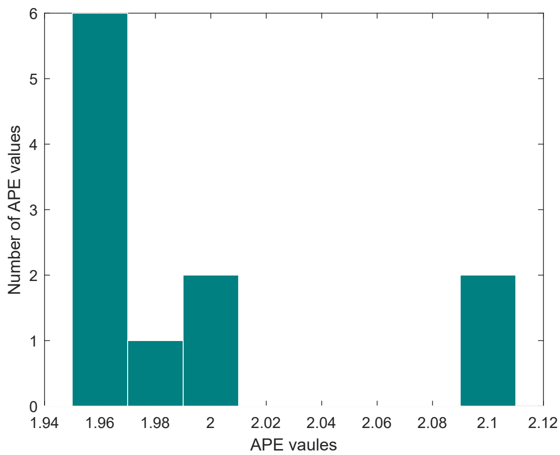

Figure 5.5: APE values for Feburary

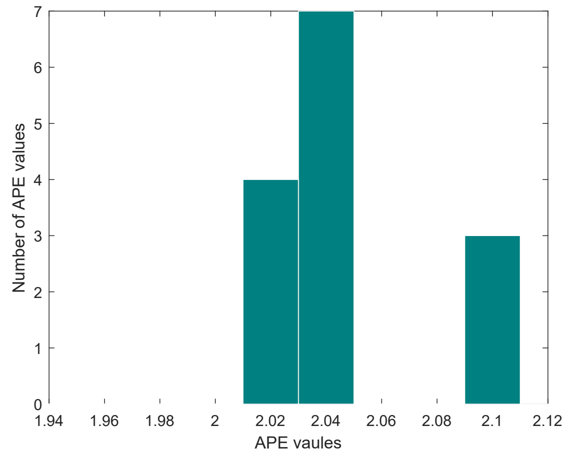

Figure 5.6: APE values for March

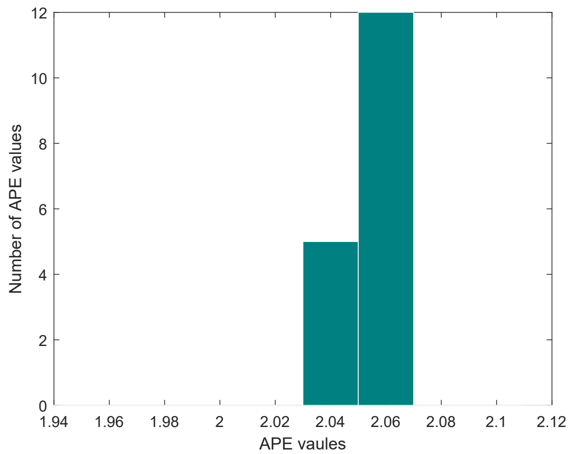

Figure 5.7: APE values for April

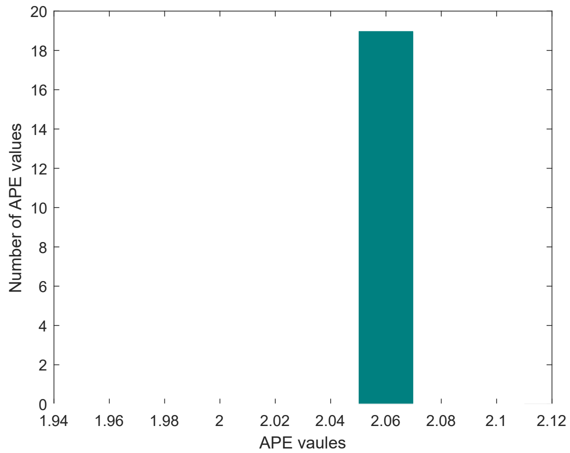

Figure 5.8: APE values for May

In addition to the APE values from each month, the APE values are found for the STC spectrum with the wavelength range 300 to 900 nm.

Table 5.6: APE value from the standard AM1.5 spectrum with the wavelength range 300-900 nm.

STC spectrum [300-900 nm]	APE [eV]
AM0 Extraterrestrial irradiance	2.11 eV
AM1.5 Global irradiance at 37° tilt	2.03 eV
AM1.5 Direct normal irradiance	1.99 eV

5.1.3 Atmospheric parameters

In this section, the APE results are compared with the atmospheric parameters AM and AOD, to see if there is any connection between the results.

Figure 5.9 plots the air mass (at solar noon) versus APE results for each month. The figure shows that in February, with higher air mass around AM3.5, most of the APE results between 1.94 - 2.01 are located. In March, the air mass is around AM2 and have APE results from 2.02 to 2.10. During April, the air mass is around AM1.5, and the APE results vary between 2.03 to 2.07. In May, the air mass is down to AM1.3, where APE values vary between 2.05 to 2.07 eV.

In addition, the correlation coefficient (R) is calculated. February and March have a correlation coefficient at 0.76 and 0.74, while March and May gets a correlation coefficient at -0.39 and 0.41. The correlation coefficient for all four months is -0.67.

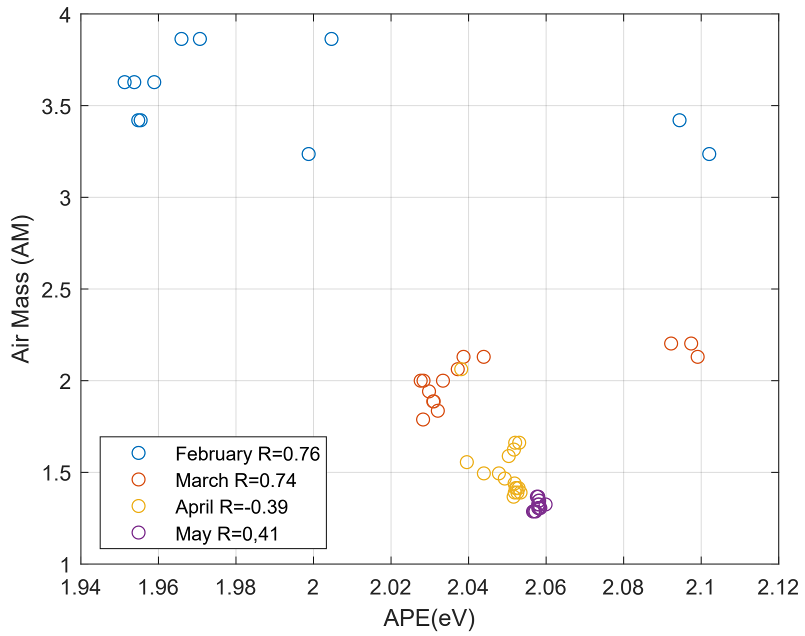

Figure 5.9: Air Mass vs APE

Figure 5.10 and 5.11 plot the Aerosol Optical Depth (AOD) versus APE for April and May. AOD from February and March was not measured because of calibration of the instrument. AOD is measured at different wavelength, which is shown in the figures. Because of the small variation in the APE results in April and May, the x-axis is scaled up to see the differences. The AOD measured at different wavelengths has a small variation, but no apparent trend visible in April and May.

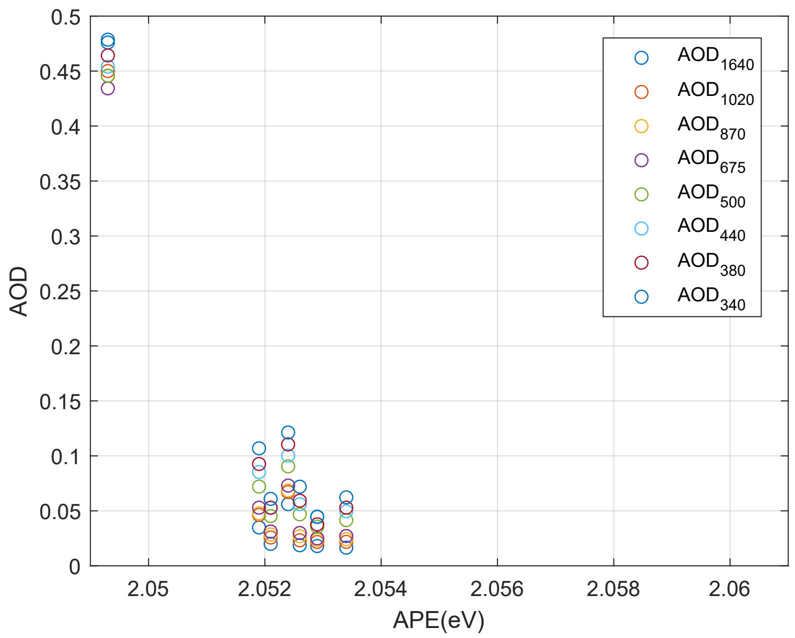

Figure 5.10: AOD vs APE in April.

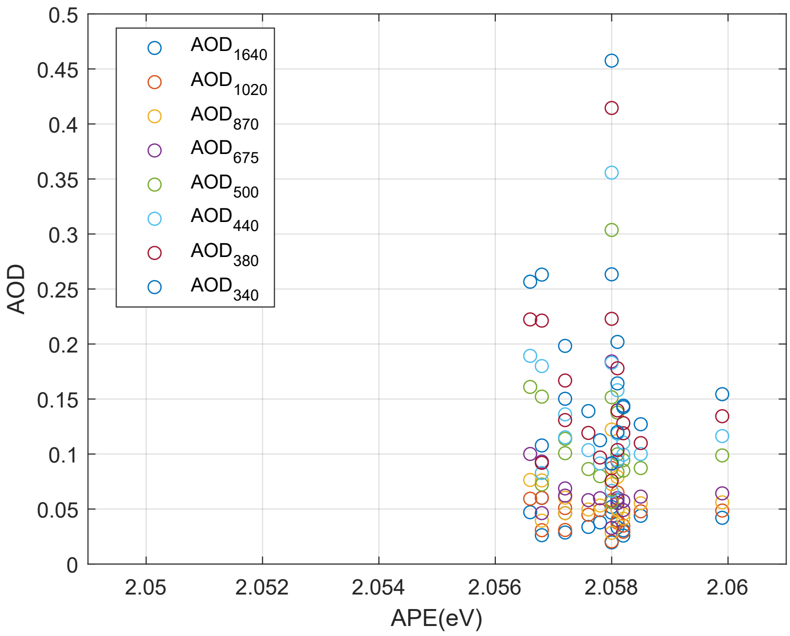

Figure 5.11: AOD vs APE in May.

5.1.4 Spectral irradiance measurements around solar noon

This section presents the spectral irradiance measurements and irradiance results for February, March, April, and May around solar noon in Grimstad. Therefore, only data during the two hours at solar noon is used in the plot and to calculate the results. This method is used to look at days with an equal period. In addition, this is when the spectral irradiance is at its highest intensity.

Figure 5.12a shows the spectral irradiance measurements at solar noon for each measured day in February, while figure 5.12b shows the average of these days. The shapes in figure 5.12a and 5.12b illustrates almost horizontal peaks with a small absorption trough around 600 nm. This is also the case with the highest spectral irradiance curved, also represented as "clear days," in figure 5.12a, where the peak value is around 1 W/m^2/nm. The mean peak in 5.1b has the peak to around 0.5 W/m^2/nm.

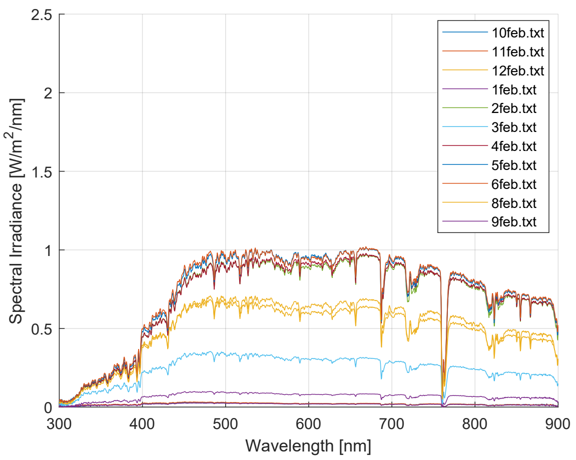

(a)

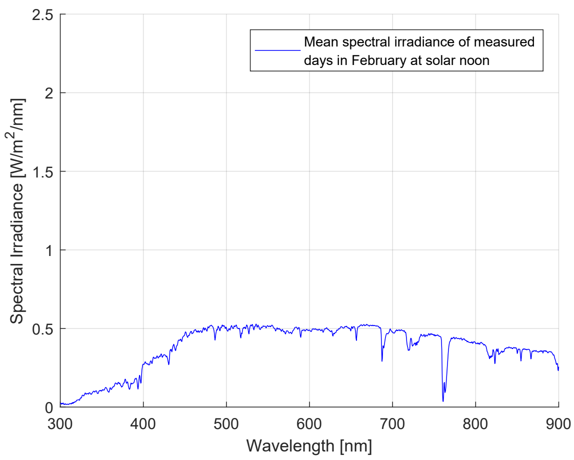

(b)

Figure 5.12: (a) Spectral irradiance measurements for each day with data in February around solar noon. (b) Mean spectral irradiance measurements for the days in February around solar noon.

Table 5.7 shows the results of the irradiance from the mean spectrum irradiance in figure 5.12b integrated into bands of 50 nm from 300 nm to 900 nm. This demonstrates the distribution of the irradiance in the spectrum at solar noon. In addition, the total irradiance from 300 nm to 900 nm is calculated, and the percent of the total irradiance is integrated to the irradiance of each band. As demonstrated in table 5.7, the total irradiance when the sun is at the highest position between 300-900 nm is only 228.14 W/m^2, but higher than the results for February in table 5.1.

Table 5.7: Mean irradiance from spectrum in February at solar noon.

Wavelength range $\Delta\lambda$ [nm]	Irradiance within $\Delta\lambda$ [W/m^2]	Spectral irradiance fraction [%]
300-350	2.95	1.29
350-400	7.23	3.17
400-450	16.96	7.43
450-500	24.51	10.75
500-550	25.10	11.00
550-600	24.79	10.87
600-650	24.46	10.72
650-700	24.69	10.82
700-750	22.38	9.81
750-800	19.43	8.52
800-850	18.27	8.01
850-900	17.36	7.61
300-900	**228.14**	**100**

Figure 5.13a Mean spectral irradiance measurements around solar noon for each measured day in March, while figure 5.13b shows the average of the month.

Compared with the shape in figure 5.12a and 5.12b from the month before, the shapes are now in figure 5.13a and 5.13b more peaked and correspond the shape to a STC spectrum like figure 2.10. However, there is still a small absorption trough around 600 nm. This is most illustrated from the days with low spectral irradiance, but it also occurs on the day with the highest spectral irradiance in figure 5.13a, which has a higher peak than 1.5 $W/m^2/nm$. The absorption trough is also illustrated in monthly average spectral irradiance in figure 5.13b, where the highest peak is around 0.9 $W/m^2/nm$.

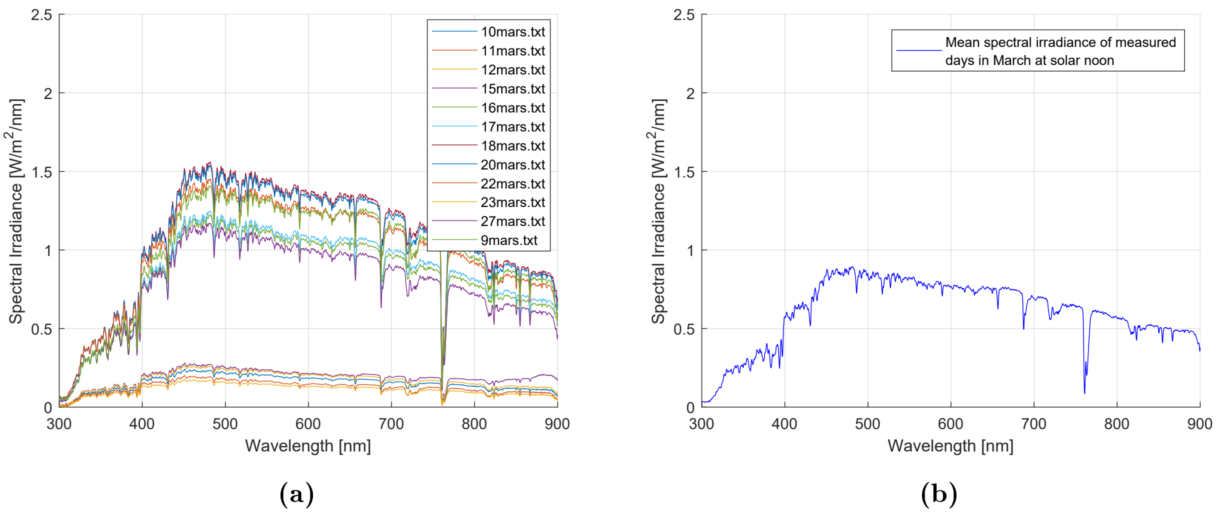

Figure 5.13: (a) Spectral irradiance measurements for each day with data in March aorund solar noon. (b) Mean spectral irradiance measurements for the days in March around solar noon.

Table 5.8 shows the results of the irradiance from the mean spectrum irradiance in figure 5.13b integrated into bands of 50 nm from 300 nm to 900 nm to demonstrate the irradiance distribution at solar noon. Moreover, the total irradiance from 300 nm to 900 nm is calculated, and the percent of the total irradiance is divided to the irradiance of each band. As demonstrated in table 5.8, the total irradiance between 300-900 nm has increased from results in previous table 5.7 to 363.39 W/m^2.

Table 5.8: Mean irradiance from spectrum in March around solar noon

Wavelength range $\Delta\lambda$ [nm]	Irradiance within $\Delta\lambda$ [W/m^2]	Spectral irradiance fraction [%]
300-350	7.61	2.10
350-400	16.52	4.55
400-450	33.09	9.11
450-500	42.75	11.76
500-550	40.89	11.25
550-600	39.49	10.87
600-650	37.42	10.3
650-700	36.05	9.92
700-750	32.304	8.89
750-800	27.57	7.59
800-850	25.73	7.08
850-900	23.95	6.59
300-900	**363.39**	**100**

Figure 5.14a shows the spectral irradiance measurements at solar noon for each measured day in April, while figure 5.14b shows the average of these days.

In figure 5.14a and 5.14b, the trend from previous month is maintained, where the shape are peaked in figure 5.13a and 5.13b, and correspond the shape to a STC spectrum like figure 2.10. The absorption trough around 600 nm that occurs in the results from previous months vanishes in the April results. The highest spectral irradiance in figure 5.14a has a peak above than 1.5 W/m^2/nm. In figure 5.14b, the monthly average spectral irradiance peak is around 1 W/m^2/nm.

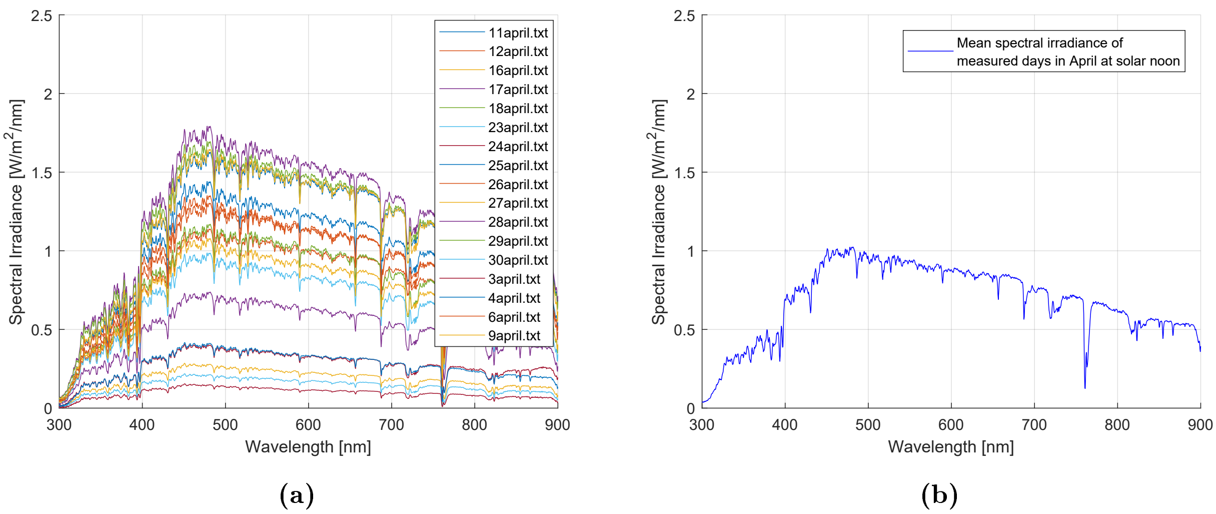

Figure 5.14: (a) Spectral irradiance measurements around solar noon for each day with data in April. (b) Mean spectral irradiance around solar noon for the days in April.

Table 5.9 shows the results of the irradiance from the mean spectrum irradiance at solar noon, in figure 5.14b, integrated into bands of 50 nm from 300 nm to 900 nm. Besides, the total irradiance from 300 nm to 900 nm is calculated, and the percent of the total irradiance is divided to the irradiance of each band. As demonstrated in table 5.9, the total irradiance between 300-900 nm has increased from the previous month to 411.35 W/m^2.

Table 5.9: Mean irradiance from spectrum in April around solar noon.

Wavelength range $\Delta\lambda$ [nm]	Irradiance within $\Delta\lambda$ [W/m^2]	Spectral irradiance fraction [%]
300-350	10.31	2.51
350-400	20.39	4.96
400-450	38.95	9.47
450-500	48.98	11.91
500-550	46.48	11.30
550-600	45.09	10.96
600-650	42.45	10.32
650-700	39.94	9.71
700-750	34.70	8.44
750-800	30.41	7.39
800-850	27.53	6.69
850-900	26.12	6.35
300-900	**411.35**	**100**

Figure 5.15a shows the spectral irradiance measurements around solar noon for each measured day in May around solar noon, while figure 5.15b shows the average of these days.

In figure 5.15a and 5.15b, the trend from previous two months still maintains, where the shapes correspond to the shape of an STC spectrum like figure 2.10. The highest spectral irradiance in figure 5.15a has a peak above 1.5 W/m^2/nm. In figure 5.15b, the monthly average spectral irradiance peaks is around 1.5 W/m^2/nm. This is closed to the global AM 1.5 spectrum, where the peak is around 1.6 W/m^2/nm

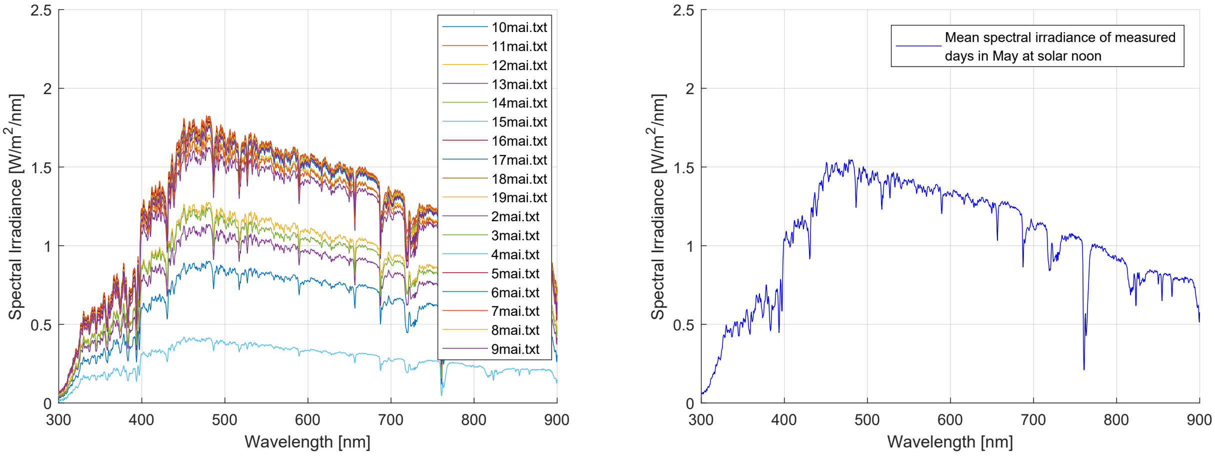

(a) (b)

Figure 5.15: (a) Spectral irradiance measurements around solar noon for each day in May. (b) Mean spectral irradiance measurements around solar noon for the days in May.

Table 5.10 shows the results of the irradiance from the mean spectrum irradiance in figure 5.15b integrated into bands of 50 nm from 300 nm to 900 nm. As demonstrated in table 5.10, the total irradiance between 300-900 nm has increased from the previous month to 618.9 W/m^2.

Table 5.10: Mean irradiance from spectrum in May at solar noon.

Wavelength range $\Delta\lambda$ [nm]	**Irradiance within $\Delta\lambda$ [W/m^2]**	**Spectral irradiance fraction [%]**
300-350	15.82	2.56
350-400	30.71	4.96
400-450	58.76	9.50
450-500	73.88	11.94
500-550	70.13	11.33
550-600	68.40	11.05
600-650	64.34	10.40
650-700	60.13	9.72
700-750	51.79	8.37
750-800	45.61	7.37
800-850	40.75	6.58
850-900	38.58	6.23
300-900	**618.9**	**100**

5.2 Sensitivity analysis

In this section, a sensitivity analysis executed with SMARTS is presented. Different atmospheric parameters are investigated to investigate how they influence the spectra.

In figure 5.16, spectra with different air masses are presented. Air mass values are chosen after the results in figure 5.9. The lowest air mass, AM1.5, gives the spectrum that corresponds to the STC spectrum. The shape changes in the spectrum with AM2, AM3.5, and AM4, where the higher the air mass is, the more the shape and peak value changes.

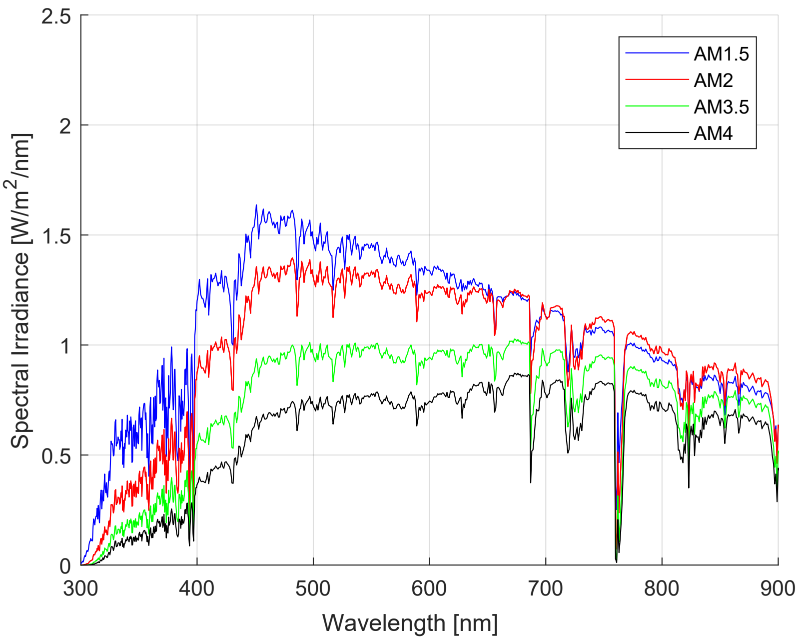

Figure 5.16: Spectral irradiance distribution with different Air Mass.

Spectral irradiance distribution with different AOD at 500 nm is presented in figure 5.17. An AOD that is 0,01 gives the highest spectral irradiance values, while an AOD that is 2 gives the lowest irradiance. AOD in the range $1 - 1,5$ give the same spectrum.

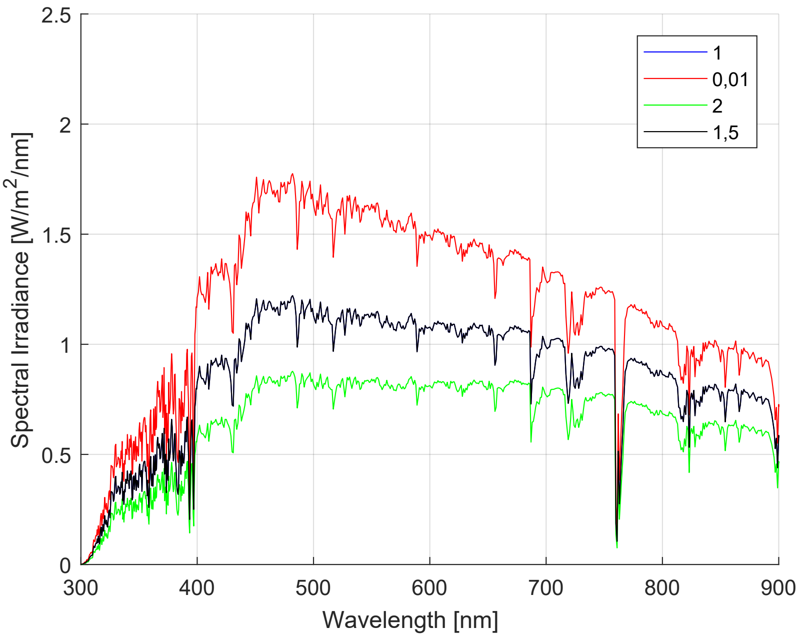

Figure 5.17: Spectral irradiance distribution with different AOD at 500 nm. AOD1 and AOD1.5 curves are overlapping

In figure 5.18, spectral irradiance distributions with different specific precipitable water variables is plotted. From 300 nm to 500 nm the spectra are, whereas the same. Between 700 nm and 800 nm difference is seen with increasing absorption for higher PW values.

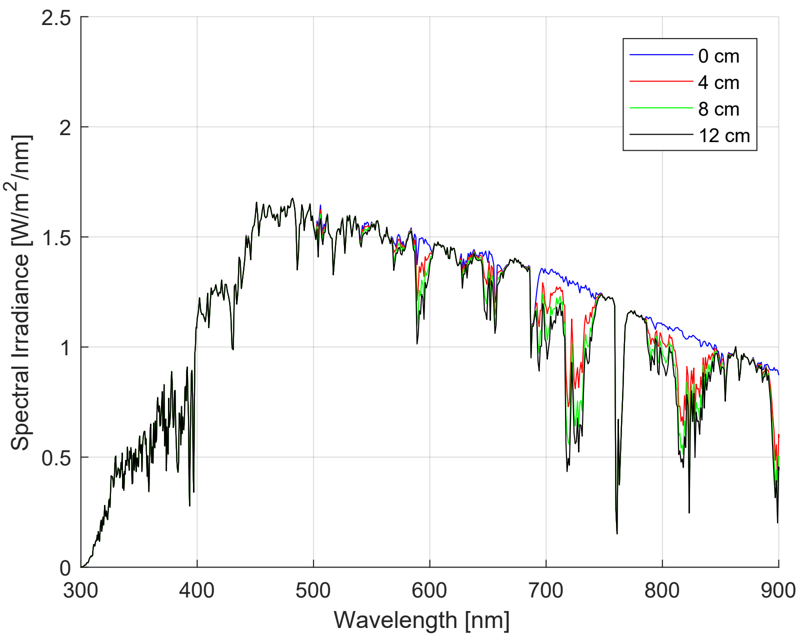

Figure 5.18: Spectral irradiance distribution with different specific precipitable water values.

In figure 5.19 and 5.20, spectral irradiance distributions with different ozone and air pressure is investigated. The values are chosen after data from earlier year from Birkenes. Figure 5.19 demonstrates that ozone affects the spectrum from 500 to 600 nm. The different ozone values from Brikenes, gives the same spectrum. Figure 5.20 does not show any visual changes with different pressure.

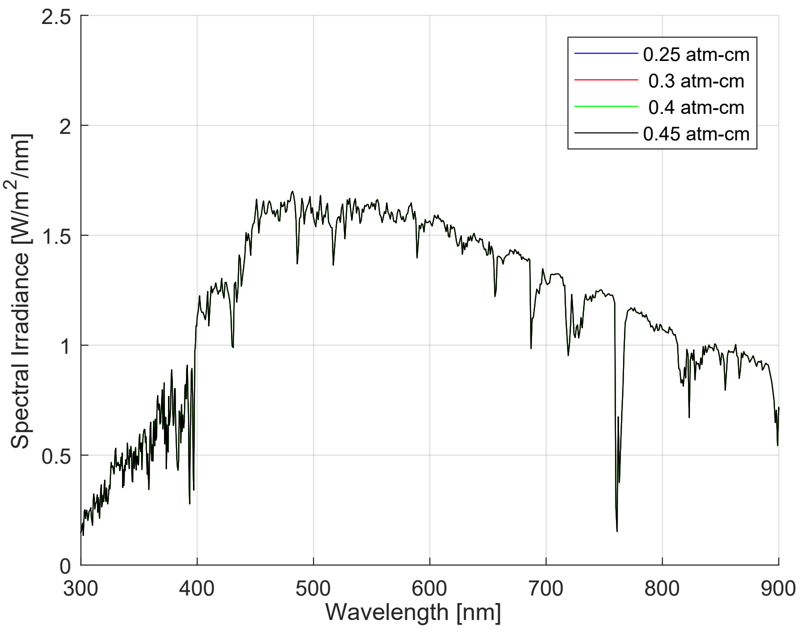

Figure 5.19: Spectral irradiance distribution with different ozone values.

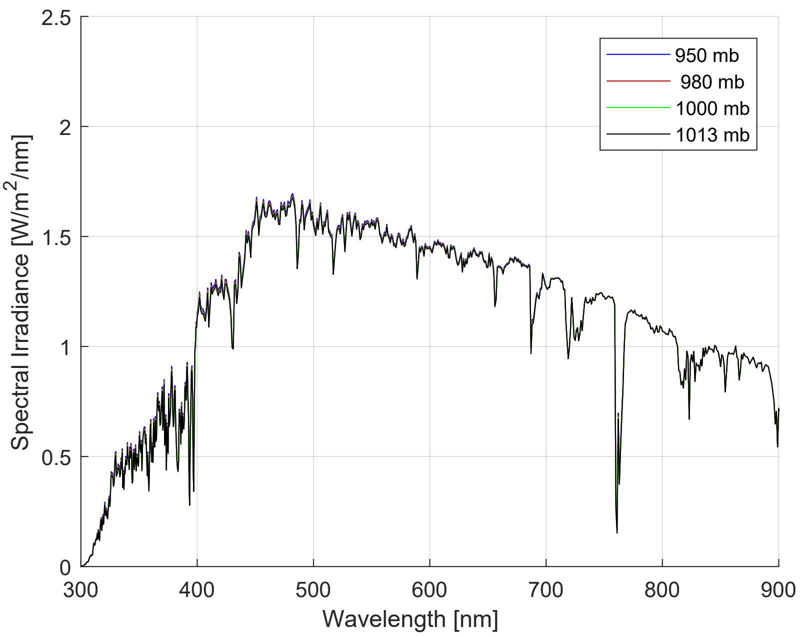

Figure 5.20: Spectral irradiance distribution with different air pressure values.

5.3 Theoretical models of the experimental results

In this section, a theoretical model is created to match one spectrum from each month. This is to create a full-range spectrum, extended beyond the measured interval 300- 900 nm, to be used for the PV analysis. The first two figures show the results from February, where figure 5.21 illustrates the SMARTS model and the reference "clear" day from February, while figure 5.22 presents the spectrum from SMARTS with the wavelength from 0 to 3000 nm. Air mass and AOD were the main parameters that were changed to match with the measured spectrum. The parameters used for the SMARTS model are shown in Appendix B.

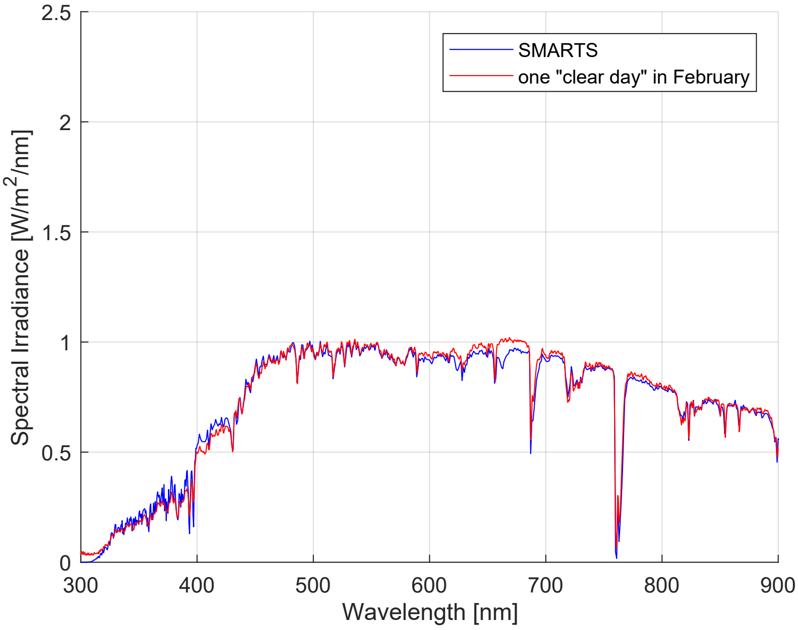

Figure 5.21: Spectral irradiance distribution from a clear day February.

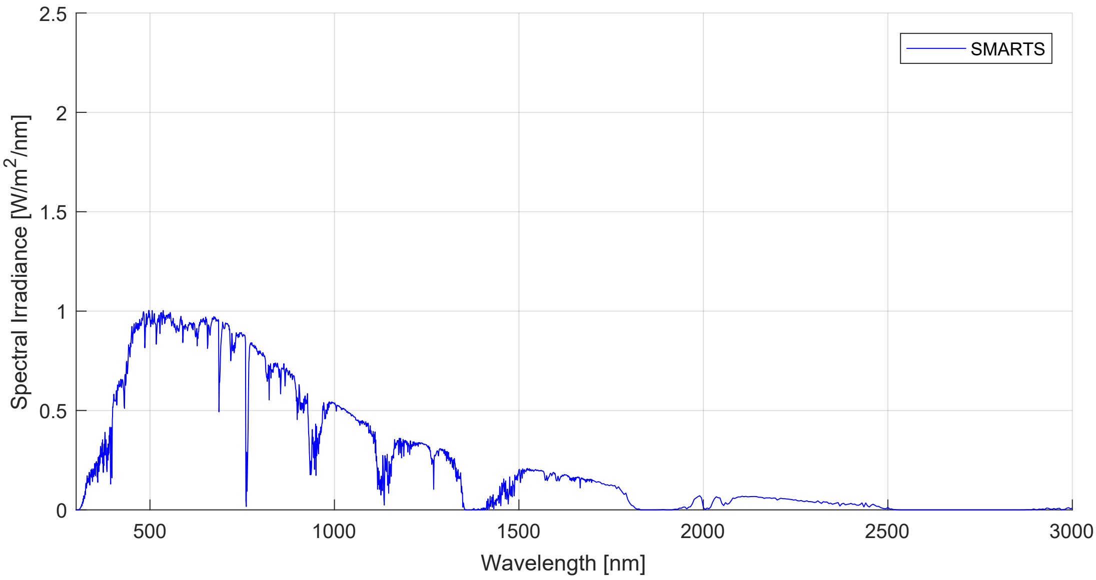

Figure 5.22: Spectral irradiance distribution made in SMARTS that match with a clear day in Feburary.

Figure 5.23 shows the SMARTS model and the reference "clear" day from March. The model is almost identical, except in the area between 600 nm and 700 nm, which was the most difficult to get identical. Air mass and AOD were the main parameters that were changed to match with the measured spectrum. This was also the problem with the model in February. Figure 5.24 demonstrates the spectrum from SMARTS with the wavelength from 0 to 3000 nm.

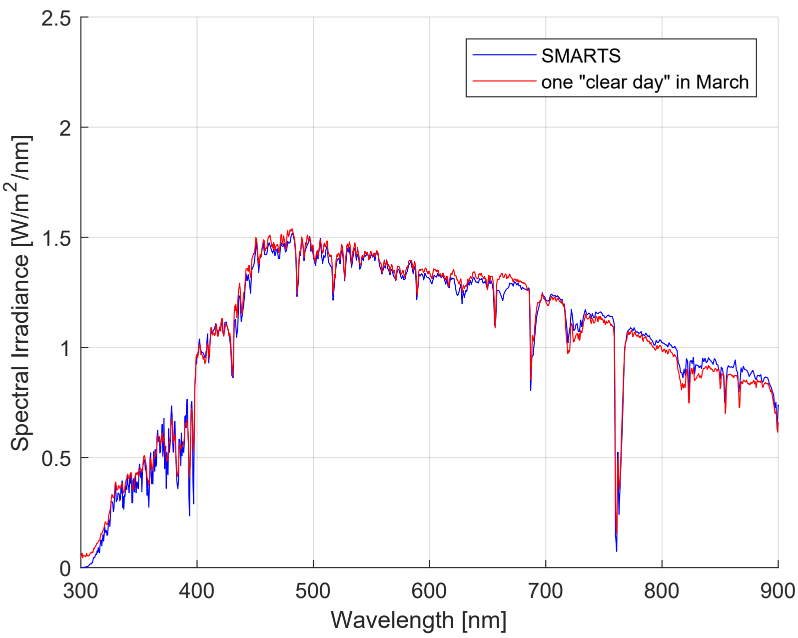

Figure 5.23: Spectral irradiance distribution from March.

Figure 5.24: Spectral irradiance distribution made in SMARTS that match with a clear day in March.

Figure 5.25 presents the SMARTS model and the reference "clear" day from April. Here, the difference between the model and reference measurements occurs mainly in the area between 600 nm and 800 nm. Figure 5.26 demonstrates the spectrum from SMARTS with the wavelength from 0 to 3000 nm. The parameter used for the SMARTS model is shown in Appendix B.

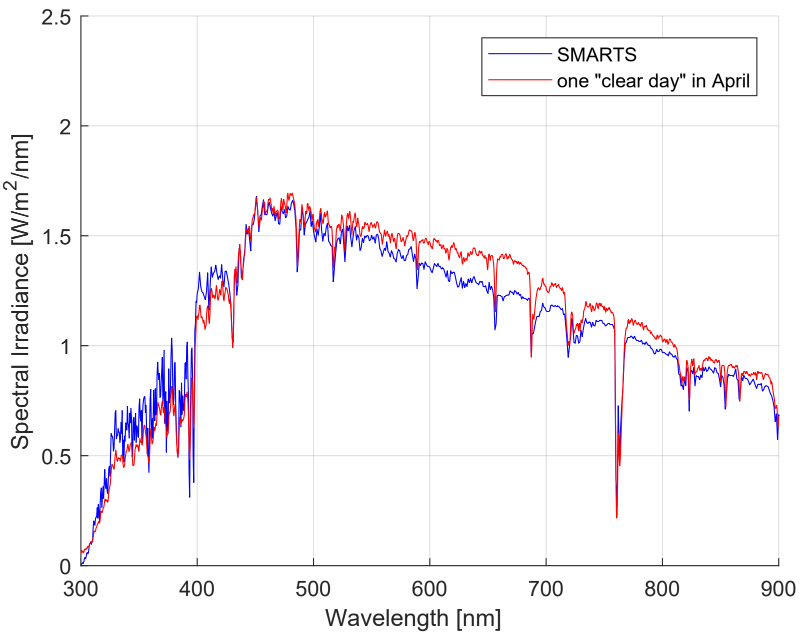

Figure 5.25: Spectral irradiance distribution from April.

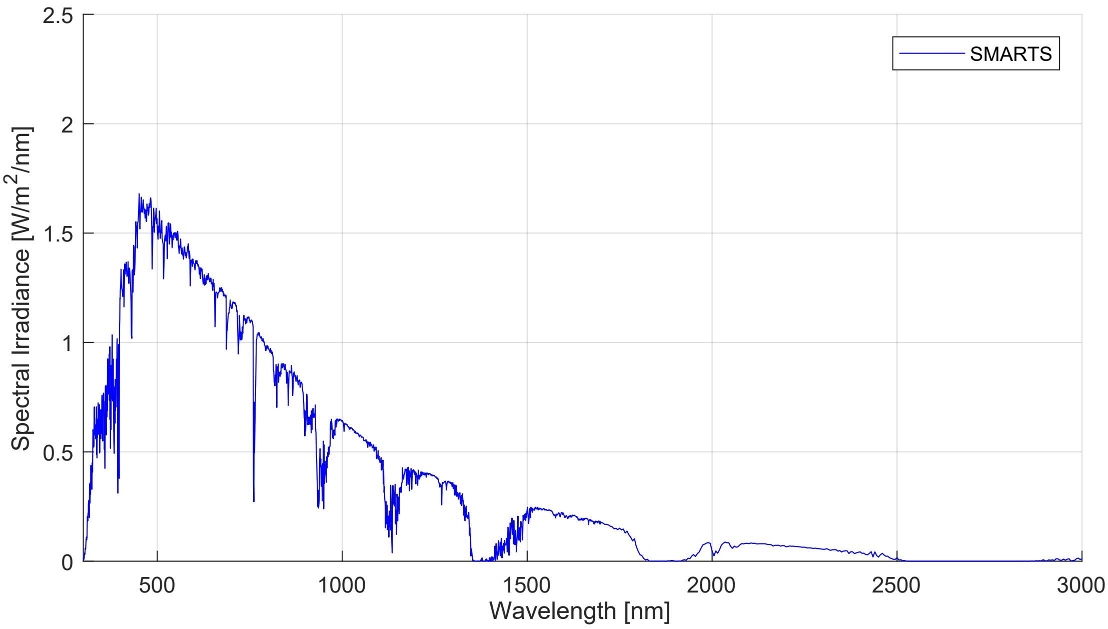

Figure 5.26: Spectral irradiance distribution made in SMARTS that match with a clear day in April.

Finally, figure 5.27 presents the SMARTS model and the reference "clear" day from May. In this case, the difference between the model and reference measurements occurs mainly in the area between 300 nm and 450 nm. Air mass, AOD PW were the main parameters that were changed to match with the measured spectrum. Further, in figure 5.28 demonstrates the spectrum from SMARTS with the wavelength from 0 to 3000 nm.

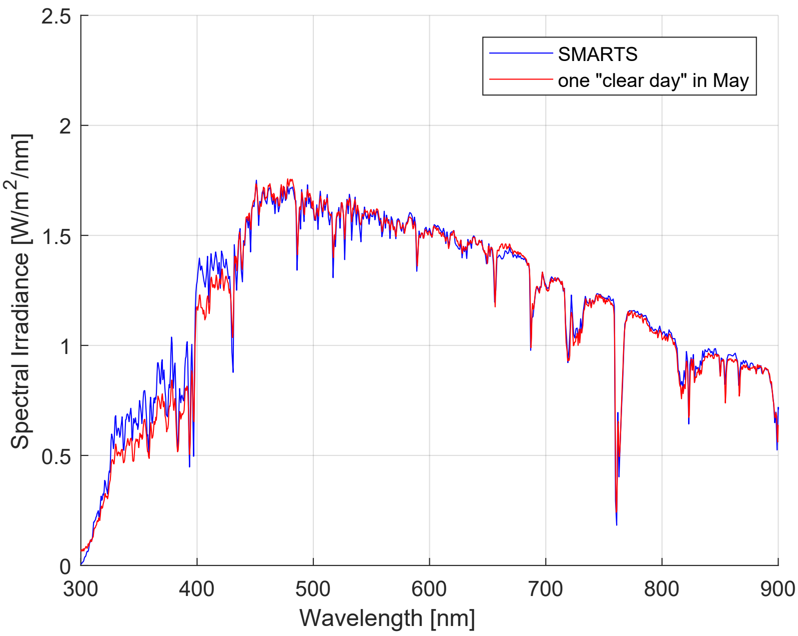

Figure 5.27: Spectral irradiance distribution a clear day from May.

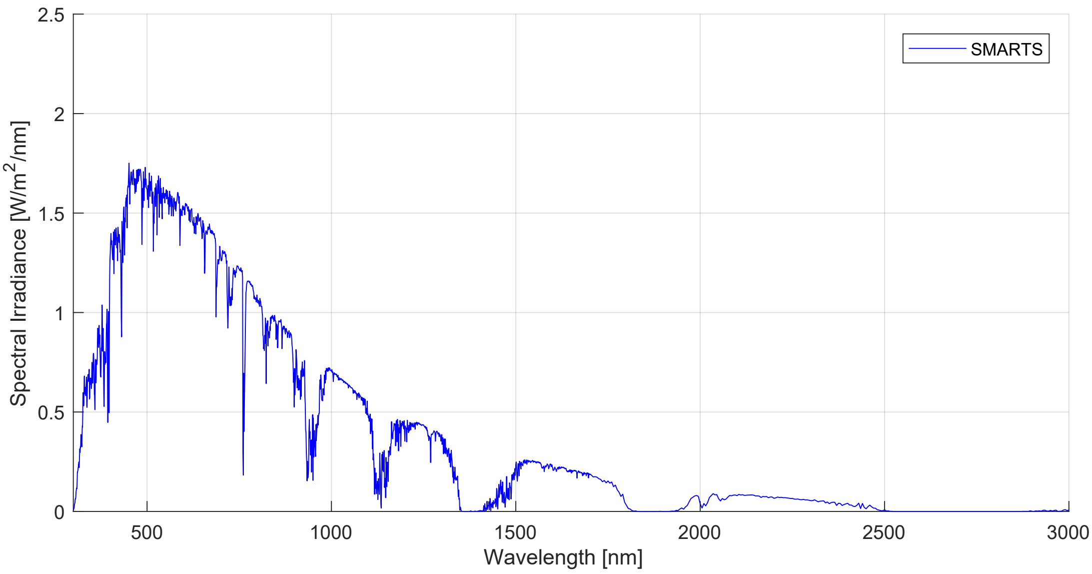

Figure 5.28: Spectral irradiance distribution made in SMARTS that match with a clear day in May.

To control the results made in SMARTS with the actual spectrum, measurements from a pyranometer are used for comparison. The pyranometer is mounted in the plane of the spectrometer 4.3 and measures the total global irradiance for the full spectrum. The SMARTS models are set with the same wavelength range to compare the flux density from the SMARTS model with the flux density from the pyranometer. This result is presented in table 5.11.

Table 5.11: Flux density from the SMARTS models and the pyranometer with same wavelength range.

	Pyranometer	**SMARTS**	**Difference (ref. Pyraonometer)**
6 February	700.92 W/m^2	669.91 W/m^2	4.52 %
20 March	912.30 W/m^2	938.48 W/m^2	2.83 %
29 April	950.79 W/m^2	955.76 W/m^2	0.521 %
17 May	977.39 W/m^2	1007.83 W/m^2	3.07 %

The results demonstrate that there is a small difference between the irradiance from the pyranometer and the SMARTS models. However, the small difference is considered acceptable for the purpose of PV model evaluation, 5.4.

5.4 PV results

This section presents an analysis of which PV technology gives the best result in southern Norway based on the recorded spectra. Figure 5.29 demonstrates the monthly average spectral irradiance distribution from February, March, April, and May together with the normalized spectral response curve for a-Si, CdTe, CIGS, and c-Si based on [35]. As the figure shows, a-Si and CdTe SP-curves fall within the 300-900 nm measured interval, whereas the larger bond-gap of CIGS and c-Si fall outside this region.

Hence, figure 5.13 shows the SMARTS model for February, April, March, and May together with the SR-curves of the PV technologies.

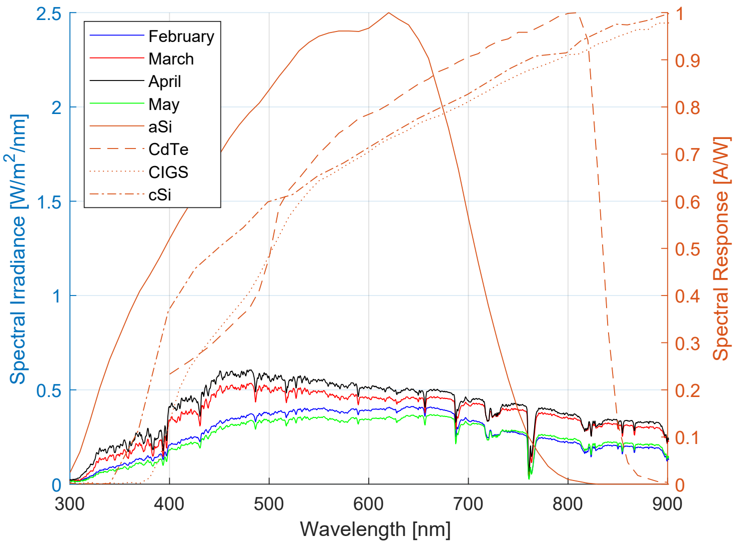

Figure 5.29: Montley average spectral irradiance distribution from February, March, April, and May plotted against spectrale response curves for different PV technologies.

Table 5.12 demonstrates the calculated short-circuit current density from these different PV technologies for the four months. Here, the results are calculated with the absolute spectral response values for the different technologies to adjust to the correct short circuit current density. The results show that CIGS gives the highest short-circuit current density in February. However, in March, April and May, c-Si gives the best results. Nevertheless, CIGS and c-Si give generally similar results in all three months.

Table 5.12: Short circuit current density based on the monthley average spectral irradiance with four PV technologies.

	February	**March**	**April**	**May**
a-Si	27.16 A/m^2	45.06 A/m^2	50.57 A/m^2	64.39 A/m^2
CdTe	38.89 A/m^2	59.23 A/m^2	64.79 A/m^2	81.8 A/m^2
CIGS	**60.59 A/m^2**	90.81 A/m^2	99.18 A/m^2	124.75 A/m^2
c-Si	59.98 A/m^2	**91.32 A/m^2**	**100.16 A/m^2**	**126.12 A/m^2**

Figure 5.13 shows the SMARTS model for February, April, March, and May together with the SR-curves of the PV technologies. Now all the PV technologies fall within the wavelength range. The SMARTS model is based on a clear day around solar noon for each month, which gives higher spectral irradiance distribution.

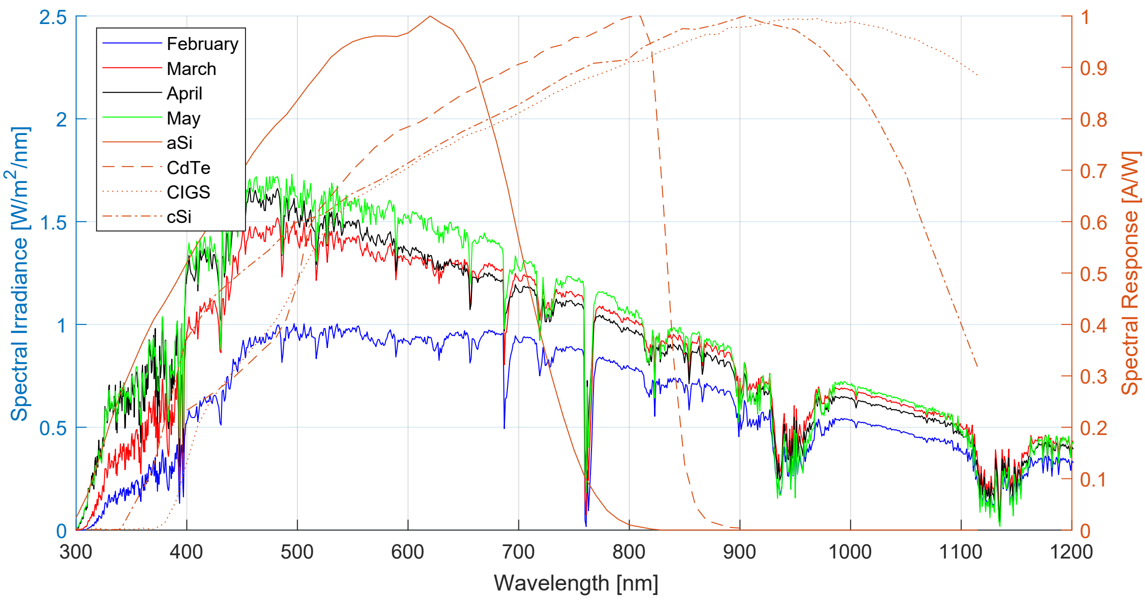

Figure 5.30: Spectral irradiance distribution made in SMARTS based on clear days around solar noon from February, March, April, and May plotted against spectrale response curves for different PV technologies.

Table 5.13 demonstrates the short-circuit current density from different PV technologies from four SMARTS models, which was made from clear days at solar noon. This gives us the result when the whole spectral response is included for all the PV device. The results show that CIGS gives the highest short-circuit current density in February, March, April, and May. This is related to CIGC having the widest range of spectral response.

Table 5.13: Short circuit current density from different days made in SMARTS with diverse PV technologies.

	February	**March**	**April**	**May**
aSi	87.24 A/m^2	127.89 A/m^2	136.66 A/m^2	147.74 A/m^2
CdTe	122.05 A/m^2	170.03 A/m^2	172.63 A/m^2	187.77 A/m^2
CIGS	**260.02 A/m^2**	**355.00 A/m^2**	**349.82 A/m^2**	**374.28 A/m^2**
cSi	232.98 A/m^2	321.40 A/m^2	321.98 A/m^2	345.82 A/m^2

However, for the best performing PV technology, the power output should be compared. The maximum power is the product of the ideal record efficiency solar cell parameters 4.6, and the short-circuit current density for the spectra modeled with SMARTS, based on measured clear days around solar noon. The resulting comparison of power output is shown in table 5.14.

Table 5.14: Maximum power output for spectra modelled with SMARTS.

	February	**March**	**April**	**May**
a-Si	55 W/m^2	87 W/m^2	86 W/m^2	93 W/m^2
CdTe	86 W/m^2	120 W/m^2	121 W/m^2	132 W/m^2
CIGS	**156 W/m^2**	**213 W/m^2**	**210 W/m^2**	**224 W/m^2**
c-Si	147 W/m^2	202 W/m^2	203 W/m^2	218 W/m^2

6 Discussion

6.1 Spectrum shape

During the measurements period from February to May, the shape of the spectrum changes significantly. Figure 5.1b and 5.1a show that the spectral shape in February is more flat, with a small drop around 600 nm. This continues in spectra from March in figure 5.2b and 5.2a, but the shape is more peaked. In April, shown in figure 5.3b and 5.3a, the shape of the spectrum corresponds more to the STC spectrum. And in May, shown in 5.4a and 5.4b, the shape is even more peaked than in April. In table 5.4, the wavelength range from 450 - 500 nm, 12 % of the mean energy from the full spectrum is distributed. This is the highest percentage in a wavelength range in this thesis. These results show that the spectrum shape changes during the season. Because of the variation of the weather during the years, the datasets from February, March, April, and May 2018 is not enough to conclude the typical spectral distribution. Therefore, to establish a monthly spectral irradiance distribution, data from a longer period over several years need to be developed.

In addition to the seasonal changes over the years, there are also some uncertainties with the measurements. In some datasets, a small period was not available because of technical problems. This does not affect the spectrum enough to make the dataset incomplete. Also, during the daylength changed, which gives a different number of spectra to average over each day. For this reason, spectral irradiance distribution during two hours around solar noon is used to compare. This period during the day is also when the spectral irradiance is at its highest intensity. In the results at solar noon, the spectral irradiance density is almost double in every month compared with the mean spectrum in section 5.1.1. Nevertheless, the shape of the spectrum at solar noon is equivalent to the shape in section 5.1.1.

6.1.1 APE results

The histogram of APE for each month shows that lowest APE values occur in February, then they increase in March and further in April and May. To conclude how the APE changes during the season, more data over several years is needed. However, it would appear that the APE increases steadily through the months from February to May because air mass decreases. This is as expected from theory 2.4.2, where long wavelength region is attenuated, increase the APE value.

Furthermore, in both February and March there are a few days that have an APE value around 2.1 eV. As mentioned about APE in section 2.4.2, this could indicate cloudy weather where the clouds absorb the longer wavelength.

There is also mention in section 2.4.2 that APE gives the opportunity to determine if the spectrum is classified as blue rich or red rich by comparing with the standard AM1.5 spectrum. In table 5.6 the APE value for the standard AM1.5 spectrum with the wavelength range 300 to 900 nm, is presented. The table shows that the APE value for AM1.5 global irradiance at 37° tilt is 2.03 eV. Therefore APE values lower than 2.03 eV can be classified as red rich, while APE values higher than 2.03 eV is blue rich. By looking at APE values for each month, shows that APE values from May and April are blue rich. In February the APE values are red rich except two APE values, which is suspected as cloudy days. In March both red rich and blue rich is represented. However, the majority is classified as blue rich. This is also shown in table 5.5, where the slope for mean spectrum irradiance spectrum is found to classified the spectrum as blue rich or red rich. The findings correspond with the APE results, where the spectrum from March, April, and May is blue rich, while February is red rich.

In the literature review in section 3.1.1, APE results from other locations are presented. Their APE results were from 1.78 – 2.04 eV, where the highest results were from Japan, and the lowest in Spain. APE from this thesis work is from 1.95 – 2.1 eV. From table 3.1, different locations in Japan have the most similar APE results to this thesis. However, it is difficult to compare the APE results from the earlier articles with the APE results from this thesis, because of the different wavelength range and period. This would be more accurate to compare if data for a more extended period is developed and should, therefore, be considered in further work.

The APE is also compared with air mass when the sun is at it highest position during the measured day. Here, it shows that the air mass decrease as the APE increase and vice versa. In addition to air mass, AOD measurements from Birkenes were also compared with. Only AOD from April and May were available because of technical problem and calibration of the instrument at Birkenes. The AOD result from April and May compared with APE only gives small variation, and no general conclusion can be made.

6.2 Sensitivity analysis with SMARTS

The sensitivity analysis done with SMARTS shows how the spectrum is affected when the parameters change. Variation of the air mass shows that the spectrum flattens when the air mass gets higher, same as seen in measured spectra. This shows the influence the air mass has on the spectra and gives a possible explanation of the measurements with the drop around 600 nm in section 5.1.1 and 5.1.4. The sensitivity analysis of precipitable water also demonstrates changes from 600 nm til 900 nm, which could also indicate influence on the measurements.

Different AOD at 500 nm were also analysed. The analysis shows that the spectral irradiance distribution flattens when the AOD is high. This is also seen in figure 5.17 that AOD 1 and 1.5 have the same spectral irradiance values. This indicates that small AOD changes do not affect the spectrum. This complements the results in figure 5.10 and 5.11, where AOD as 0.05 or 0.5 gives the same APE.

Typical air pressure and ozone for this location were also investigated. Figure 5.20 does not show any changes in the spectra with the different pressure values. The sensitivity analysis of ozone showed in figure 5.19, which the spectrum changes from the STC spectrum. Although, all the typical ozone values gives for Birkens have to small varation to give real impact. In overall, the sensitivity analysis shows that air mass, AOD, and PW probably will have impact on the measured spectra for this location.

6.3 SMARTS model

For each month a theoretical model is made with SMARTS. Each model is made to match one clear day at solar noon for each month. The results show that the easiest model to make was February, March, and May, while in the model in April does not adequately duplicate the measured day. Not having measurements on all the different parameters, detain it difficult to make an absolute match with the SMARTS program. However, the model with the SMARTS program can give a good indication of the full spectrum despite the small difference in the spectrum between 600 to 800 nm.

6.4 PV results

The average of each month is in the results calculated with the SR from each of the PV technologies to find the short-circuit current density. The results in table 5.12, shows that c-Si gives the best result for the monthly average spectra for March, April, and May, while in February GIGS gives the best result.

However, in table 5.13, the short-circuit current density is presented when the SMARTS models are used instead of the average measurements. Now, the whole SR curve is included in the calculations. Moreover, then, CIGS gives the best result in the four months. However, for the best performing PV technology, the maximum power output is calculated and compared from the short-circuit current density to the SMARTS models. The maximum power output gets the same conclusion as the short-circuit current density. This demonstrates that when the whole spectrum is included, the outcome changes. Nevertheless, the results from GIGS and c-Si gives similar short-circuit current density in both outcomes, and therefore both could PV technologies could be used.

Since there is not complete data for a full year, it is not possible to conclude final recommendation on which PV technology is best for the Southern Norway conditions. Nevertheless, with the presently available data, CIGS gives the best short-circuit current density and maximum power output results.

7 Further Work

Due to limitations with this thesis, where only data from February, March, and April is obtained, further work in this investigation would continue measuring the spectral irradiance to get data from every month over several years. This will also give the opportunity to compare results with models using the real astronomical parameters results from Birkenes. And it will also give the opportunity to compare with the APE results from the literature review in section 3.1.1.

Another investigation could be to characterize other locations and irradiance conditions in Norway. It would be interesting to collect global and spectral irradiance measurements for several locations in the Nordics, to be analyzed and compared with the measurements from UiA. There is little research on the spectral irradiance distribution in the Nordics, and therefore it is suggested that measurements should be performed in different locations to observe the effects of seasonal variation, climate, and latitude.

In this thesis, only the model with the SMARTS program was made. SMARTS only models the clear sky spectral irradiance distribution, and because of the changing weather in Norway, another program that handles cloudy weather could be too useful for modeling diffuse spectra.

In addition, a further investigation of the PV performance can be done and compared with outdoor measurements to confirm how to short-circuit density and maximum power output changes with the season and atmospheric conditions.

8 Conclusion

The outdoor performance of PV modules depends on solar irradiation, module temperature, and solar spectrum. Different locations would, therefore, give a variation in outcome for different PV technologies. In this thesis, measurements and analysis of the spectral irradiance distribution in Southern Norway have been investigated.

The spectral irradiance has been measured with a spectrometer at the University of Agder during the period February to May 2018 to analyse the changes through the months. The spectrum in February has a flattened shape, with increasing peak value in March, April, and May. This is affected by the air mass during these periods. The air mass influence the shape of the spectrum, which is investigated in sensitivity analysis with the help of SMARTS. The sensitivity analyses also investigate the effect of AOD, precipitable water, ozone, and air pressure on the spectrum.

APE results from other locations are presented in a literature review. Their APE results were from $1.78 - 2.04$ eV, where the highest results were from Japan, and the lowest in Spain. APE from this thesis work is from $1.95 - 2.1$ eV. However, it is difficult to compare the APE results from the earlier articles with the APE results from this thesis, because of the different wavelength range and period. The APE value for standard AM1.5 spectrum is found to determine if the spectra are classified as blue rich or red rich. APE values from May and April are blue rich, while in February the majority of APE values are red rich.

The APE is also compared with air mass during the months, which shows that the air mass decrease as the APE increase and vice versa. Only AOD from April and May were available because of technical problem and calibration of the instrument at Birkenes. The AOD result from April and May compared with APE only gives small variation, and no general conclusion can be made.

The SMARTS program is also used to make a model of a clear day around solar noon for each month. This is to create a spectrum with a complete wavelength range for use in the calculations of the performance of four PV technologies. The SMARTS model successful reproduce spectra in February, March, and May, however, in April there is has some mismatch between 600 nm and 800 nm.

The monthly average spectral irradiance of each month is used to calculate the short-circuit current density with the SR from each PV technologies. The four SMARTS models where also used to calculate the short-circuit current density and the maximum power output. CIGS gives the highest short-circuit current density and the maximum power output in the four months. Nevertheless, the results for CIGS and c-Si is close and are both suitable PV technologies to use at this location.

Further work in this investigation, would be to continue measuring the spectral irradiance distribution to get a complete dataset over several years. This would give the opportunity to see if the PV performance rating changes during the season. Spectral irradiance measurements from other location in Norway and Nordics could also to be of interest to observe the effects of seasonal variation, climate, and latitude.

References

[1] BP, "Solar energy," 2017. [Online]. Available: https://www.bp.com/en/global/corporate/energy-economics/statistical-review-of-world-energy/renewable-energy/solar-energy.html

[2] I. E. Agency, "Renewables 2017," 2017. [Online]. Available: https://www.iea.org/renewables/

[3] D. Dirnberger, G. Blackburn, B. Müller, and C. Reise, "On the impact of solar spectral irradiance on the yield of different pv technologies," *Solar Energy Materials and Solar Cells*, vol. 132, pp. 431 – 442, 2015. [Online]. Available: http://www.sciencedirect.com/science/article/pii/S0927024814005169

[4] T. Ishii, K. Otani, A. Itagaki, and K. Utsunomiya, "A simplified methodology for estimating solar spectral influence on photovoltaic energy yield using average photon energy," *Energy Science & Engineering*, vol. 1, no. 1, pp. 18–26, 2013. [Online]. Available: http://dx.doi.org/10.1002/ese3.3

[5] G. Nofuentes, C. Gueymard, J. Aguilera, M. Pérez-Godoy, and F. Charte, "Is the average photon energy a unique characteristic of the spectral distribution of global irradiance?" *Solar Energy*, vol. 149, no. Supplement C, pp. 32 – 43, 2017. [Online]. Available: http://www.sciencedirect.com/science/article/pii/S0038092X17302797

[6] R. G. Barry and R. J. Chorley, *Atmosphere Weather and Climate 8th ed*, 8th ed. Routledge, 2003. [Online]. Available: http://danida.vnu.edu.vn/cpis/files/Books/Atmosphere%20Weather%20and%20Climate%208th%20ed%20-%20R%20Barry%20R%20Chorley%20-%20Routledge%202003%20WW.pdf

[7] S. Wenham, M. Green, M. Watt, and R. Corkish, *Applied Photovoltaics*, 2nd ed. Earthscan, 2007.

[8] PVeducation, "Declination angle," PVeducation.org, Mar. 2018. [Online]. Available: https://www.pveducation.org/pvcdrom/properties-of-sunlight/declination-angle

[9] R. Eke, T. Betts, and G. R., "Spectral irradiance effects on the outdoor performance of photovoltaic modules," *Renewable and Sustainable Energy Reviews*, vol. 69, pp. 429 – 434, 2017. [Online]. Available: http://www.sciencedirect.com/science/article/pii/S1364032116307079

[10] azo materials, "Introduction to solar simulators," azo materials, 2017, picture. [Online]. Available: https://www.azom.com/article.aspx?ArticleID=10817

[11] G. spec, "Solar radiation instruments information," 2017, figure. [Online]. Available: http://www.globalspec.com/learnmore/sensors_transducers_detectors/weather_sensing/solar_radiation_instruments

[12] NASA, "Measuring areosols," Earth Obseravtory, Nov. 2017. [Online]. Available: https://earthobservatory.nasa.gov/Features/Aerosols/page5.php

[13] Appropedia, "File:am1 5 spectrum.jpg," 2017, figure. [Online]. Available: http://www.appropedia.org/File:Am1_5_spectrum.jpg

[14] S. direct, "Solar electric photovoltaic modules," 2018. [Online]. Available: http://www.solardirect.com/pv/pvlist/pvlist.htm

[15] E. Publishers, "Solar pv module faults and failings," EE Publishers, Apr. 2018. [Online]. Available: http://www.ee.co.za/article/solar-pv-module-faults-failings.html

[16] M. A. M. (energy informaitive), "Best thin film solar panels - amorphous, cadmium telluride or cigs?" energyinformative.org. [Online]. Available: http://energyinformative.org/best-thin-film-solar-panels-amorphous-cadmium-telluride-cigs/

[17] national renewable energy laboratory, "Cadmium telluride solar cells," nrel.gov, May 2018. [Online]. Available: https://www.nrel.gov/pv/cadmium-telluride-solar-cells.html

[18] NREL, "Copper indium gallium diselenide solar cells," nrel.gov, May 2018. [Online]. Available: https://www.nrel.gov/pv/copper-indium-gallium-diselenide-solar-cells.html

[19] M. Padilla, B. Michl, B. Thaidigsmann, W. Warta, and M. Schubert, "Short-circuit current density mapping for solar cells," *Solar Energy Materials and Solar Cells*, vol. 120, pp. 282 – 288, 2014. [Online]. Available: http://www.sciencedirect.com/science/article/pii/S0927024813004881

[20] PVeducation.org, "Solar cell efficiency," Apr. 2018. [Online]. Available: https://www.pveducation.org/pvcdrom/solar-cell-operation/solar-cell-efficiency

[21] T. Veeken, "S-q charts," Life Management in New Photovaltic Materials, Feb. 2018. [Online]. Available: http://www.lmpv.nl/sq/

[22] T. N. R. E. L. (NREL), "Reference solar spectral irradiance: Air mass 1.5," Nov. 2017. [Online]. Available: http://rredc.nrel.gov/solar/spectra/am1.5/

[23] C. Honsberg and S. Bowden, "Spectral irradiance," PV education. org. [Online]. Available: http://www.pveducation.org/pvcdrom/properties-of-sunlight/spectral-irradiance

[24] ——, "Photon flux," PV education. org. [Online]. Available: http://www.pveducation.org/pvcdrom/properties-of-sunlight/photon-flux

[25] C. Gueymard, "Daily spectral effects on concentrating pv solar cells as affected by realistic aerosol optical depth and other atmospheric conditions," Proceedings of SPIE - The International Society for Optical Engineering., 2009.

[26] G. Nofuentes, J. de la Casa, M. Torres-Ramírez, and M. Alonso-Abella, "Solar spectral and module temperature influence on the outdoor performance of thin film pv modules deployed on a sunny inland site," *International Journal of Photoenergy*, 2013. [Online]. Available: https://www.hindawi.com/journals/ijp/2013/620127/abs/

[27] S. Nann and C. Riordan, "Solar spectral irradiance under clear and cloudy skies: Measurements and a semiempirical model," *Journal of Applied Meteorology*, vol. 30, no. 4, pp. 447–462, 1991. [Online]. Available: https://doi.org/10.1175/1520-0450(1991)030<0447:SSIUCA>2.0.CO;2

[28] T. Minemoto, Y. Nakada, H. Takahashi, and H. Takakura, "Uniqueness verification of solar spectrum index of average photon energy for evaluating outdoor performance of photovoltaic

modules," *Solar Energy*, vol. 83, no. 8, pp. 1294 – 1299, 2009, picture page 5. [Online]. Available: http://www.sciencedirect.com/science/article/pii/S0038092X09000577

[29] M. Norton, A. G. Amillo, and R. Galleano, "Comparison of solar spectral irradiance measurements using the average photon energy parameter," *Solar Energy*, vol. 120, no. Supplement C, pp. 337 – 344, 2015. [Online]. Available: http://www.sciencedirect.com/science/article/pii/S0038092X1500331X

[30] A. Louwen, A. C. de Waal, and W. G. J. H. M. van Sark, "Evaluation of different indicators for representing solar spectral variation," in *2016 IEEE 43rd Photovoltaic Specialists Conference (PVSC)*, June 2016, pp. 0133–0137.

[31] M. . e. a. KRAWCZYNSKI, "Spectral irradiance measurements for photovoltaic systems in maritime climates," 2011, iN: Proceedings of the 7th Photovoltaic Science Applications and Technology Conference (PVSAT-7), 1st-3rd April 2011, Heriot-Watt University, Edinburgh, pp. 277-280. [Online]. Available: https://dspace.lboro.ac.uk/2134/9216

[32] T. Minemoto, S. Nagae, and H. Takakura, "Impact of spectral irradiance distribution and temperature on the outdoor performance of amorphous si photovoltaic modules," *Solar Energy Materials and Solar Cells*, vol. 91, no. 10, pp. 919 – 923, 2007. [Online]. Available: http://www.sciencedirect.com/science/article/pii/S0927024807000712

[33] T. Minemoto, M. Toda, S. Nagae, M. Gotoh, A. Nakajima, K. Yamamoto, H. Takakura, and Y. Hamakawa, "Effect of spectral irradiance distribution on the outdoor performance of amorphous si//thin-film crystalline si stacked photovoltaic modules," *Solar Energy Materials and Solar Cells*, vol. 91, no. 2, pp. 120 – 122, 2007. [Online]. Available: http://www.sciencedirect.com/science/article/pii/S0927024806003369

[34] A. Gracia Amillo, T. Huld, P. Vourlioti, R. Müller, and M. Norton, "Application of satellite-based spectrally-resolved solar radiation data to pv performance studies," vol. 8, pp. 3455–3488, 05 2015.

[35] D. Dirnberger, G. Blackburn, B. Müller, and C. Reise, "On the impact of solar spectral irradiance on the yield of different pv technologies," *Solar Energy Materials and Solar Cells*, vol. 132, pp. 431 – 442, 2015. [Online]. Available: http://www.sciencedirect.com/science/article/pii/S0927024814005169

[36] A. Bagheri, "Work report solar spectral measurement at uia (pv lab.), characterization of hr2000 +," 2017, unpublished.

[37] mssl.ucl.ac.uk, "An introduction to ccd operation," mssl.ucl.ac.uk, Mar. 2018. [Online]. Available: http://www.mssl.ucl.ac.uk/www_detector/ccdgroup/optheory/ccdoperation.html

[38] O. Optics, "Patch cords," May 2018. [Online]. Available: https://oceanoptics.com/product-category/patch-cords/

[39] ——, "Cosine correctors," OceanOptics.com, May 2018. [Online]. Available: https://oceanoptics.com/product/cosine-correctors/

[40] B. et al., "A guide to measuring solar uv spectra using array spectroradiometers," AIP Conference Proceedings, May 2013. [Online]. Available: https://aip.scitation.org/doi/abs/10.1063/1.4804892

[41] G. Seckmeyer, A. Bais, G. Bernhard, M. Blumthaler, S. Drueke, P. Kiedron, K. Lantz, R. McKenzie, and S. Riechelmann, "Instruments to measure solar ultraviolet radiation part 4: Array spectroradiometers (wmo td no. 1538)," p. pp. 43, 01 2010.

[42] S. et al., "Instruments to measure solar ultraviolet radiation," WORLD METEOROLOGICAL ORGANIZATION GLOBAL ATMOSPHERE WATCH, 2010. [Online]. Available: https://www.researchgate.net/profile/Alkiviadis_Bais/publication/227860175_Instruments_to_measure_solar_ultraviolet_irradiance_Part_1_Spectral_instruments/links/55a28ced08aec9ca1e64f6d9/Instruments-to-measure-solar-ultraviolet-irradiance-Part-1-Spectral-instruments.pdf

[43] O. Optics, "Hd-2000 familiy," Ocean Optics. [Online]. Available: https://oceanoptics.com/product/dh-2000-family/

[44] R. Poling, "What is a solar pyranometer?" Solar Power World, Mar. 2015. [Online]. Available: https://www.solarpowerworldonline.com/2015/03/what-is-a-solar-pyranometer/

[45] hukseflux.com, "Sr20 pyranometer," https://www.hukseflux.com/product/sr20-pyranometer. [Online]. Available: https://www.hukseflux.com/product/sr20-pyranometer

[46] N. . N. I. for Air Research, "Monitoring of the atmospheric ozone layer and natural ultraviolet radiation: Annual report 2014," Miljødirektoratet, Apr. 2018. [Online]. Available: http://www.miljodirektoratet.no/no/Publikasjoner/2015/September-2015/Monitoring-of-the-atmospheric-ozone-layer-and-natural-ultraviolet-radiation-Annual-Report-2014/

[47] Nrel, "About smarts," nrel.gov, Mar. 2018. [Online]. Available: https://www.nrel.gov/rredc/smarts/about.html

[48] U. D. o. E. Sandia National Laboratories, "Spectral response," PV Performance modelling collaborative, May 2018. [Online]. Available: https://pvpmc.sandia.gov/modeling-steps/2-dc-module-iv/effective-irradiance/spectral-response/

A Appendix - Specifications

A.1 Calibration instument

Table A.1: DH-2000 Family specifications [43]

Engineering Specifications	**DH-2000-DUV Series**
Sources:	Deep-UV Deuterium & Tungsten Halogen
Wavelength range:	190-2500 nm
Nominal bulb power:	26 W (deuterium) 20 W (tungsten halogen)
Typical output power:	See chart below
Warm-up time:*	25 minutes
Source lifetime:	1,000 hours
Stability of light source output:	$\leq$0.1%/hour @ 254 nm (deuterium) $\leq$0.1%/hour @ 700 nm (tungsten halogen)
Drift:	$\leq$0.1%/hour @ 254 nm (deuterium) $\leq$0.1%/hour @ 700 nm (tungsten halogen)
Shutter:	DH2000-S-DUV & DH2000-S-DUV-TTL only
Remote shutter control:	DH2000-S-DUV-TTL only
Integrated filter holder:	DH2000-FHS-DUV only
Operating temperature:	5 °C - 35 °C
Operating humidity:	5-95% without condensation at 40 °C
Power requirements:	85-264 V, 50/60 Hz
Power consumption:	Approximately 78VA
Dimensions (W x H x L):	15 x 13.5 x 28.5 cm
Weight:	5 kg
Safety & regulatory:	CE; ROHS, WEEE
Replacement bulbs:	DH-2000-DUV-B (deuterium) DH-2000-BH (tungsten halogen)

* Warm-up time @23 °C ambient, free airflow, no vibrations

A.2 Spectrometer

Table A.2: DR2000+ spectrometer specifications

Engineering Specifications	**HR2000+ Custom (user configured)**
PHYSICAL	
Dimensions: (L x W x H) mm and inches	148.6 x 104.8 x 45.1 mm (5.9 x 4.1 x 1.8 in.)
Weight: kg and lb	0.57 kg (1.26 lbs.)
DETECTOR	
Type:	Sony ILX511B
Range:	190 – 1100 nm
SPECTROSCOPIC	
Wavelength range:	190 – 1100 nm
Integration time:	1 millisecond – 65 seconds (20 seconds typical)
Dynamic range:	2 x 108 (system); 1300:1 for a single acquisition
Signal-to-noise ratio:	250:1 (at full signal)
Grating:	H1 – H14; HC-1
Slit:	5, 10, 25, 50, 100 or 200 μm wide slits
Optical resolution:	~0.035 to 6.8 nm (FWHM)
Stray light:	<0.05% at 600 nm; <0.10% at 435 nm
Buffering:	no
Fiber optic connector:	SMA 905 to single-strand optical fiber (0.22 NA)
ELECTRONICS	
Power consumption:	220 mA at +5 VDC
Strobe functions:	2 programmable strobe signals (single/continuous)
Interfaces:	USB 2.0, 480 Mbps; 2-wire RS-232; I2C 2 wire serial bus
Temperature:	-30° to +70° C Storage & -10° to +50° C Operation
Humidity:	0% – 90% non-condensing

A.3 Fiber certificate

Ocean Optics

Part #: QP600-025-SR
Date: May 4, 2016
Assembly #: OOS-004928-03
Connector 1 #: QSMA
Connector 2 #: QSMA
Sales Order # STOCK

www.OceanOptics.com
Phone:727-733-2447
Fax:727-733-3962
Info@OceanOptics.com
830 Douglas Ave
Dunedin, FL 34698

Ask about our custom line of Optical Probes and Assemblies.

Fiber Type: UV-SR
Fiber Core Diameter:(um) 600um

Jacketing: Monocoil
Length (meters): 0.25

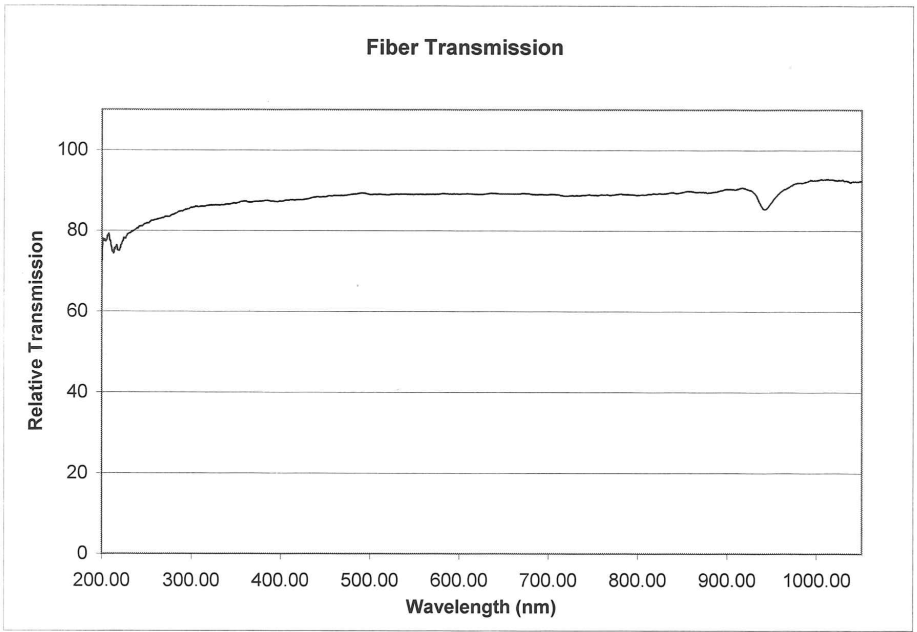

Inspection Checklist X
Polish: X
Concentricity: X
Cap Placement: X
Labeling: X
Color Coding: X
Ferrule length: X

Tested by: Van Foster

Inspected by: Van Foster

Your Fiber was tested for performance prior to shipment. Please check your Fiber for breakage upon receipt.
Ocean Optics will replace under warranty any broken Fiber returned within three weeks after customer receipt.

RoHS - Compliant

B Appendix - SMARTS

B.1 Input file for SMARTS model in February

```
'USSA_AOD=0.084_ASTM_G173'
1
985 0 0
1
'SAW'
1
1
0
3
400
0
'S&F_RURAL'
0
0,5
41
1
51 37. 180.
280 4000 1 1200
2
280 4000 .5
3
8 9 10
1
0 2.9 0
0
0
0
2
3,5
```

B.2 Output file for SMARTS model in February

```
*****************  SMARTS, version 2.9.5  ******************
 Simple Model of the Atmospheric Radiative Transfer of Sunshine
    Chris A. Gueymard, Solar Consulting Services
              December 2005
   This model is documented in FSEC Report PF-270-95
 and in a Solar Energy paper, vol. 71, No.5, 325-346 (2001)
 NOTE: These references describe v. 2.8 or earlier!!!
 See the User's Manual for details on the considerable
 changes that followed...
**************************************************************
  Reference for this run: USSA_AOD=0.084_ASTM_G173
----------------------------------------------------------------
* ATMOSPHERE : SAW        AEROSOL TYPE: S&F_RURAL
* INPUTS:
    Pressure (mb) =  985.000   Ground Altitude (km) =   0.0000
    Height above ground (km) =   0.0000
    Relative Humidity (%) = 80.460   Precipitable Water (cm) =  0.4161
    Ozone (atm-cm) = 0.3759 or 375.9 Dobson Units
  AEROSOLS:  Optical Depth at 500 nm = 0.0000      Optical depth at 550 nm = 0.0000
      Angstrom's Beta = 0.0000       Schuepp's B = 0.0000
    Meteorological Range (km) =  999.0   Visibility (km) =  764.9
    Alpha1 = 0.8909  Alpha2 = 1.2600   Mean Angstrom's Alpha = 1.0755
    Season = FALL/WINTER
* TEMPERATURES:
    Instantaneous at site's altitude = 257.1 K
    Daily average (reference) at site's altitude = 257.1 K
    Stratospheric Ozone and NO2 (effective) = 217.3 K
** WARNING #13 *********
\\ Ground reflectance data for RED_BRICK
\\ extend only from 0.3000 to 4.0000 µm,
\\ whereas the wavelength limits for this run are 0.2800 and 4.0000 µm.
```

\\ Consequently, reflectance is fixed at 0.028 below 0.3000 µm and at 0.382 above 4.0000 µm.

** WARNING #13 *********

\\ Ground reflectance data for DRY_LONG_GRASS

\\ extend only from 0.2771 to 2.9760 µm,

\\ whereas the wavelength limits for this run are 0.2800 and 4.0000 µm.

\\ Consequently, reflectance is fixed at 0.008 below 0.2771 µm and at 0.003 above 2.9760 µm.

The following spectral variables will be output to file: smarts295.ext.txt

* Global_tilted_irradiance

* Beam_normal_+circumsolar

* Difuse_horiz-circumsolar

Spectral ZONAL albedo data: RED_BRICK

with a reflection process: NON_LAMBERTIAN

* GEOMETRY (half-angles) OF THE SIMULATED RADIOMETER (deg.):

Slope = 0.00   Aperture = 2.90   Limit = 0.00

** WARNING #11*********

\\ The radiometer's Slope and Limit angles are not provided.

\\ Circumsolar calculations will therefore be performed for

\\ an average geometry corresponding to the Aperture angle.

Spectral LOCAL albedo data: DRY_LONG_GRASS

with a reflection process: NON_LAMBERTIAN

==
==================

* SOLAR POSITION (deg.):

Zenith Angle (apparent) = 70.671 Azimuth (from North) = 180.00

RELATIVE OPTICAL MASSES:

- Rayleigh = 3.000

- Water Vapor = 3.017

- Ozone = 2.962

- NO2 = 2.968

- Aerosols = 3.015

CO2 Mixing Ratio (ppmv): 400.0

Total column abundances (atm-cm) for all gases except H2O, and for normal/standard conditions:

BrO CH2O CH4 ClNO3 CO CO2 HNO2 HNO3 NH3

0.2500E-05 0.3000E-03 0.1241E+01 0.1200E-03 0.8743E-01 0.3121E+03 0.1000E-03 0.3373E-03 0.1731E-03

NO NO2 NO3 N2 N2O O2 O3 O4 SO2

0.2962E-03 0.1863E-03 0.5000E-04 0.3856E+06 0.2346E+00 0.1631E+06 0.3759E+00 0.1631E+06 0.1074E-03

Corrected total column abundances for all gases (atm-cm)

with these realistic conditions: MODERATE POLLUTION

BrO CH2O CH4 ClNO3 CO CO2 HNO2 HNO3 NH3

0.2500E-05 0.1000E-02 0.1271E+01 0.1200E-03 0.1224E+00 0.3121E+03 0.3000E-03 0.1537E-02 0.1731E-03

NO NO2 NO3 N2 N2O O2 O3 O4 SO2

0.2030E-01 0.2186E-02 0.5500E-04 0.3856E+06 0.2346E+00 0.1631E+06 0.3812E+00 0.1631E+06 0.5107E-02

* ANGLES (deg.) FOR TILTED SURFACE CALCULATIONS:

Surface Tilt = 37.000 Surface Azimuth (from North) = 180.000

Incidence Angle = 33.671

Diffuse irradiance ratios (tilted plane/horizontal):

0.8993 (isotropic approximate conversion--for reference)

1.5591 (anisotropic conversion model--used here)

* *

** SPECTRUM:

Total (0-100 µm) Extraterrestrial Irradiance used here = 1200.00 W/m2

(i.e., 1.0000 times the selected solar constant, 1200.00 W/m2, due to the actual Sun-Earth distance.)

Source for selected solar spectrum: Gueymard_2003

To account for the chosen Solar Constant value, the selected solar spectrum has been uniformly multiplied

by this scaling coefficient = 0.8784

Wavelength Range = 280.0 to 4000.0 nm; Number of Wavelengths = 2002

*** BROADBAND IRRADIANCES (W/m2):

* DIRECT BEAM AT NORMAL INCIDENCE:

Extraterrestrial = 1184.13 Terrestrial = 762.03 Atmospheric Transmittance = 0.6435

* FOR THE HORIZONTAL PLANE:

Direct Beam = 252.23 Diffuse = 33.21 Global = 285.44 Clearness index, KT = 0.2379

Diffuse irradiance origination details:

Sky diffuse = 31.10 Back-scattered diffuse = 2.11

* FOR THE TILTED PLANE:

Direct Beam = 634.19 Sky Diffuse = 41.73 Ground Reflected = 11.86 Global = 675.92

* EXPERIMENTAL (WITH CIRCUMSOLAR CORRECTION):

Direct Beam, Normal Incidence = 762.22 Diffuse Horizontal = 33.15 Global Horizontal = 285.44

B.3 Input file for SMARTS model in March

```
'USSA_AOD=0.084_ASTM_G173'
1
1013.25 0 0
1
'SAW'
1
1
0
2
400
0
'S&F_RURAL'
0
0,07
41
1
51 37. 180.
280 4000 1.0 1366.1
2
280 4000 .5
3
8 9 10
1
0 2.9 0
0
0
0
2
2,5
```

B.4 Output file for SMARTS model in March

``` 
*****************  SMARTS, version 2.9.5  *******************
 Simple Model of the Atmospheric Radiative Transfer of Sunshine
    Chris A. Gueymard, Solar Consulting Services
               December 2005
   This model is documented in FSEC Report PF-270-95
 and in a Solar Energy paper, vol. 71, No.5, 325-346 (2001)
 NOTE: These references describe v. 2.8 or earlier!!!
 See the User's Manual for details on the considerable
 changes that followed...
**************************************************************
   Reference for this run: USSA_AOD=0.084_ASTM_G173
--------------------------------------------------------------
* ATMOSPHERE : SAW        AEROSOL TYPE: S&F_RURAL
* INPUTS:
    Pressure (mb) = 1013.250   Ground Altitude (km) =   0.0000
    Height above ground (km) =   0.0000
    Relative Humidity (%) = 80.460   Precipitable Water (cm) =  0.4161
    Ozone (atm-cm) = 0.3759 or 375.9 Dobson Units
  AEROSOLS:  Optical Depth at 500 nm = 0.0000      Optical depth at 550 nm = 0.0000
      Angstrom's Beta = 0.0000       Schuepp's B = 0.0000
    Meteorological Range (km) =  999.0   Visibility (km) =  764.9
    Alpha1 = 0.8909  Alpha2 = 1.2600   Mean Angstrom's Alpha = 1.0755
  Season = FALL/WINTER
* TEMPERATURES:
    Instantaneous at site's altitude = 257.1 K
    Daily average (reference) at site's altitude = 257.1 K
    Stratospheric Ozone and NO2 (effective) = 217.3 K
** WARNING #13 *********
\\ Ground reflectance data for RED_BRICK
\\ extend only from 0.3000 to 4.0000 µm,
\\ whereas the wavelength limits for this run are 0.2800 and 4.0000 µm.
```

\\ Consequently, reflectance is fixed at 0.028 below 0.3000 µm and at 0.382 above 4.0000 µm.

** WARNING #13 *********

\\ Ground reflectance data for DRY_LONG_GRASS

\\ extend only from 0.2771 to 2.9760 µm,

\\ whereas the wavelength limits for this run are 0.2800 and 4.0000 µm.

\\ Consequently, reflectance is fixed at 0.008 below 0.2771 µm and at 0.003 above 2.9760 µm.

The following spectral variables will be output to file: smarts295.ext.txt

 * Global_tilted_irradiance

 * Beam_normal_+circumsolar

 * Difuse_horiz-circumsolar

 Spectral ZONAL albedo data: RED_BRICK

 with a reflection process: NON_LAMBERTIAN

* GEOMETRY (half-angles) OF THE SIMULATED RADIOMETER (deg.):

 Slope = 0.00 Aperture = 2.90 Limit = 0.00

** WARNING #11*********

\\ The radiometer's Slope and Limit angles are not provided.

\\ Circumsolar calculations will therefore be performed for

\\ an average geometry corresponding to the Aperture angle.

 Spectral LOCAL albedo data: DRY_LONG_GRASS

 with a reflection process: NON_LAMBERTIAN

==
==================

==
==================

* SOLAR POSITION (deg.):

 Zenith Angle (apparent) = 60.085 Azimuth (from North) = 180.00

 RELATIVE OPTICAL MASSES:

 - Rayleigh = 2.000

 - Water Vapor = 2.004

 - Ozone = 1.993

 - NO2 = 1.997

 - Aerosols = 2.004

CO2 Mixing Ratio (ppmv): 400.0

Total column abundances (atm-cm) for all gases except H2O, and for normal/standard conditions:

BrO CH2O CH4 ClNO3 CO CO2 HNO2 HNO3 NH3

0.2500E-05 0.3000E-03 0.1281E+01 0.1200E-03 0.9077E-01 0.3211E+03 0.1000E-03 0.3385E-03 0.1840E-03

NO NO2 NO3 N2 N2O O2 O3 O4 SO2

0.3029E-03 0.1868E-03 0.5000E-04 0.4067E+06 0.2423E+00 0.1678E+06 0.3759E+00 0.1678E+06 0.1140E-03

Corrected total column abundances for all gases (atm-cm)

with these realistic conditions: LIGHT POLLUTION

BrO CH2O CH4 ClNO3 CO CO2 HNO2 HNO3 NH3

0.2500E-05 0.4000E-03 0.1301E+01 0.1200E-03 0.9077E-01 0.3211E+03 0.1500E-03 0.1539E-02 0.1840E-03

NO NO2 NO3 N2 N2O O2 O3 O4 SO2

0.7803E-02 0.6868E-03 0.5100E-04 0.4067E+06 0.2423E+00 0.1678E+06 0.3782E+00 0.1678E+06 0.1114E-02

* ANGLES (deg.) FOR TILTED SURFACE CALCULATIONS:

Surface Tilt = 37.000 Surface Azimuth (from North) = 180.000

Incidence Angle = 23.085

Diffuse irradiance ratios (tilted plane/horizontal):

0.8993 (isotropic approximate conversion--for reference)

1.3661 (anisotropic conversion model--used here)

* *

** SPECTRUM:

Total (0-100 µm) Extraterrestrial Irradiance used here = 1366.10 W/m2

(i.e., 1.0000 times the selected solar constant, 1366.10 W/m2, due to the actual Sun-Earth distance.)

Source for selected solar spectrum: Gueymard_2003

Wavelength Range = 280.0 to 4000.0 nm; Number of Wavelengths = 2002

*** BROADBAND IRRADIANCES (W/m2):

* DIRECT BEAM AT NORMAL INCIDENCE:

Extraterrestrial = 1348.03 Terrestrial = 963.98 Atmospheric Transmittance = 0.7151

* FOR THE HORIZONTAL PLANE:

Direct Beam = 480.74 Diffuse = 46.90 Global = 527.64 Clearness index, KT = 0.3862

Diffuse irradiance origination details:

Sky diffuse = 43.38 Back-scattered diffuse = 3.52

* FOR THE TILTED PLANE:

Direct Beam = 886.78 Sky Diffuse = 60.41 Ground Reflected = 18.24 Global = 947.20

* EXPERIMENTAL (WITH CIRCUMSOLAR CORRECTION):

Direct Beam, Normal Incidence = 964.18 Diffuse Horizontal = 46.80 Global Horizontal = 527.64

B.5 Input file for SMARTS model in April

```
'USSA_AOD=0.084_ASTM_G173'
1
1013.25 0 0
1
'SAW'
0
1
1
0
3
400
0
'S&F_MARIT'
0
0,03
66
1
66 39 180
280 4000 1 1500
2
280 4000 .5
3
8 9 10
1
0 2,9 0
0
0
0
2
1,4
```

B.6 Output file for SMARTS model in April

```
*****************  SMARTS, version 2.9.5  ******************
 Simple Model of the Atmospheric Radiative Transfer of Sunshine
    Chris A. Gueymard, Solar Consulting Services
              December 2005
   This model is documented in FSEC Report PF-270-95
 and in a Solar Energy paper, vol. 71, No.5, 325-346 (2001)
 NOTE: These references describe v. 2.8 or earlier!!!
 See the User's Manual for details on the considerable
 changes that followed...
***************************************************************
  Reference for this run: USSA_AOD=0.084_ASTM_G173
----------------------------------------------------------------
* ATMOSPHERE : SAW        AEROSOL TYPE: S&F_MARIT
* INPUTS:
    Pressure (mb) = 1013.250   Ground Altitude (km) =   0.0000
    Height above ground (km) =   0.0000
    Relative Humidity (%) = 80.460   Precipitable Water (cm) =  1.0000
    Ozone (atm-cm) = 0.3759 or 375.9 Dobson Units
  AEROSOLS:  Optical Depth at 500 nm = 0.0000      Optical depth at 550 nm = 0.0000
     Angstrom's Beta = 0.0000       Schuepp's B = 0.0000
    Meteorological Range (km) =  999.0   Visibility (km) =  764.9
    Alpha1 = 0.3110  Alpha2 = 0.3043   Mean Angstrom's Alpha = 0.3077
    Season = FALL/WINTER
* TEMPERATURES:
    Instantaneous at site's altitude = 257.1 K
    Daily average (reference) at site's altitude = 257.1 K
    Stratospheric Ozone and NO2 (effective) = 217.3 K
** WARNING #13 *********
\\ Ground reflectance data for SPRUCE_TREE
\\ extend only from 0.3900 to 0.8450 µm,
\\ whereas the wavelength limits for this run are 0.2800 and 4.0000 µm.
```

\\ Consequently, reflectance is fixed at 0.009 below 0.3900 µm and at 0.231 above 0.8450 µm.

The following spectral variables will be output to file: smarts295.ext.txt

* Global_tilted_irradiance

* Beam_normal_+circumsolar

* Difuse_horiz-circumsolar

Spectral ZONAL albedo data: SPRUCE_TREE

with a reflection process: NON_LAMBERTIAN

* GEOMETRY (half-angles) OF THE SIMULATED RADIOMETER (deg.):

Slope = -5.00 Aperture = 2.00 Limit = 9.00

Spectral LOCAL albedo data: SPRUCE_TREE

with a reflection process: NON_LAMBERTIAN

==

==

* SOLAR POSITION (deg.):

Zenith Angle (apparent) = 0.000 Azimuth (from North) = 180.00

RELATIVE OPTICAL MASSES:

- Rayleigh = 1.000

- Water Vapor = 1.000

- Ozone = 1.000

- NO2 = 1.000

- Aerosols = 1.000

CO2 Mixing Ratio (ppmv): 400.0

Total column abundances (atm-cm) for all gases except H2O, and for normal/standard conditions:

BrO CH2O CH4 ClNO3 CO CO2 HNO2 HNO3 NH3

0.2500E-05 0.3000E-03 0.1281E+01 0.1200E-03 0.9077E-01 0.3211E+03 0.1000E-03 0.3385E-03 0.1840E-03

NO NO2 NO3 N2 N2O O2 O3 O4 SO2

0.3029E-03 0.1868E-03 0.5000E-04 0.4067E+06 0.2423E+00 0.1678E+06 0.3759E+00 0.1678E+06 0.1140E-03

Corrected total column abundances for all gases (atm-cm) with these realistic conditions: MODERATE POLLUTION

BrO CH2O CH4 ClNO3 CO CO2 HNO2 HNO3 NH3

0.2500E-05 0.1000E-02 0.1311E+01 0.1200E-03 0.1258E+00 0.3211E+03 0.3000E-03 0.1539E-02 0.1840E-03

NO NO2 NO3 N2 N2O O2 O3 O4 SO2

0.2030E-01 0.2187E-02 0.5500E-04 0.4067E+06 0.2423E+00 0.1678E+06 0.3812E+00 0.1678E+06 0.5114E-02

* ANGLES (deg.) FOR TILTED SURFACE CALCULATIONS:

Surface Tilt = 39.000 Surface Azimuth (from North) = 180.000

Incidence Angle = 39.000

Diffuse irradiance ratios (tilted plane/horizontal):

0.8886 (isotropic approximate conversion--for reference)

1.1369 (anisotropic conversion model--used here)

* *

** SPECTRUM:

Total (0-100 µm) Extraterrestrial Irradiance used here = 1500.00 W/m2

(i.e., 1.0000 times the selected solar constant, 1500.00 W/m2, due to the actual Sun-Earth distance.)

Source for selected solar spectrum: Gueymard_2003

To account for the chosen Solar Constant value, the selected solar spectrum has been uniformly multiplied

by this scaling coefficient = 1.0980

Wavelength Range = 280.0 to 4000.0 nm; Number of Wavelengths = 2002

*** BROADBAND IRRADIANCES (W/m2):

* DIRECT BEAM AT NORMAL INCIDENCE:

Extraterrestrial = 1480.16 Terrestrial = 1155.11 Atmospheric Transmittance = 0.7804

* FOR THE HORIZONTAL PLANE:

Direct Beam = 1155.11 Diffuse = 58.84 Global = 1213.96 Clearness index, KT = 0.8093

Diffuse irradiance origination details:

Sky diffuse = 56.51 Back-scattered diffuse = 2.33

* FOR THE TILTED PLANE:

Direct Beam = 897.69 Sky Diffuse = 66.82 Ground Reflected = 14.53 Global = 964.51

* EXPERIMENTAL (WITH CIRCUMSOLAR CORRECTION):

Direct Beam, Normal Incidence = 1155.15   Diffuse Horizontal = 58.81   Global Horizontal = 1213.96

B.7 Input file for SMARTS model in May

```
'USSA_AOD=0.084_ASTM_G173'
1
1013.25 0 0
1
'USSA'
1
1
1
400
1
'S&F_MARIT'
0
1
41
1
51 37. 180.
280 4000 1 1352
2
280 4000 .5
3
8 9 10
1
0 2.9 0
0
0
0
2
1,2
```

B.8 Output file for SMARTS model in May

****************** SMARTS, version 2.9.5 *******************

Simple Model of the Atmospheric Radiative Transfer of Sunshine

Chris A. Gueymard, Solar Consulting Services

December 2005

This model is documented in FSEC Report PF-270-95

and in a Solar Energy paper, vol. 71, No.5, 325-346 (2001)

NOTE: These references describe v. 2.8 or earlier!!!

See the User's Manual for details on the considerable

changes that followed...

****

Reference for this run: USSA_AOD=0.084_ASTM_G173

----

* ATMOSPHERE : USSA AEROSOL TYPE: S&F_MARIT

* INPUTS:

Pressure (mb) = 1013.250 Ground Altitude (km) = 0.0000

Height above ground (km) = 0.0000

Relative Humidity (%) = 46.040 Precipitable Water (cm) = 1.4160

Ozone (atm-cm) = 0.3438 or 343.8 Dobson Units

AEROSOLS: Optical Depth at 500 nm = 1.0000 Optical depth at 550 nm = 0.9472

Angstrom's Beta = 0.6740 Schuepp's B = 0.4343

Meteorological Range (km) = 6.5 Visibility (km) = 5.0

Alpha1 = 0.4877 Alpha2 = 0.5692 Mean Angstrom's Alpha = 0.5284

Season = SPRING/SUMMER

* TEMPERATURES:

Instantaneous at site's altitude = 288.1 K

Daily average (reference) at site's altitude = 288.1 K

Stratospheric Ozone and NO2 (effective) = 225.3 K

** WARNING #13 *********

\\ Ground reflectance data for RED_BRICK

\\ extend only from 0.3000 to 4.0000 µm,

\\ whereas the wavelength limits for this run are 0.2800 and 4.0000 µm.

\\ Consequently, reflectance is fixed at 0.028 below 0.3000 µm and at 0.382 above 4.0000 µm.

** WARNING #13 *********

\\ Ground reflectance data for DRY_LONG_GRASS

\\ extend only from 0.2771 to 2.9760 µm,

\\ whereas the wavelength limits for this run are 0.2800 and 4.0000 µm.

\\ Consequently, reflectance is fixed at 0.008 below 0.2771 µm and at 0.003 above 2.9760 µm.

The following spectral variables will be output to file: smarts295.ext.txt

 * Global_tilted_irradiance

 * Beam_normal_+circumsolar

 * Difuse_horiz-circumsolar

 Spectral ZONAL albedo data: RED_BRICK

 with a reflection process: NON_LAMBERTIAN

* GEOMETRY (half-angles) OF THE SIMULATED RADIOMETER (deg.):

 Slope = 0.00 Aperture = 2.90 Limit = 0.00

** WARNING #11*********

\\ The radiometer's Slope and Limit angles are not provided.

\\ Circumsolar calculations will therefore be performed for

\\ an average geometry corresponding to the Aperture angle.

 Spectral LOCAL albedo data: DRY_LONG_GRASS

 with a reflection process: NON_LAMBERTIAN

==

* SOLAR POSITION (deg.):

 Zenith Angle (apparent) = 0.000 Azimuth (from North) = 180.00

 RELATIVE OPTICAL MASSES:

 - Rayleigh = 1.000

 - Water Vapor = 1.000

 - Ozone = 1.000

 - NO2 = 1.000

 - Aerosols = 1.000

 CO2 Mixing Ratio (ppmv): 400.0

 Total column abundances (atm-cm) for all gases except H2O, and for normal/standard conditions:

BrO CH2O CH4 ClNO3 CO CO2 HNO2 HNO3 NH3

0.2500E-05 0.3000E-03 0.1326E+01 0.1200E-03 0.8859E-01 0.3211E+03 0.1000E-03 0.3637E-03 0.1751E-03

NO NO2 NO3 N2 N2O O2 O3 O4 SO2

0.3145E-03 0.2044E-03 0.5000E-04 0.3827E+06 0.2473E+00 0.1678E+06 0.3438E+00 0.1678E+06 0.1100E-03

* ANGLES (deg.) FOR TILTED SURFACE CALCULATIONS:

Surface Tilt = 37.000 Surface Azimuth (from North) = 180.000

Incidence Angle = 37.000

Diffuse irradiance ratios (tilted plane/horizontal):

0.8993 (isotropic approximate conversion--for reference)

1.1555 (anisotropic conversion model--used here)

* *

** SPECTRUM:

Total (0-100 µm) Extraterrestrial Irradiance used here = 1352.00 W/m2

(i.e., 1.0000 times the selected solar constant, 1352.00 W/m2, due to the actual Sun-Earth distance.) Source for selected solar spectrum: SMARTS_Gueymard

To account for the chosen Solar Constant value, the selected solar spectrum has been uniformly multiplied

by this scaling coefficient = 0.9890

Wavelength Range = 280.0 to 4000.0 nm; Number of Wavelengths = 2002

*** BROADBAND IRRADIANCES (W/m2):

* DIRECT BEAM AT NORMAL INCIDENCE:

Extraterrestrial = 1333.15 Terrestrial = 468.49 Atmospheric Transmittance = 0.3514

* FOR THE HORIZONTAL PLANE:

Direct Beam = 468.49 Diffuse = 531.49 Global = 999.98 Clearness index, KT = 0.7396

Diffuse irradiance origination details:

Sky diffuse = 506.33 Back-scattered diffuse = 25.16

* FOR THE TILTED PLANE:

Direct Beam = 374.15 Sky Diffuse = 641.22 Ground Reflected = 27.35 Global = 1015.37

* EXPERIMENTAL (WITH CIRCUMSOLAR CORRECTION):

Direct Beam, Normal Incidence = 486.08 Diffuse Horizontal = 513.90 Global Horizontal = 999.98

C Appendix - Matlab

C.1 Average of one day

The script that was used to make an average of each day.

```
function [] = TestLoadData();
format long;


files = dir('*.txt');
Names={files.name};
data= dlmread(files(1).name,'',15,0);    %,'',15,0) % read first file
[r,c] = size(data);                  % data size, here row r=2048, column c=2
nFile=length(files);                 % number of files in dataset

CONV = 10^(-2); %Measurement: uW/cm2/nm = 10(-6)W/10(-4)m2/nm = 10(-2)W/m2/nm

dataMean=zeros(r,c);                 % preallocate for results
allData=zeros(c,r);                  % temporary matrix that will contain all irradiances from all files
dataMean(:,1)=data(:,1);             % column 1 = wavelenghts (nm)
for i=1:nFile                        % for all file-names
data=dlmread(files(i).name,'',15,0);  %i=1,2
allData(i,:)=data(:,2).*CONV;          % column 2 = irradiance (W/nm2/nm)
end

for i=1:nFile
for j=1:r                        %for all rows of irradiance data
dataMean(j,2)=dataMean(j,2) + allData(i,j); % Adding all irradiance data, for a given wavelength
end
end
dataMean(:,2) = (dataMean(:,2)/nFile); %Dividing by the number of files to find the mean irradiance



figure(1)
plot(dataMean(:,1),dataMean(:,2),'m-')
hold on
% plot(dataMean(:,1),allData(1,:),'c-')
% plot(dataMean(:,1),allData(2,:),'b-')
```

```
legend('Mean irradiance')
title(['mean measured spectra']) %,'fontsize',11,'fontweight','bold','
    position',[3 (YMAX*0.7)]);
xlabel('Wavelength (nm)');
ylabel('Irradiance (W/m2/nm)')
ylim([0,2.5])
xlim([300 900])
hold off
grid minor

fileID=fopen('16april.txt','wt');

for ii=1:size(dataMean,1)
fprintf(fileID,'%g %g \n',dataMean(ii,1),dataMean(ii,2));
end

%  dataMean = mean(means,2)     % and the grand mean since mean(mean(data))
    =mean(allData)

% dlmwrite('112.txt', dataMean);

return
```

C.2 February, and Air Mass VS APE

All calculations from February, and Air Mass VS APE from each month.

```
content...%function [] = TestLoadData3();
clear all
close all
clc
format long;

files=dir('*.txt');
files.name;
N = length(files);


dir_to_search = 'C:\Users\Helene Arnesen Hasla\Desktop\mars';
files2 = fullfile(dir_to_search, '*.txt');
files3 = dir(files2);
files3.name;
N2= length(files3);
% M=dlmread(files3(1).name,'',[2 2 0 2])

dir_to_search2 = 'C:\Users\Helene Arnesen Hasla\Desktop\april';
files4 = fullfile(dir_to_search2, '*.txt');
files5 = dir(files4);
files5.name;
N3= length(files5);

dir_to_search3 = 'C:\Users\Helene Arnesen Hasla\Desktop\SR';
filesASI = fullfile(dir_to_search3, 'aSi.txt');
filesCDTE = fullfile(dir_to_search3, 'CdTe.txt');
filesCIGS = fullfile(dir_to_search3, 'CIGS.txt');
filesCSI = fullfile(dir_to_search3, 'cSi.txt');
M=dlmread(filesASI,'',1,0);
M1=dlmread(filesCDTE,'',1,0);
M2=dlmread(filesCIGS,'',1,0);
M3=dlmread(filesCSI,'',1,0);

%Define wavelength limits for APE integration
LLIM = 300; %lower wavelength limit, nm
HLIM = 900; %upper wavelength limit, nm

ener=0;
flux=0;
```

```
ener1=0;
flux1=0;
ener2=0;
flux2=0;

%Define constants
h = 6.63*10^(-34); %J*s
c = 3.00*10^(8); %m/s
q = 1.60*10^(-19); %J/eV conversion factor
%1 eV = 1.60*10^(-19) C * 1 J/C = 1.60*10^(-19) J

% for k=1:N2
%       B=load(files2(k).name);
%        [l,o]=size(B);
% %        sumB=sum(B(:,2))
% end
MeanEner1=0;
MeanEner2=0;
MeanEner3=0;
MeanEner4=0;
MeanEner5=0;
MeanEner6=0;
MeanEner7=0;
MeanEner8=0;
MeanEner9=0;
MeanEner10=0;


for i=1:N
A = load(files(i).name);
[m,n] = size(A);
deltaLAM1=zeros(m,1); deltaLAM1(1) = A(2,1)-A(1,1);

for j=2:m
deltaLAM1(j)=A(j,1)-A((j-1),1);
end
sumA = sum(A(:,2).*deltaLAM1(:));


%        disp(['Integrated spectrum (300-900 nm), ',files(i).name,': ',
    num2str(sumA),' W/m^{2}.']);

%Alternative:
```

```
%vstr = genvarname(sprintf('%s',files(i).name));
%disp(['Integrated spectrum (300-900 nm), file ',vstr,': ',num2str(sumA),'
    W/m^{2}.']);

for k=1:m
if A(k,1) >= LLIM && A(k,1) <= HLIM
%APE
ener = ener + (A(k,2)*deltaLAM1(k));
flux = flux + (A(k,2)*A(k,1)*10^(-9)/(h*c)*deltaLAM1(k));
end
end


APE= ener/(q*flux);


disp(['Integrated spectrum (300-900 nm)','APE : ',num2str(APE),'eV ',
    files(i).name,':' ,num2str(sumA), ' W/m^{2}.']);

mat(i)=APE;

end

for ii=1:N2

B = load(files3(ii).name);
[s,t] =size(B);
deltaLAM2=zeros(s,1); deltaLAM2(1) = B(2,1)-B(1,1);


for jj=2:s
deltaLAM2(jj)=B(jj,1)-B((jj-1),1);
end
sumB = sum(B(:,2).*deltaLAM2(:));


for kk=1:s
if B(kk,1) >= LLIM && B(kk,1) <= HLIM
%APEmars
ener1 = ener1 + (B(kk,2)*deltaLAM2(kk));
flux1 = flux1 + (B(kk,2)*B(kk,1)*10^(-9)/(h*c)*deltaLAM2(kk));
end
end
```

```
APE2=ener1/(q*flux1);
mat2(ii)=APE2;

end

for iii=1:N3

C = load(files5(iii).name);
[v,tt] =size(C);
deltaLAM3=zeros(v,1); deltaLAM3(1) = C(2,1)-C(1,1);


for jjj=2:v
deltaLAM3(jjj)=C(jjj,1)-C((jjj-1),1);
end
sumC = sum(C(:,2).*deltaLAM3(:));


for kkk=1:v
if C(kkk,1) >= LLIM && C(kkk,1) <= HLIM
%APEapril
ener2 = ener2 + (C(kkk,2)*deltaLAM3(kkk));
flux2 = flux2 + (C(kkk,2)*C(kkk,1)*10^(-9)/(h*c)*deltaLAM3(kkk));
end
end
APE3=ener2/(q*flux2);
mat3(iii)=APE3;

end

histogram


data= dlmread(files(1).name);    %,'',15,0) % read first file
[r,c] = size(data);              % data size, here row r=2048, column c=2
nFile=length(files);             % number of files in dataset


dataMean=zeros(r,c);             % preallocate for results
allData=zeros(c,r);              % temporary matrix that will contain all
    irradiances from all files
dataMean(:,1)=data(:,1);         % column 1 = wavelenghts (nm)
for i=1:nFile                    % for all file-names
```

```
data=dlmread(files(i).name);  %i=1,2
allData(i,:)=data(:,2);        % column 2 = irradiance (W/nm2/nm)
end

for i=1:nFile
for j=1:r                      %for all rows of irradiance data
dataMean(j,2)=dataMean(j,2) + allData(i,j); % Adding all irradiance data,
    for a given wavelength
end
end
dataMean(:,2) = (dataMean(:,2)/nFile); %Dividing by the number of files to
     find the mean irradiance

AAA =(dataMean > 300 & dataMean < 350);
dataMean(AAA);

fileID=fopen('febs.txt','wt');

for ii=1:size(dataMean,1)
fprintf(fileID,'%g %g \n',dataMean(ii,1),dataMean(ii,2));
end


ener1=0; ener2=0; ener3=0; ener4=0; ener5=0; ener6=0;
ener7=0; ener8=0; ener9=0; ener10=0; ener11=0; ener13=0;
ener16=0; ener12=0; ener13=0; ener14=0; ener15=0; ener17=0;

delta300=zeros(r,1); delta300(1) = dataMean(2,1)-dataMean(1,1);

for ii2=2:r
delta300(ii2)=dataMean(ii2,1)-dataMean((ii2-1),1);
end

for j3=1:m
if dataMean(j3,1) >= 300 && dataMean(j3,1) < 350
ener1 = ener1 + (dataMean(j3,2)*delta300(j3)); %J/s/m2
end
if dataMean(j3,1) >= 350 && dataMean(j3,1) < 400
ener2 = ener2 + (dataMean(j3,2)*delta300(j3)); %J/s/m2
end
if dataMean(j3,1) >= 400 && dataMean(j3,1) < 450
ener3 = ener3 + (dataMean(j3,2)*delta300(j3)); %J/s/m2
end
```

```
if dataMean(j3,1) >= 450 && dataMean(j3,1) < 500
ener4 = ener4 + (dataMean(j3,2)*delta300(j3)); %J/s/m2
end
if dataMean(j3,1) >= 500 && dataMean(j3,1) < 550
ener5 = ener5 + (dataMean(j3,2)*delta300(j3)); %J/s/m2
end
if dataMean(j3,1) >= 550 && dataMean(j3,1) < 600
ener6 = ener6 + (dataMean(j3,2)*delta300(j3)); %J/s/m2
end
if dataMean(j3,1) >= 600 && dataMean(j3,1) < 650
ener7 = ener7 + (dataMean(j3,2)*delta300(j3)); %J/s/m2
end
if dataMean(j3,1) >= 650 && dataMean(j3,1) < 700
ener8 = ener8 + (dataMean(j3,2)*delta300(j3)); %J/s/m2
end
if dataMean(j3,1) >= 700 && dataMean(j3,1) < 750
ener9 = ener9 + (dataMean(j3,2)*delta300(j3)); %J/s/m2
end
if dataMean(j3,1) >= 750 && dataMean(j3,1) < 800
ener10 = ener10 + (dataMean(j3,2)*delta300(j3)); %J/s/m2
end
if dataMean(j3,1) >= 800 && dataMean(j3,1) < 850
ener11 = ener11 + (dataMean(j3,2)*delta300(j3)); %J/s/m2
end
if dataMean(j3,1) >= 850 && dataMean(j3,1) < 900
ener12 = ener12 + (dataMean(j3,2)*delta300(j3)); %J/s/m2
end
if dataMean(j3,1) >= 300 && dataMean(j3,1) < 900
ener13 = ener13 + (dataMean(j3,2)*delta300(j3)); %J/s/m2
end
end

prosent1=(ener1/ener13)*100;
prosent2=(ener2/ener13)*100;
prosent3=(ener3/ener13)*100;
prosent4=(ener4/ener13)*100;
prosent5=(ener5/ener13)*100;
prosent6=(ener6/ener13)*100;
prosent7=(ener7/ener13)*100;
prosent8=(ener8/ener13)*100;
prosent9=(ener9/ener13)*100;
prosent10=(ener10/ener13)*100;
prosent11=(ener11/ener13)*100;
```

```
prosent12=(ener12/ener13)*100;

disp(['Mean energy from integrated spectrum (300-350 nm):', num2str(ener1), ' W/m^{2}.', '% of full sectrum:', num2str(prosent1), '%']);
disp(['Mean energy from integrated spectrum (350-400 nm):', num2str(ener2), ' W/m^{2}.','% of full sectrum:', num2str(prosent2), '%']);
disp(['Mean energy from integrated spectrum (400-450 nm):', num2str(ener3), ' W/m^{2}.','% of full sectrum:', num2str(prosent3), '%']);
disp(['Mean energy from integrated spectrum (450-500 nm):', num2str(ener4), ' W/m^{2}.','% of full sectrum:', num2str(prosent4), '%']);
disp(['Mean energy from integrated spectrum (500-550 nm):', num2str(ener5), ' W/m^{2}.','% of full sectrum:', num2str(prosent5), '%']);
disp(['Mean energy from integrated spectrum (550-600 nm):', num2str(ener6), ' W/m^{2}.','% of full sectrum:', num2str(prosent6), '%']);
disp(['Mean energy from integrated spectrum (600-650 nm):', num2str(ener7), ' W/m^{2}.','% of full sectrum:', num2str(prosent7), '%']);
disp(['Mean energy from integrated spectrum (650-700 nm):', num2str(ener8), ' W/m^{2}.','% of full sectrum:', num2str(prosent8), '%']);
disp(['Mean energy from integrated spectrum (700-750 nm):', num2str(ener9), ' W/m^{2}.','% of full sectrum:', num2str(prosent9), '%']);
disp(['Mean energy from integrated spectrum (750-800 nm):', num2str(ener10), ' W/m^{2}.','% of full sectrum:', num2str(prosent10), '%']);
disp(['Mean energy from integrated spectrum (800-850 nm):', num2str(ener11), ' W/m^{2}.','% of full sectrum:', num2str(prosent11), '%']);
disp(['Mean energy from integrated spectrum (850-900 nm):', num2str(ener12), ' W/m^{2}.','% of full sectrum:', num2str(prosent12), '%']);
disp(['Mean energy from integrated spectrum (300-900 nm):', num2str(ener13), ' W/m^{2}.']);

yq=interp1(M(:,1),M(:,2),dataMean(:,1));
yq1=interp1(M1(:,1),M1(:,2),dataMean(:,1));
yq2=interp1(M2(:,1),M2(:,2),dataMean(:,1));
yq3=interp1(M3(:,1),M3(:,2),dataMean(:,1));

[mm,nn] = size(dataMean);
delta=zeros(mm,1); delta(1) = dataMean(2,1)-dataMean(1,1);

aSii=0;
CdTe=0;
CIGS=0;
cSi=0;

for i7=2:mm
```

```
if dataMean(i7,1) >= 300 && dataMean(i7,1) <= 900
delta(i7)=dataMean(i7,1)-dataMean((i7-1),1);
aSii=aSii+(yq(i7)*dataMean(i7,2)*delta(i7));
aSi=aSii*0.35;

CIGS=CIGS+(yq2(i7)*dataMean(i7,2)*delta(i7));
CIGS1=CIGS*0.65;
cSi=cSi+(yq3(i7)*dataMean(i7,2)*delta(i7));
cSi1=cSi*0.6;

%         yq(i7);
%         dataMean(i7,2);
%         disp([dataMean(i7,2)]);
end
if dataMean(i7,1) >= 400 && dataMean(i7,1) <= 900
delta(i7)=dataMean(i7,1)-dataMean((i7-1),1);
CdTe=CdTe+(yq1(i7)*dataMean(i7,2)*delta(i7));
CdTe1=CdTe*0.45;
end
end

disp(['PV - aSi:', num2str(aSi), 'A/m2'])
disp(['PV - CdTe:', num2str(CdTe1), 'A/m2'])
disp(['PV - CIGS:', num2str(CIGS1), 'A/m2'])
disp(['PV - cSi:', num2str(cSi1), 'A/m2'])


% aSii
% CdTe
% CIGS
% cSi


figure(5)
hold on
grid on
% plotyy(dataMean(:,1),yq(:,1),dataMean(:,1),dataMean(:,2))
% % plot(dataMean(:,1),dataMean(:,2))
%  set(gca,'XLim',[300 900]);
%  set(gca,'YLim',[0 1]);
x = dataMean(:,1);
y = (yq(:,1));
y1 = (yq1(:,1));
```

```
y2 = (yq2(:,1));
y3 = (yq3(:,1));
yyaxis right
plot(x,y)
plot(x,y1)
plot(x,y2)
plot(x,y3)
ylim([0 1])
legend('aSi','CdTe','CIGS','cSi')
ylabel('Spectral Response [A/W]')
z = (dataMean(:,2));
yyaxis left
plot(x,z)
ylim ([0 2.5])
xlim([300 900])
legend('February','aSi','CdTe','CIGS','cSi')
xlabel('Wavelenght [nm]')
ylabel('Spectral Irradiance [W/m^{2}/nm]')
title('Spectral Irradiance Measurements and Spectral Response');
hold off

a=[x y y1 y2 y3 z]
dlmwrite('data.txt',a)

% sumdataMean1=sum(dataMean1)
figure(1)
clf;
hold on
grid on
for i=1:N
A = load(files(i).name);
plot(A(:,1),A(:,2));
end
legend(files.name)
% plot(dataMean(:,1),dataMean(:,2),'m')
% legend('Mean irradiance in February')
set(gca,'XLim',[300 900]);
set(gca,'YLim',[0 2.5]);
xlabel('Wavelength [nm]');
ylabel('Spectral Irradiance [W/m^{2}/nm]');
title('Spectral Irradiance Measurements UiA');
hold off
```

```
figure(4)
%% s(1) = subplot(dataMean(:,1),dataMean(:,2),'m-');
%%
%% X = 0:25;
%% Y = [exp(0.1*X); -exp(.05*X)]';
%% stem(s(1),X,Y)
%  area(dataMean(:,1),dataMean(:,2),'m-')
% plot(dataMean(:,1),allData(1,:),'c-')
% plot(dataMean(:,1),allData(2,:),'b-')
legend('Mean irradiance')
title(['mean measured spectra']) %,'fontsize',11,'fontweight','bold','
    position',[3 (YMAX*0.7)]);
xlabel('Wavelength (nm)');
ylabel('Irradiance (W/m2/nm)')
ylim([0,0.5])
xlim([250 950])
hold off
grid minor


luftfebs= xlsread('luft febs');
%  luftfebs = data(:,3)
for r=1:N
figure(5)
Labels=files(r).name;
%   Labels2=Labels(r);

plot(mat,luftfebs(:,3),'*')
% text(mat,luftfebs(:,3),Labels);
end
xlabel('APE(eV)');
ylabel('Air Temperature (^oC)');
title('Air Temperature vs APE');
ylim([-3 8]);
xlim([1.94 2.12])
grid

Airmas= xlsread('Airmasfeb');
Airmas2= xlsread('AirmasMars');
Airmas3=xlsread('Airmasapril');

figure(6)
```

```
plot(mat,Airmas(:,3),'o')
hold on
plot(mat2,Airmas2(:,3),'o')
plot(mat3,Airmas3(:,3),'o')
Co1=corrcoef(mat,Airmas(:,3));
Co2=corrcoef(mat2,Airmas2(:,3));
Co3=corrcoef(mat3,Airmas3(:,3));
Co1(2,1);
Co2(2,1);
Co3(2,1);

hold off

legend('February R=0.76','March R=0.74','April R=-0.39')
xlabel('APE(eV)');
ylabel('Air Mass (AM)');
title('Air Mass vs APE');
%  ylim([-3 8]);
xlim([1.94 2.12])
grid


figure(3);
hist(mat,[1.94 1.96 1.98 2 2.02 2.04 2.06 2.08 2.1 2.12]);
h = findobj(gca,'Type','patch');
h.FaceColor = [0 0.5 0.5];
h.EdgeColor = 'w';
title(['Histogram results of APE'])
xlabel('APE vaules');
ylabel('Number of APE values')
xlim([1.94 2.12])

%plott APE
figure(2);
bar(mat)
set(gca,'XTickLabel',{files.name})
ylabel('APE')



%return
```

C.3 March

All calculations from March.

```
content...%function  [] = TestLoadData3();
format long;
clear all
close all
clc

files=dir('*.txt');
files.name;
N = length(files);
C=0;

dir_to_search = 'C:\Users\Helene Arnesen Hasla\Desktop\SR';
filesASI = fullfile(dir_to_search, 'aSi.txt');
filesCDTE = fullfile(dir_to_search, 'CdTe.txt');
filesCIGS = fullfile(dir_to_search, 'CIGS.txt');
filesCSI = fullfile(dir_to_search, 'cSi.txt');
M=dlmread(filesASI,'',1,0);
M1=dlmread(filesCDTE,'',1,0);
M2=dlmread(filesCIGS,'',1,0);
M3=dlmread(filesCSI,'',1,0);

% for i=1:N
%         C= C+files.name;
% end
% A(1,1)

%Define wavelength limits for APE integration
LLIM = 300; %lower wavelength limit, nm
HLIM = 900; %upper wavelength limit, nm

ener=0;
flux=0;

MeanEner1=0;
MeanEner2=0;
MeanEner3=0;
MeanEner4=0;
MeanEner5=0;
MeanEner6=0;
MeanEner7=0;
```

```
MeanEner8=0;
MeanEner9=0;
MeanEner10=0;

%Define constants
h = 6.63*10^(-34); %J*s
c = 3.00*10^(8); %m/s
q = 1.60*10^(-19); %J/eV conversion factor
%1 eV = 1.60*10^(-19) C * 1 J/C = 1.60*10^(-19) J

for i=1:N
A = load(files(i).name);
[m,n] = size(A);
deltaLAM1=zeros(m,1); deltaLAM1(1) = A(2,1)-A(1,1);

for j=2:m
deltaLAM1(j)=A(j,1)-A((j-1),1);
end
sumA = sum(A(:,2).*deltaLAM1(:));
%       disp(['Integrated spectrum (300-900 nm), ',files(i).name,': ',
    num2str(sumA),' W/m^{2}.']);

%Alternative:
%vstr = genvarname(sprintf('%s',files(i).name));
%disp(['Integrated spectrum (300-900 nm), file ',vstr,': ',num2str(sumA),'
     W/m^{2}.']);

for k=1:m
if A(k,1) >= LLIM && A(k,1) <= HLIM
%APE
ener = ener + (A(k,2)*deltaLAM1(k));
flux = flux + (A(k,2)*A(k,1)*10^(-9)/(h*c)*deltaLAM1(k));
end
end
APE= ener/(q*flux);

disp(['Integrated spectrum (300-900 nm)','APE : ',num2str(APE),'eV  ',
    files(i).name,':' ,num2str(sumA), ' W/m^{2}.']);

mat(i)=APE;


end
```

```
%histogram


data= dlmread(files(1).name);    %,'',15,0) % read first file
[r,c] = size(data);              % data size, here row r=2048, column c=2
nFile=length(files);             % number of files in dataset


dataMean=zeros(r,c);             % preallocate for results
allData=zeros(c,r);              % temporary matrix that will contain all
    irradiances from all files
dataMean(:,1)=data(:,1);         % column 1 = wavelenghts (nm)
for i=1:nFile                    % for all file-names
data=dlmread(files(i).name);  %i=1,2
allData(i,:)=data(:,2);       % column 2 = irradiance (W/nm2/nm)
end

for i=1:nFile
for j=1:r                     %for all rows of irradiance data
dataMean(j,2)=dataMean(j,2) + allData(i,j); % Adding all irradiance data,
    for a given wavelength
end
end
dataMean(:,2) = (dataMean(:,2)/nFile); %Dividing by the number of files to
     find the mean irradiance


ener1=0; ener2=0; ener3=0; ener4=0; ener5=0; ener6=0;
ener7=0; ener8=0; ener9=0; ener10=0; ener11=0; ener13=0;
ener16=0; ener12=0; ener13=0; ener14=0; ener15=0; ener17=0;

delta300=zeros(r,1); delta300(1) = dataMean(2,1)-dataMean(1,1);

for ii2=2:r
delta300(ii2)=dataMean(ii2,1)-dataMean((ii2-1),1);
end

for j3=1:m
if dataMean(j3,1) >= 300 && dataMean(j3,1) < 350
ener1 = ener1 + (dataMean(j3,2)*delta300(j3)); %J/s/m2
end
if dataMean(j3,1) >= 350 && dataMean(j3,1) < 400
ener2 = ener2 + (dataMean(j3,2)*delta300(j3)); %J/s/m2
```

```
end
if dataMean(j3,1) >= 400 && dataMean(j3,1) < 450
ener3 = ener3 + (dataMean(j3,2)*delta300(j3)); %J/s/m2
end
if dataMean(j3,1) >= 450 && dataMean(j3,1) < 500
ener4 = ener4 + (dataMean(j3,2)*delta300(j3)); %J/s/m2
end
if dataMean(j3,1) >= 500 && dataMean(j3,1) < 550
ener5 = ener5 + (dataMean(j3,2)*delta300(j3)); %J/s/m2
end
if dataMean(j3,1) >= 550 && dataMean(j3,1) < 600
ener6 = ener6 + (dataMean(j3,2)*delta300(j3)); %J/s/m2
end
if dataMean(j3,1) >= 600 && dataMean(j3,1) < 650
ener7 = ener7 + (dataMean(j3,2)*delta300(j3)); %J/s/m2
end
if dataMean(j3,1) >= 650 && dataMean(j3,1) < 700
ener8 = ener8 + (dataMean(j3,2)*delta300(j3)); %J/s/m2
end
if dataMean(j3,1) >= 700 && dataMean(j3,1) < 750
ener9 = ener9 + (dataMean(j3,2)*delta300(j3)); %J/s/m2
end
if dataMean(j3,1) >= 750 && dataMean(j3,1) < 800
ener10 = ener10 + (dataMean(j3,2)*delta300(j3)); %J/s/m2
end
if dataMean(j3,1) >= 800 && dataMean(j3,1) < 850
ener11 = ener11 + (dataMean(j3,2)*delta300(j3)); %J/s/m2
end
if dataMean(j3,1) >= 850 && dataMean(j3,1) < 900
ener12 = ener12 + (dataMean(j3,2)*delta300(j3)); %J/s/m2
end
if dataMean(j3,1) >= 300 && dataMean(j3,1) < 900
ener13 = ener13 + (dataMean(j3,2)*delta300(j3)); %J/s/m2
end
end

prosent1=(ener1/ener13)*100;
prosent2=(ener2/ener13)*100;
prosent3=(ener3/ener13)*100;
prosent4=(ener4/ener13)*100;
prosent5=(ener5/ener13)*100;
prosent6=(ener6/ener13)*100;
prosent7=(ener7/ener13)*100;
```

```matlab
prosent8=(ener8/ener13)*100;
prosent9=(ener9/ener13)*100;
prosent10=(ener10/ener13)*100;
prosent11=(ener11/ener13)*100;
prosent12=(ener12/ener13)*100;

disp(['Mean energy from integrated spectrum (300-350 nm):', num2str(ener1), ' W/m^{2}.', '% of full sectrum:', num2str(prosent1), '%']);
disp(['Mean energy from integrated spectrum (350-400 nm):', num2str(ener2), ' W/m^{2}.','% of full sectrum:', num2str(prosent2), '%']);
disp(['Mean energy from integrated spectrum (400-450 nm):', num2str(ener3), ' W/m^{2}.','% of full sectrum:', num2str(prosent3), '%']);
disp(['Mean energy from integrated spectrum (450-500 nm):', num2str(ener4), ' W/m^{2}.','% of full sectrum:', num2str(prosent4), '%']);
disp(['Mean energy from integrated spectrum (500-550 nm):', num2str(ener5), ' W/m^{2}.','% of full sectrum:', num2str(prosent5), '%']);
disp(['Mean energy from integrated spectrum (550-600 nm):', num2str(ener6), ' W/m^{2}.','% of full sectrum:', num2str(prosent6), '%']);
disp(['Mean energy from integrated spectrum (600-650 nm):', num2str(ener7), ' W/m^{2}.','% of full sectrum:', num2str(prosent7), '%']);
disp(['Mean energy from integrated spectrum (650-700 nm):', num2str(ener8), ' W/m^{2}.','% of full sectrum:', num2str(prosent8), '%']);
disp(['Mean energy from integrated spectrum (700-750 nm):', num2str(ener9), ' W/m^{2}.','% of full sectrum:', num2str(prosent9), '%']);
disp(['Mean energy from integrated spectrum (750-800 nm):', num2str(ener10), ' W/m^{2}.','% of full sectrum:', num2str(prosent10), '%']);
disp(['Mean energy from integrated spectrum (800-850 nm):', num2str(ener11), ' W/m^{2}.','% of full sectrum:', num2str(prosent11), '%']);
disp(['Mean energy from integrated spectrum (850-900 nm):', num2str(ener12), ' W/m^{2}.','% of full sectrum:', num2str(prosent12), '%']);
disp(['Mean energy from integrated spectrum (300-900 nm):', num2str(ener13), ' W/m^{2}.']);



figure(1)
clf;
hold on
grid on
for i=1:N
A = load(files(i).name);
plot(A(:,1),A(:,2));
end
```

```
legend(files.name)
% plot(dataMean(:,1),dataMean(:,2),'m')
% legend('Mean spectral irradiance in March')
set(gca,'XLim',[300 900]);
set(gca,'YLim',[0 2.5]);
xlabel('Wavelength [nm]');
ylabel('Spectral Irradiance [W/m^{2}/nm]');
title('Spectral Irradiance Measurements UiA');
hold off


% figure(4)
% % % s(1) = subplot(dataMean(:,1),dataMean(:,2),'m-');
% % %
% % % X = 0:25;
% % % Y = [exp(0.1*X); -exp(.05*X)]';
% % % stem(s(1),X,Y)
% %  area(dataMean(:,1),dataMean(:,2),'m-')
% % plot(dataMean(:,1),allData(1,:),'c-')
% % plot(dataMean(:,1),allData(2,:),'b-')
% legend('Mean irradiance')
% title(['mean measured spectra']) %,'fontsize',11,'fontweight','bold','position',[3 (YMAX*0.7)]);
% xlabel('Wavelength (nm)');
% ylabel('Irradiance (W/m2/nm)')
% ylim([0,0.5])
% xlim([250 950])
% hold off
% grid minor

%  luftfebs= xlsread('luftmars');
% %  luftfebs = data(:,3)
%  for r=1:N
% figure(5)
% %     Labels=files(r).name;
% %    Labels2=Labels(r);
%
% plot(mat,luftfebs(:,2),'*')
% % text(mat,luftfebs(:,3),Labels);
%  end
%
% xlabel('APE(eV)');
% ylabel('Air Temperature (^oC)');
```

```
% title('Air Temperature vs APE');
%  ylim([-3 8]);
%  xlim([1.94 2.12])
% grid
%
%  Airmas= xlsread('AirmasMars');
%
% figure(6)
% plot(mat,Airmas(:,3),'o')
%
% xlabel('APE(eV)');
% ylabel('AM');
% title('AM vs APE');
%%  ylim([-3 8]);
%  xlim([1.94 2.12])
% grid

yq=interp1(M(:,1),M(:,2),dataMean(:,1));
yq1=interp1(M1(:,1),M1(:,2),dataMean(:,1));
yq2=interp1(M2(:,1),M2(:,2),dataMean(:,1));
yq3=interp1(M3(:,1),M3(:,2),dataMean(:,1));

[mm,nn] = size(dataMean);
delta=zeros(mm,1); delta(1) = dataMean(2,1)-dataMean(1,1);

aSii=0;
CdTe=0;
CIGS=0;
cSi=0;

for i7=2:mm
if dataMean(i7,1) >= 300 && dataMean(i7,1) <= 900
delta(i7)=dataMean(i7,1)-dataMean((i7-1),1);
aSii=aSii+(yq(i7)*dataMean(i7,2)*delta(i7));
aSi=aSii*0.35;

CIGS=CIGS+(yq2(i7)*dataMean(i7,2)*delta(i7));
CIGS1=CIGS*0.65;
cSi=cSi+(yq3(i7)*dataMean(i7,2)*delta(i7));
cSi1=cSi*0.6;

%       yq(i7);
%       dataMean(i7,2);
```

```
%          disp([dataMean(i7,2)]);
end
if dataMean(i7,1) >= 400 && dataMean(i7,1) <= 900
delta(i7)=dataMean(i7,1)-dataMean((i7-1),1);
CdTe=CdTe+(yq1(i7)*dataMean(i7,2)*delta(i7));
CdTe1=CdTe*0.45;
end
end

disp(['PV - aSi:', num2str(aSi), 'A/m2'])
disp(['PV - CdTe:', num2str(CdTe1), 'A/m2'])
disp(['PV - CIGS:', num2str(CIGS1), 'A/m2'])
disp(['PV - cSi:', num2str(cSi1), 'A/m2'])


% aSii
% CdTe
% CIGS
% cSi


figure(3);
hist(mat,[1.94 1.96 1.98 2 2.02 2.04 2.06 2.08 2.1 2.12]);
h = findobj(gca,'Type','patch');
h.FaceColor = [0 0.5 0.5];
h.EdgeColor = 'w';
title(['Histogram results of APE'])
xlabel('APE vaules');
ylabel('Number of APE values')
xlim([1.94 2.12])

% %plott APE
% figure(2);
% bar(mat)
% set(gca,'XTickLabel',{files.name})
% ylabel('APE')

figure(5)
hold on
grid on
% plotyy(dataMean(:,1),yq(:,1),dataMean(:,1),dataMean(:,2))
% % plot(dataMean(:,1),dataMean(:,2))
%  set(gca,'XLim',[300 900]);
```

```
%   set(gca,'YLim',[0  1]);
x = dataMean(:,1);
y = (yq(:,1));
y1 = (yq1(:,1));
y2 = (yq2(:,1));
y3 = (yq3(:,1));
yyaxis right
plot(x,y)
plot(x,y1)
plot(x,y2)
plot(x,y3)
ylim([0  1])
legend('aSi','CdTe','CIGS','cSi')
ylabel('Spectral Response [A/W]')
z = (dataMean(:,2));
yyaxis left
plot(x,z)
ylim ([0  2.5])
xlim([300  900])
legend('March','aSi','CdTe','CIGS','cSi')
xlabel('Wavelenght [nm]')
ylabel('Spectral Irradiance [W/m^{2}/nm]')
title('Spectral Irradiance Measurements and Spectral Response');
hold off

a=[x y y1 y2 y3 z]
dlmwrite('data.txt',a)

%return
```

C.4 April

All calculations form April, included AOD VS APE results.

```
%function [] = TestLoadData3();
format long;
clear all
close all
clc

files=dir('*.txt');
files.name;
N = length(files);
C=0;

dir_to_search = 'C:\Users\Helene Arnesen Hasla\Desktop\SR';
filesASI = fullfile(dir_to_search, 'aSi.txt');
filesCDTE = fullfile(dir_to_search, 'CdTe.txt');
filesCIGS = fullfile(dir_to_search, 'CIGS.txt');
filesCSI = fullfile(dir_to_search, 'cSi.txt');
M=dlmread(filesASI,'',1,0);
M1=dlmread(filesCDTE,'',1,0);
M2=dlmread(filesCIGS,'',1,0);
M3=dlmread(filesCSI,'',1,0);

%Define wavelength limits for APE integration
LLIM = 300; %lower wavelength limit, nm
HLIM = 900; %upper wavelength limit, nm

ener=0;
flux=0;


%Define constants
h = 6.63*10^(-34); %J*s
c = 3.00*10^(8); %m/s
q = 1.60*10^(-19); %J/eV conversion factor
%1 eV = 1.60*10^(-19) C * 1 J/C = 1.60*10^(-19) J

for i=1:N
A = load(files(i).name);
[m,n] = size(A);
deltaLAM1=zeros(m,1); deltaLAM1(1) = A(2,1)-A(1,1);

```

```
for j=2:m
deltaLAM1(j)=A(j,1)-A((j-1),1);
end
sumA = sum(A(:,2).*deltaLAM1(:));
%      disp(['Integrated spectrum (300-900 nm), ',files(i).name,': ', num2str(sumA),' W/m^{2}.']);

%Alternative:
%vstr = genvarname(sprintf('%s',files(i).name));
%disp(['Integrated spectrum (300-900 nm), file ',vstr,': ',num2str(sumA),' W/m^{2}.']);

for k=1:m
if A(k,1) >= LLIM && A(k,1) <= HLIM
%APE
ener = ener + (A(k,2)*deltaLAM1(k));
flux = flux + (A(k,2)*A(k,1)*10^(-9)/(h*c)*deltaLAM1(k));
end
end
APE= ener/(q*flux);

% disp(['Integrated spectrum (300-900 nm)','APE : ',num2str(APE),'eV ', files(i).name,':' ,num2str(sumA), ' W/m^{2}.']);

mat(i)=APE;


end
%histogram


data= dlmread(files(1).name);   %,'',15,0) % read first file
[r,c] = size(data);             % data size, here row r=2048, column c=2
nFile=length(files);            % number of files in dataset


dataMean=zeros(r,c);            % preallocate for results
allData=zeros(c,r);             % temporary matrix that will contain all irradiances from all files
dataMean(:,1)=data(:,1);        % column 1 = wavelenghts (nm)
for i=1:nFile                   % for all file-names
data=dlmread(files(i).name);  %i=1,2
allData(i,:)=data(:,2);       % column 2 = irradiance (W/nm2/nm)
```

```
end

for i=1:nFile
for j=1:r                        %for all rows of irradiance data
dataMean(j,2)=dataMean(j,2) + allData(i,j); % Adding all irradiance data, for a given wavelength
end
end
dataMean(:,2) = (dataMean(:,2)/nFile); %Dividing by the number of files to find the mean irradiance


ener1=0; ener2=0; ener3=0; ener4=0; ener5=0; ener6=0;
ener7=0; ener8=0; ener9=0; ener10=0; ener11=0; ener13=0;
ener16=0; ener12=0; ener13=0; ener14=0; ener15=0; ener17=0;

delta300=zeros(r,1); delta300(1) = dataMean(2,1)-dataMean(1,1);

for ii2=2:r
delta300(ii2)=dataMean(ii2,1)-dataMean((ii2-1),1);
end

for j3=1:m
if dataMean(j3,1) >= 300 && dataMean(j3,1) < 350
ener1 = ener1 + (dataMean(j3,2)*delta300(j3)); %J/s/m2
end
if dataMean(j3,1) >= 350 && dataMean(j3,1) < 400
ener2 = ener2 + (dataMean(j3,2)*delta300(j3)); %J/s/m2
end
if dataMean(j3,1) >= 400 && dataMean(j3,1) < 450
ener3 = ener3 + (dataMean(j3,2)*delta300(j3)); %J/s/m2
end
if dataMean(j3,1) >= 450 && dataMean(j3,1) < 500
ener4 = ener4 + (dataMean(j3,2)*delta300(j3)); %J/s/m2
end
if dataMean(j3,1) >= 500 && dataMean(j3,1) < 550
ener5 = ener5 + (dataMean(j3,2)*delta300(j3)); %J/s/m2
end
if dataMean(j3,1) >= 550 && dataMean(j3,1) < 600
ener6 = ener6 + (dataMean(j3,2)*delta300(j3)); %J/s/m2
end
if dataMean(j3,1) >= 600 && dataMean(j3,1) < 650
ener7 = ener7 + (dataMean(j3,2)*delta300(j3)); %J/s/m2
```

```
end
if dataMean(j3,1) >= 650 && dataMean(j3,1) < 700
ener8 = ener8 + (dataMean(j3,2)*delta300(j3)); %J/s/m2
end
if dataMean(j3,1) >= 700 && dataMean(j3,1) < 750
ener9 = ener9 + (dataMean(j3,2)*delta300(j3)); %J/s/m2
end
if dataMean(j3,1) >= 750 && dataMean(j3,1) < 800
ener10 = ener10 + (dataMean(j3,2)*delta300(j3)); %J/s/m2
end
if dataMean(j3,1) >= 800 && dataMean(j3,1) < 850
ener11 = ener11 + (dataMean(j3,2)*delta300(j3)); %J/s/m2
end
if dataMean(j3,1) >= 850 && dataMean(j3,1) < 900
ener12 = ener12 + (dataMean(j3,2)*delta300(j3)); %J/s/m2
end
if dataMean(j3,1) >= 300 && dataMean(j3,1) < 900
ener13 = ener13 + (dataMean(j3,2)*delta300(j3)); %J/s/m2
end
end

prosent1=(ener1/ener13)*100;
prosent2=(ener2/ener13)*100;
prosent3=(ener3/ener13)*100;
prosent4=(ener4/ener13)*100;
prosent5=(ener5/ener13)*100;
prosent6=(ener6/ener13)*100;
prosent7=(ener7/ener13)*100;
prosent8=(ener8/ener13)*100;
prosent9=(ener9/ener13)*100;
prosent10=(ener10/ener13)*100;
prosent11=(ener11/ener13)*100;
prosent12=(ener12/ener13)*100;

% disp(['Mean energy from integrated spectrum (300-350 nm):', num2str(
    ener1), ' W/m^{2}.', '% of full sectrum:', num2str(prosent1), '%']);
% disp(['Mean energy from integrated spectrum (350-400 nm):', num2str(
    ener2), ' W/m^{2}.','% of full sectrum:', num2str(prosent2), '%']);
% disp(['Mean energy from integrated spectrum (400-450 nm):', num2str(
    ener3), ' W/m^{2}.','% of full sectrum:', num2str(prosent3), '%']);
% disp(['Mean energy from integrated spectrum (450-500 nm):', num2str(
    ener4), ' W/m^{2}.','% of full sectrum:', num2str(prosent4), '%']);
% disp(['Mean energy from integrated spectrum (500-550 nm):', num2str(
```

```
ener5), ' W/m^{2}.','% of full sectrum:', num2str(prosent5), '%']);
% disp(['Mean energy from integrated spectrum (550-600 nm):', num2str(
    ener6), ' W/m^{2}.','% of full sectrum:', num2str(prosent6), '%']);
% disp(['Mean energy from integrated spectrum (600-650 nm):', num2str(
    ener7), ' W/m^{2}.','% of full sectrum:', num2str(prosent7), '%']);
% disp(['Mean energy from integrated spectrum (650-700 nm):', num2str(
    ener8), ' W/m^{2}.','% of full sectrum:', num2str(prosent8), '%']);
% disp(['Mean energy from integrated spectrum (700-750 nm):', num2str(
    ener9), ' W/m^{2}.','% of full sectrum:', num2str(prosent9), '%']);
% disp(['Mean energy from integrated spectrum (750-800 nm):', num2str(
    ener10), ' W/m^{2}.','% of full sectrum:', num2str(prosent10), '%']);
% disp(['Mean energy from integrated spectrum (800-850 nm):', num2str(
    ener11), ' W/m^{2}.','% of full sectrum:', num2str(prosent11), '%']);
% disp(['Mean energy from integrated spectrum (850-900 nm):', num2str(
    ener12), ' W/m^{2}.','% of full sectrum:', num2str(prosent12), '%']);
% disp(['Mean energy from integrated spectrum (300-900 nm):', num2str(
    ener13), ' W/m^{2}.']);
%


yq=interp1(M(:,1),M(:,2),dataMean(:,1));
yq1=interp1(M1(:,1),M1(:,2),dataMean(:,1));
yq2=interp1(M2(:,1),M2(:,2),dataMean(:,1));
yq3=interp1(M3(:,1),M3(:,2),dataMean(:,1));

[mm,nn] = size(dataMean);
delta=zeros(mm,1); delta(1) = dataMean(2,1)-dataMean(1,1);

aSii=0;
CdTe=0;
CIGS=0;
cSi=0;

for i7=2:mm
if dataMean(i7,1) >= 300 && dataMean(i7,1) <= 900
delta(i7)=dataMean(i7,1)-dataMean((i7-1),1);
aSii=aSii+(yq(i7)*dataMean(i7,2)*delta(i7));
aSi=aSii*0.35;

CIGS=CIGS+(yq2(i7)*dataMean(i7,2)*delta(i7));
CIGS1=CIGS*0.65;
cSi=cSi+(yq3(i7)*dataMean(i7,2)*delta(i7));
cSi1=cSi*0.6;
```

```
%        yq(i7);
%        dataMean(i7,2);
%        disp([dataMean(i7,2)]);
end
if dataMean(i7,1) >= 400 && dataMean(i7,1) <= 900
delta(i7)=dataMean(i7,1)-dataMean((i7-1),1);
CdTe=CdTe+(yq1(i7)*dataMean(i7,2)*delta(i7));
CdTe1=CdTe*0.45;
end
end

disp(['PV - aSi:', num2str(aSi), 'A/m2'])
disp(['PV - CdTe:', num2str(CdTe1), 'A/m2'])
disp(['PV - CIGS:', num2str(CIGS1), 'A/m2'])
disp(['PV - cSi:', num2str(cSi1), 'A/m2'])


% aSii
% CdTe
% CIGS
% cSi


figure(5)
hold on
grid on
% plotyy(dataMean(:,1),yq(:,1),dataMean(:,1),dataMean(:,2))
%% plot(dataMean(:,1),dataMean(:,2))
%  set(gca,'XLim',[300 900]);
%  set(gca,'YLim',[0 1]);
x = dataMean(:,1);
y = (yq(:,1));
y1 = (yq1(:,1));
y2 = (yq2(:,1));
y3 = (yq3(:,1));
yyaxis right
plot(x,y)
plot(x,y1)
plot(x,y2)
plot(x,y3)
ylim([0 1])
legend('aSi','CdTe','CIGS','cSi')
```

```
ylabel('Spectral Response [A/W]')
z = (dataMean(:,2));
yyaxis left
plot(x,z)
ylim ([0 2.5])
xlim([300 900])
legend('April','aSi','CdTe','CIGS','cSi')
xlabel('Wavelenght [nm]')
ylabel('Spectral Irradiance [W/m^{2}/nm]')
title('Spectral Irradiance Measurements and Spectral Response');
hold off

a=[x y y1 y2 y3 z];
dlmwrite('data.txt',a);

% figure(1)
% clf;
% hold on
% grid on
% % for i=1:N
% %     A = load(files(i).name);
% %     plot(A(:,1),A(:,2));
% % end
% % legend(files.name)
% plot(dataMean(:,1),dataMean(:,2),'m')
% legend('Mean spectral irradiance of measured days in April ')
% set(gca,'XLim',[300 900]);
% set(gca,'YLim',[0 2.5]);
% xlabel('Wavelength [nm]');
% ylabel('Spectral Irradiance [W/m^{2}/nm]');
% title('Spectral Irradiance Measurements UiA');
% hold off



%  luftfebs= xlsread('luftmars');
% %  luftfebs = data(:,3)
%  for r=1:N
% figure(5)
% %     Labels=files(r).name;
% %    Labels2=Labels(r);
%
% plot(mat,luftfebs(:,2),'*')
```

```
% % text(mat,luftfebs(:,3),Labels);
%  end
%
% xlabel('APE(eV)');
% ylabel('Air Temperature (^oC)');
% title('Air Temperature vs APE');
%  ylim([-3 8]);
%  xlim([1.94 2.12])
% grid
%
%  Airmas= xlsread('AODapril');
%
% figure(6)
% plot(Airmas(:,2),Airmas(:,3),'o')
% hold on
% plot(Airmas(:,2),Airmas(:,4),'o')
% plot(Airmas(:,2),Airmas(:,5),'o')
% plot(Airmas(:,2),Airmas(:,6),'o')
% plot(Airmas(:,2),Airmas(:,7),'o')
% plot(Airmas(:,2),Airmas(:,8),'o')
% plot(Airmas(:,2),Airmas(:,9),'o')
% plot(Airmas(:,2),Airmas(:,10),'o')
% hold off
% legend('AOD_{1640}','AOD_{1020}','AOD_{870}','AOD_{675}','AOD_{500}','
    AOD_{440}','AOD_{380}','AOD_{340}')
% xlabel('APE(eV)');
% ylabel('AOD');
% title('AOD vs APE');
% %  ylim([-3 8]);
% % xlim([1.94 2.12])
% grid

% figure(3);
% hist(mat,[1.94 1.96 1.98 2 2.02 2.04 2.06 2.08 2.1 2.12]);
% h = findobj(gca,'Type','patch');
% h.FaceColor = [0 0.5 0.5];
% h.EdgeColor = 'w';
% title(['Histogram results of APE'])
% xlabel('APE vaules');
% ylabel('Number of APE values')
% xlim([1.94 2.12])

% %plott APE
```

```
% figure(2);
% bar(mat)
% set(gca,'XTickLabel',{files.name})
% ylabel('APE')



%return
```

C.5 SMARTS

All calculations done with SMARTS in matlab.

```

close all


% dir_to_search = 'C:\Users\Helene Arnesen Hasla\Desktop\SMARTS_295_PC';
% filesEXT = fullfile(dir_to_search, 'smarts295.ext');
% M=dlmread(filesEXT,'',1,0);

S=smarts295;
S1=smarts1;
S2=smarts2;
S3=smarts3;

[m1,n1] = size(S1);
[m,n] = size(S);
[m2,n2] = size(S2);
[m3,n3] = size(S3);


x=S(:,1);
y=S(:,2);
x1=S1(:,1);
y1=S1(:,2);
x2=S2(:,1);
y2=S2(:,2);
x3=S3(:,1);
y3=S3(:,2);


a = table2array(x);
b = table2array(y);
a1 = table2array(x1);
b1 = table2array(y1);
a2 = table2array(x2);
b2 = table2array(y2);
a3 = table2array(x3);
b3 = table2array(y3);

figure(1)
grid on
```

```
hold on
plot(a,b,'b')
plot(a1,b1,'r')
plot(a2,b2,'g')
plot(a3,b3,'k')
legend('AM1.5','AM2','AM3.5','AM4')
xlabel('Wavelenght [nm]')
ylabel('Spectral Irradiance [W/m^{2}/nm]')
title('Spectral Irradiance Distibution with different Air Mass');
xlim ([300 900])
ylim ([0 2.5])
hold off

%%


close all

S=smarts295;
S1=smarts1;
S2=smarts2;
S3=smarts3;

[m1,n1] = size(S1);
[m,n] = size(S);
[m2,n2] = size(S2);
[m3,n3] = size(S3);


x=S(:,1);
y=S(:,2);
x1=S1(:,1);
y1=S1(:,2);
x2=S2(:,1);
y2=S2(:,2);
x3=S3(:,1);
y3=S3(:,2);


a = table2array(x);
b = table2array(y);
a1 = table2array(x1);
b1 = table2array(y1);
```

```
a2 = table2array(x2);
b2 = table2array(y2);
a3 = table2array(x3);
b3 = table2array(y3);

figure(1)
grid on
hold on
plot(a,b,'b')
plot(a1,b1,'r')
plot(a2,b2,'g')
%plot(a3,b3,'k')
legend('1','0,01','2','1,5')
xlabel('Wavelenght [nm]')
ylabel('Spectral Irradiance [W/m^{2}/nm]')
title('Spectral Irradiance Distibution with different AOD at 500 nm');
xlim ([300 900])
ylim ([0 2.5])
hold off

%%

S=smarts295;
S1=smarts1;
S2=smarts2;
S3=smarts3;

[m1,n1] = size(S1);
[m,n] = size(S);
[m2,n2] = size(S2);
[m3,n3] = size(S3);


x=S(:,1);
y=S(:,2);
x1=S1(:,1);
y1=S1(:,2);
x2=S2(:,1);
y2=S2(:,2);
x3=S3(:,1);
y3=S3(:,2);


```

```
a = table2array(x);
b = table2array(y);
a1 = table2array(x1);
b1 = table2array(y1);
a2 = table2array(x2);
b2 = table2array(y2);
a3 = table2array(x3);
b3 = table2array(y3);

figure(1)
grid on
hold on
plot(a,b,'b')
plot(a1,b1,'r')
plot(a2,b2,'g')
plot(a3,b3,'k')
legend('0 cm','4 cm','8 cm','12 cm');
xlabel('Wavelenght [nm]')
ylabel('Spectral Irradiance [W/m^{2}/nm]')
title('Spectral Irradiance Distibution with different Specific
    Precipitable Water');
xlim ([300 900])
ylim ([0 2.5])
hold off
%%

S=smarts295;
S1=smarts1;
S2=smarts2;
S3=smarts3;

[m1,n1] = size(S1);
[m,n] = size(S);
[m2,n2] = size(S2);
[m3,n3] = size(S3);


x=S(:,1);
y=S(:,2);
x1=S1(:,1);
y1=S1(:,2);
x2=S2(:,1);
y2=S2(:,2);
```

```
x3=S3(:,1);
y3=S3(:,2);


a = table2array(x);
b = table2array(y);
a1 = table2array(x1);
b1 = table2array(y1);
a2 = table2array(x2);
b2 = table2array(y2);
a3 = table2array(x3);
b3 = table2array(y3);

figure(1)
grid on
hold on
plot(a,b,'b')
plot(a1,b1,'r')
plot(a2,b2,'g')
plot(a3,b3,'k')
legend('950 mb',' 980 mb','1000 mb','1013 mb');
xlabel('Wavelenght [nm]')
ylabel('Spectral Irradiance [W/m^{2}/nm]')
title('Spectral Irradiance Distibution with different site Pressure');
xlim ([300 900])
ylim ([0 2.5])
hold off



%%
%

close all

dir_to_search = 'C:\Users\Helene Arnesen Hasla\Desktop\MASTER MAPPER\april
    - Kopi';
file = fullfile(dir_to_search, '29april.txt');
M=dlmread(file);

S=smarts295;


```

```
[m1,n1] = size(M);
[m,n] = size(S);



x=S(:,1);
y=S(:,2);
x1=M(:,1);
y1=M(:,2);



a = table2array(x);
b = table2array(y);

dataMean1=a;
dataMean2=b;
dataMean=[dataMean1,dataMean2];
[r,c] = size(dataMean);
% dataMean=zeros(r,c);              % preallocate for results



ener1=0;



delta300=zeros(r,1); delta300(1) = dataMean1(2,1)-dataMean1(1,1);

for ii2=2:r
delta300(ii2)=dataMean1(ii2,1)-dataMean1((ii2 -1),1);
end

for j3=1:m
if dataMean1(j3,1) >= 300 && dataMean1(j3,1) < 3000
ener1 = ener1 + (dataMean2(j3,1)*delta300(j3)); %J/s/m2
end
end

disp(['Mean energy from integrated spectrum (300-3000 nm):', num2str(ener1
    ), ' W/m^{2}']);
```

```
figure(1)
grid on
hold on
plot(a,b,'b')
%  plot(x1,y1,'r')
legend('SMARTS','one "clear day" in April')
xlabel('Wavelenght [nm]')
ylabel('Spectral Irradiance [W/m^{2}/nm]')
%  title('Spectral Irradiance Distibution');
title({'Spectral Irradiance Distibution made ' , ' in SMARTS that match
    with a day in April.'});
xlim ([300 900])
xlim ([300 3000])
ylim ([0 2.5])
hold off

%%



close all

dir_to_search = 'C:\Users\Helene Arnesen Hasla\Desktop\MASTER MAPPER\
    februar - Kopi';
file = fullfile(dir_to_search, '6feb.txt');
M=dlmread(file);

S=smarts295;

x=S(:,1);
y=S(:,2);
x1=M(:,1);
y1=M(:,2);

[m,n] = size(S);
[m1,n1] = size(M);


a = table2array(x);
b = table2array(y);

dataMean1=a;
dataMean2=b;
```

```
% [r,c] = size(dataMean);
% dataMean=zeros(r,c);              % preallocate for results



ener1=0;

delta300=zeros(r,1); delta300(1) = dataMean1(2,1)-dataMean1(1,1);

for ii2=2:r
delta300(ii2)=dataMean1(ii2,1)-dataMean1((ii2 -1),1);
end

for j3=1:m
if dataMean1(j3,1) >= 280 && dataMean1(j3,1) < 4000
ener1 = ener1 + (dataMean2(j3,1)*delta300(j3)); %J/s/m2
end
end

disp(['Mean energy from integrated spectrum (300-3000 nm): ', num2str(ener1
    ), ' W/m^{2}']);

figure(1)
grid on
hold on
plot(a,b,'b')
plot(x1,y1,'r')
legend('SMARTS','one "clear day" in February')
xlabel('Wavelenght [nm]')
ylabel('Spectral Irradiance [W/m^{2}/nm]')
title('Spectral Irradiance Distibution with');
xlim ([300 900])
ylim ([0 2.5])
hold off

%%
dir_to_search = 'C:\Users\Helene Arnesen Hasla\Desktop\SR';
filesASI = fullfile(dir_to_search, 'aSi.txt');
filesCDTE = fullfile(dir_to_search, 'CdTe.txt');
filesCIGS = fullfile(dir_to_search, 'CIGS.txt');
filesCSI = fullfile(dir_to_search, 'cSi.txt');
M=dlmread(filesASI,'',1,0);
M1=dlmread(filesCDTE,'',1,0);
```

```
M2=dlmread(filesCIGS,'',1,0);
M3=dlmread(filesCSI,'',1,0);

S=smarts295;

x=S(:,1);
y=S(:,2);

a = table2array(x);
b = table2array(y);

yq=interp1(M(:,1),M(:,2),a);
yq1=interp1(M1(:,1),M1(:,2),a);
yq2=interp1(M2(:,1),M2(:,2),a);
yq3=interp1(M3(:,1),M3(:,2),a);

[mm,nn] = size(a);
delta=zeros(mm,1); delta(1) = a(2,1)-a(1,1);

aSii=0;
CdTe=0;
CIGS=0;
cSi=0;

for i7=2:mm
if a(i7,1) >= 300 && a(i7,1) <= 1000
delta(i7)=a(i7,1)-a((i7-1),1);
aSii=aSii+(yq(i7)*b(i7,1)*delta(i7));
aSi=aSii*0.35;
end
if a(i7,1) >= 300 && a(i7,1) <= 1300
delta(i7)=a(i7,1)-a((i7-1),1);
CIGS=CIGS+(yq2(i7)*b(i7,1)*delta(i7));
CIGS1=CIGS*0.65;
end
if a(i7,1) >= 300 && a(i7,1) <= 1100
delta(i7)=a(i7,1)-a((i7-1),1);
cSi=cSi+(yq3(i7)*b(i7,1)*delta(i7));
cSi1=cSi*0.6;


%        yq(i7);
%        dataMean(i7,2);
```

```
%           disp([dataMean(i7,2)]);
end
if a(i7,1) >= 400 && a(i7,1) <= 900
delta(i7)=a(i7,1)-a((i7-1),1);
CdTe=CdTe+(yq1(i7)*b(i7,1)*delta(i7));
CdTe1=CdTe*0.45;
end
end

disp(['PV - aSi:', num2str(aSi), 'A/m2'])
disp(['PV - CdTe:', num2str(CdTe1), 'A/m2'])
disp(['PV - CIGS:', num2str(CIGS1), 'A/m2'])
disp(['PV - cSi:', num2str(cSi1), 'A/m2'])
```